Republic of Iraq

Ministry of Higher Education and Scientific Research

University of Babylon

College of Engineering

Structural Behavior of Sustainable Rubberized Reinforced Concrete Columns

A Thesis

Submitted to the College of Engineering at University of Babylon in Partial Fulfillment of the Requirements for the Degree of Master in the Civil Engineering (Structures)

By

Tabarak Hussein Abood

(B.Sc. Civil Engineering, 2018)

Supervised By

Prof. Dr. Hayder M.K. Al-Mutairee

Asst. Prof. Dr. Majid M. A. Kadhim

2022 A.D ***1444 A.H***

بسم الله الرحمن الرحيم

(و يسألونك عن الروح قل الروح من أمر ربي وما أوتيتم من العلم إلا قليلا)

صدق الله العلي العظيم

سورة الاسراء (الآية 85)

Certificate

We certify that the thesis titled **"*Structural Behavior of Sustainable Rubberized Reinforced Concrete Columns*"**, was prepared by **"*Tabarak Hussein Abood",*** under our supervision at University of Babylon as a fulfillment of the partial requirements for the degree of master in Civil Engineering / Structures.

Signature:

Name**: Prof. Dr. Hayder M.K. Al-Mutairee**

Date: / / 2023

Signature:

Name**: Asst. Prof. Dr. Majid M. A. Kadhim**

Date: / / 2023

In view of available recommendations, we forward this thesis for debate by the examining committee.

Signature

Name: **Prof. Dr. Thair J. Mizhir Alfatlawi**

(Head of Civil Engineering Department)

Date: / / 2023

CERTIFICATE OF THE EXAMINING COMMITTEE

We certify as an Examining Committee that we have read this thesis titled "***Structural Behavior of Sustainable Rubberized Reinforced Concrete Columns"*** and examined the student "**Tabarak Hussein Abood**" in its content and what related to it, and found it meets the standard of thesis for the degree of Master of science in Civil Engineering (Structural Engineering).

Signature:
Name: ***Prof. Dr. Hayder M.K. Al-Mutairee***
(Supervisor)
Date: / /2023

Signature:
Name**: *Asst. Prof. Dr. Majid M. A. Kadhim***
(Supervisor)
Date: / /2023

Signature:
Name: ***Asst. Prof. Dr. Nabeel Hasan Al- Salim***
(Member)
Date: / /2022

Signature:
Name: ***Asst. Prof. Abd al Riadah Salah Al-Fatlawi***
(Member)
Date: / /2022

Signature:
Name: ***Prof. Dr. Mayasser M. Jomaaha***
(Chairman)
Date: / /2022

Approved by the Head of the Civil Engineering Department

Signature:
Name: **Prof. Dr. Thair J. Mizhir Alfatlawi**
(The Head of the Civil Engineering Department)
Date: / / 2022

Approved by the Dean of the College of Engineering

Signature:
Name: **Prof. Dr. Hatem Hadi Obeid**
(The Dean of the College of Engineering)
Date: / / 2022

Dedication

To my mother

To my brothers and sisters

To my husband and dear

To my supervisor Prof. Dr. Hayder M.K. Al-Mutairee

To the one with great humanity, respect and humility, my supervisor Asst. Prof. Dr. Majid M. A. Kadhim

"To my loved ones and my smile in life, especially my nephew who left me halfway (my father)"

With respect

ACKNOWLEDGEMENT

In the name of **ALLAH**, the most compassionate the most merciful. Praise be to **ALLAH** and pray and peace be on his prophet Mohammed and his family.

I express my deep appreciation to my supervisor Prof. Dr. Hayder M.K. Al-Mutairee and Asst. Prof. Dr. Majid M. A. Kadhim for their valuable guidance and support during the various stages of this project.

I wish to acknowledge my parents, my husband, my brothers and sisters for their encouragement and support during the course of this work.

I would like to record my thanks to the staff of civil engineering department during the period of study at the University of Babylon.

Finally, thanks to all my friends for their forceful encouragement during the progress of this work

Tabarak Hussein

2022

ABSTRACT

The purpose of this study is investigating the behavior of reinforced concrete columns using considerable recycling and reuse of crumb rubber as a substitute for aggregate particles. This study consists of two parts: the first one is experimental work, which includes preparation and test of eight concrete column models, subdivided into two groups to study the effect of :(replacement of the fine aggregate with crumb rubbers in three various proportions by volume (5 %, 10 %, and 15 %), eccentricity of the applied load), on the cracking load, ultimate load, service deformation, cracking pattern, ductility, stiffness, and failure mode. The tests were carried out over eight square cross-section columns with varying rubber content. All the column models have same dimensions (120*120*1000) mm, and tested under eccentric load.

The presence of rubber affects the mechanical properties and the behavior of the rubberized concrete. Compared to normal concrete mixes, the mechanical properties of rubberised concrete containing 15% crumb rubber reduce by (33.49, and 28.10) % for compressive strength, and splitting strength, respectively. On the other hand, the ultimate load carrying capacity decrease with increasing rubber content from 0 % to 15 % with eccentricities of (45 and 75) mm by (25.45 and 12.88) %, respectively. Also, with the increasing eccentricity (e) from 45 mm to 75 mm, the ultimate load capacity decreased about (42.02, 40.41, 36.52, and 32.24) % for the columns without rubber, columns with 5% rubber, and columns with 10% rubber, and columns with 15 % rubber, respectively. It has been noted, the ratio of crumb rubber to fine aggregate substitution reduces the failure load of reinforced concrete columns, as well as, a significant development in cracking load, and ductility compared with the same specimen without replacement. While the

stiffness of the column specimens that were replaced with rubber after applying load at various levels deteriorated dramatically as the applied load level increased.

The second section of the study uses a nonlinear three-dimensional finite element approach to depict the nonlinear behavior of the materials using the computer application ABAQUS/standard 6.14 and numerical methods for mathematical analysis to examine the tested columns. In terms of load-deformation response, ultimate load, and cracking propagation, numerical results and the obtained experimental findings were compared. The results of the finite element model showed a difference in the ultimate load by about (4.743%) for normal concrete (with eccentricity about 45 mm) and reasonable agreement with the experimental data. A parametric study included the effects of various parameters: concrete type with different ratio of reinforcement. In addition to the ratio employed in the experimental models and with the same number of reinforcing bars, two additional steel percentages are discussed in this study, where increasing the steel ratio of the column from (0.021 to 0.043) mm resulted in the following: a significant increment in the maximum load of about (20.49) % for specimen (without rubber and with eccentricities of 45 mm), about (29.26) % for specimen (with 10% of crumb rubber and with eccentricities of 45 mm), and about (20.20) % for G1F15 specimen (with 15% of crumb rubber and with eccentricities of 45 mm), respectively. While decreasing the steel ratio of the column from (0.021 to 0.014) mm resulted in the following: a significant decrement in the maximum load of about 15.24% for specimen (without rubber and with eccentricities of 45 mm), about (20.28) % for specimen (with 10% of crumb rubber and with eccentricities of 45 mm), and about (32.46) % for specimen (with 15% of crumb rubber and with eccentricities of 45 mm), respectively.

LIST OF CONTENTS

NOTATION AND SYMBOLS

The major part of the symbols used in the text is listed below; others are defined with their equations where they first appear.

Symbol	Definition	Unit
A_b	Area of reinforcement bar.	mm^2
A_c	Net area of concrete section.	mm^2
Ag	Gross area of concrete section.	mm^2
As	Area of longitudinal tension reinforcement.	mm^2
A_s`	Area of longitudinal compression reinforcement	mm^2
A_{st}	Total area of longitudinal reinforcement.	mm^2
a	Depth of equivalent compression stress block.	mm
b	Width of compression face	mm
d	Effective depth.	mm
e	Eccentricity of the axial load.	mm
EC	Modulus of elasticity of concrete.	MPa
ES	Modulus of elasticity of steel reinforcement	MPa
f_t	Tension strength of concrete.	MPa
f_c'	Cylinder compressive strength of concrete.	MPa
fcu	Cube concrete compressive strength.	MPa
f_r	Modulus of rupture of concrete	MPa

fsp	Splitting tensile strength of concrete	MPa
f_y	Yield stress of reinforcement	MPa
h	Effective dimension of the column	mm
h_f	Top flange thickness of hollow core slab	mm
ℓd	Reinforcement development length	mm
P_{cr}	Applied load corresponding to initial crack	kN
P	Axial applied load	kN
Pu	Ultimate load	kN
β1	concrete stress-block factor controlling the block height	….
ϕ	ACI strength reduction factor	….
ø	Diameter of reinforcement bars.	mm
ε_c	Strain of concrete.	….
εc	Concrete compressive strain	….
εs	Strain of steel reinforcement.	….
μ	Ductility factor.	….
k	Stiffness factor.	….
υ	Poisson`s ratio.	….
ρ	Reinforcement ratio.	….
σ1, σ2, σ3	Principal stresses	MPa

Abbreviations

Symbol	Definition
ACI	American Concrete Institute.
ASTM	American Society for Testing and Materials.
B.C.	Boundary Condition.
BS	British Standard.
CDP	Concrete Damage Plasticity.
C3D8	Eight-node brick element with integration.
DIC	Digital Image Correlation Technique.
EC	Eurocode.
E1	Eccentricity type 1.
E2	Eccentricity type 2.
EXP.	Experimental.
Eq.	Equation.
et al.	And others.
FEA	Finite Element Analysis.
FEM	Finite Element Method.
IQS	Iraqi Specification.
MPa	Mega Pascal (N/mm^2).
NSC	Normal Strength Concrete.

OPC	Ordinary Portland Cement.
Rebar	Reinforcing Bar.
RC	Reinforced Concrete.
RuC	Rubberized Concrete.
T3D2	Two-node truss element.
w/c	Water to Cement ratio.

Chapter one

Introduction

1-1 General

A column is any structure that has a ratio of length to minimum lateral dimension of at least 3 and is primarily intended to carry axial compressive loads **[1]**. Columns are also one of the most important components because they transfer loads to supports and foundations, and failure of columns in critical locations can lead to significant damage to the structure.

As shown in Figure (1-1), concrete columns are usually reinforced with longitudinal and transverse steel reinforcement. Columns can be divided into three groups based on transverse reinforcement **[2].**

1. Tied columns: is a column in which the longitudinal reinforcement bars are tied together with separate smaller diameter transverse bars (ties) spaced at some interval along the column height. It may be rectangular, round, or square columns.

2. Spirally reinforced columns: These columns have a circular or square cross-section and are reinforced with longitudinal bars in a circular shape and spirals that are closely spaced. There are two main advantages to using spirally-reinforced columns over tied ones: Improved safety for your structure and Assembly on site.

3. Composite columns: longitudinally reinforced with structural steel forms, pipes or tubing with or without extra bars, as well as lateral reinforcement. Composite columns have been widely used in high-rise composite buildings, bridges and offshore structures due to their high structural performance.

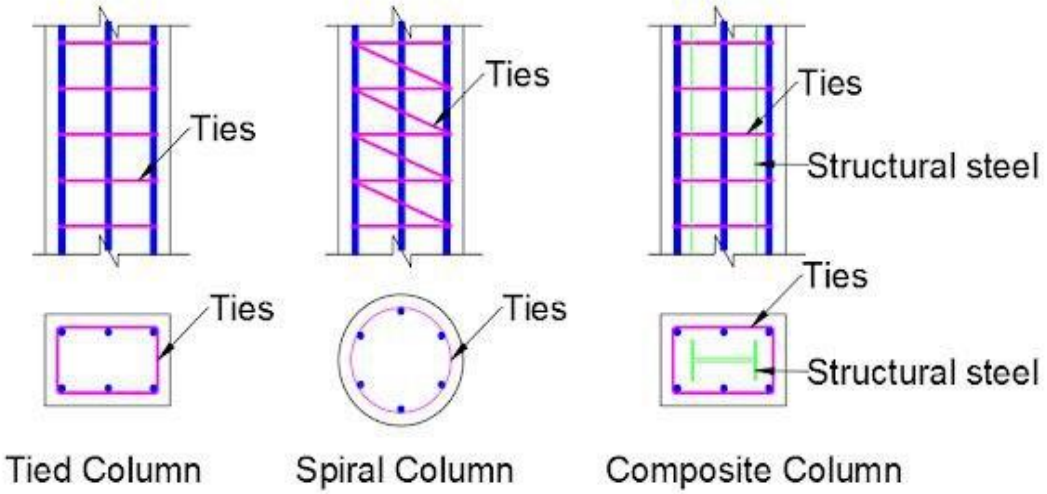

Figure (1-1): Types of reinforced concrete columns [2].

Reinforced concrete is a common structural material which is durable, cost-effective, and easy to work with. However, many constructions, particularly those subjected to harsh environmental conditions, have shown early durability. It is well understood that the durability of materials and structures is determined by both environmental factors and the material's resistance to aggressive substances **[3].** The use of scrap tire rubber as a partial or total replacement for fine aggregate improves many features of concrete. It was believed that adding rubber fibers to concrete would improve shock wave abrasion, reduce heat transmission, reduce noise, and increase acid rain resistance. In addition, incorporating scrap tire rubber particles into concrete results in increased resiliency, durability, and elasticity. Furthermore, the use of discarded tire rubber as a concrete ingredient, namely rubberized concrete, can improve the durability and elasticity of concrete structures in harsh environments.

1-2 Rubberized Concrete

The exponential rise in population and transportation growth is driving up tire manufacture for automobiles. Tires that are no longer useful produce a significant amount of rubber waste. Given that the globe produced more than 2.9 billion tires annually in 2017, "Raffoul et al" **[4]**. It is alleged that the amount of tire waste produced is almost proportional. Rubber is a crucial component used in numerous industrial areas. One of these industries is the manufacture of automobiles, where rubber is utilized for a variety of purposes, including rubber tires. Rubber tire production each year can be roughly estimated in the billions. One billion tires a year are thought to reach the end of their useful lives. A sizable portion of this number is solely dumped untreated in landfills. Land is used up significantly when tires are disposed of in landfills. There is an urgent need to properly and environmentally dispose of used tires **[5].** As was already indicated, one of these solutions to this problem and to enhance some undesirable concrete qualities is to utilize recycled tire rubber in place of fine aggregate in concrete.

1-2-1 Waste Tires Rubber Classification

According to their size, the classification of waste tire rubber is as follows:

1. Chipped rubber (shredded): Because of their huge size, chipped rubber (shredded) is commonly used to substitute coarse aggregate or gravels. This sort of rubber requires two phases of shredding and cutting: the first reduces the size of rubber particles until they achieve a particular dimension of 430-300 mm length and 230-150 mm breadth. The second stage creates a rubber cube with dimensions of 150-100 mm on each side. Chips particles with diameters of 5 to 76 mm are created if the cutting process is sustained.

2. Crumb rubber: Which is used to replace fine aggregate. This type is manufactured in factories using special mills that convert chip rubber particles into smaller particles ranging in diameter from 4.75 to 0.425 mm.
3. Ground rubber: The finest sort of rubber utilized in cement replacement is ground rubber. To convert crumb rubber to ground rubber with a size range of 0.475 mm to 0.075 mm, complex micro-milling techniques are required.

1-2-2 The Effect of Rubberized Material on Structural Properties of Concrete:

It is important to apprehend how rubber impacts the mechanical features of concrete, which include its compressive strength, tensile strength, and modulus of elasticity.

1-2-2-1 Compressive Strength

Generally, compressive strength of normal concrete is higher than that of rubberized concrete. Using natural aggregates with a size range of 0.075mm to 6mm, concrete with a rubber component of between 5 and 50% loses strength by roughly 4 to 70% **[6][7]**. Some studies have noticed that the compression strength reduced when the content of the rubber increased in the concrete. Also, the studies showed that the increasing in the crumb rubber when up to 10% will get a linear relationship between the increasing of the rubber types and the reduction in the compression strength as showing in Figure (1-2), where it was noticed that a loss in compressive strength reached about 24% of the total compressive strength at adding 10% of rubber content **[8]**. The size, shape, mechanical characteristics, and substitution fraction of the RA all affect the loss in overall strength of RuC [9]. Studies have shown a variety of causes for the diminishing trend in RuC compressive strength with rising rubber content. One of the essential motives of this declining tendency is the extraordinarily terrible adhesion of rubber and mortar in concrete, which consequences in cavities in the concrete matrix and lowers

matrix density **[9][10].** Poor adherence to the mortar may result from a smooth rubber surface.

Another cause that reduces power is untimely cracking of RuC, which takes location when RuC is put underneath compressive stress due to the fact of tensile anxiety alongside the rubber particles and related grout. **[11]**.

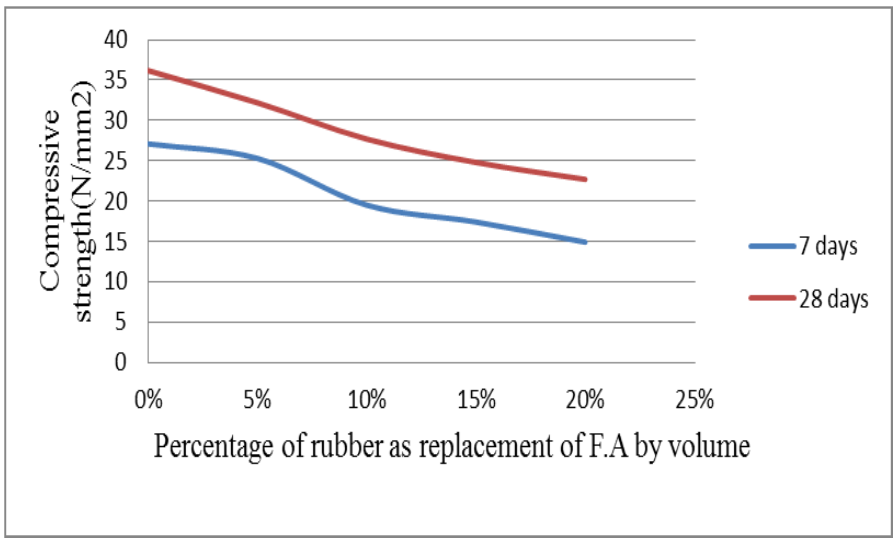

Figure (1-2): "Variation of compressive strength with crump rubber concrete" [8].

1-2-2-2 Tensile Strength

Usually, the tensile strength of the RuC (rubberized concrete) specimen is less than that of the NC (normal concrete) specimen **[12]**. The tensile strength of concrete was found to be reduced by 41% when using 4% crumb rubber in place of fine aggregate and by 58% when using 16% crumb rubber, according to Akinyele et al. **[13]**. Increased RA (rubberized aggregate) led to decreased strength. When aggregates consisting of chipped rubber are used instead of cement, the tensile strength of concrete is decreased more than when rubber powder is used in place of cement in RuC. Figure (1-3) illustrates the relationship between size and RA content in RuC's split tensile strength **[14]**.

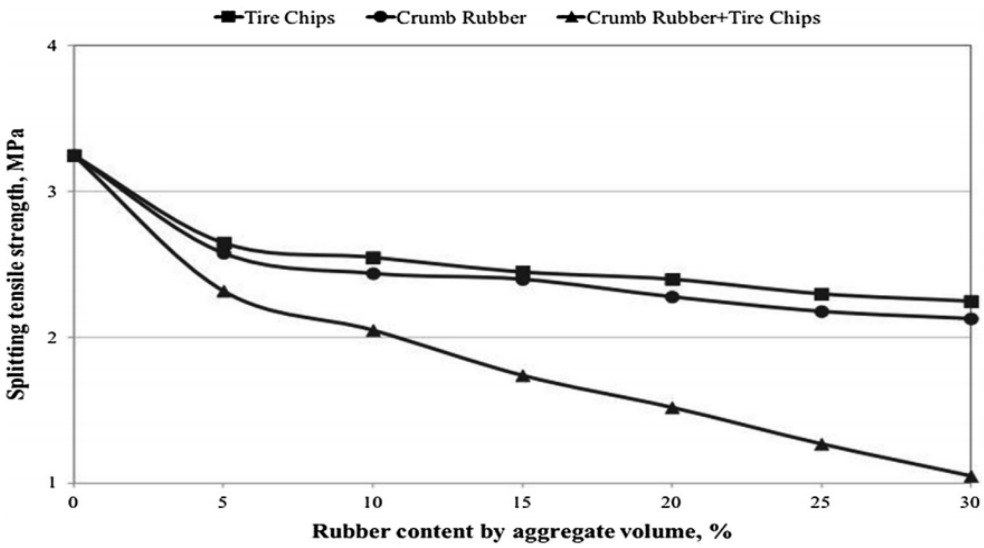

Figure (1-3): Rubber content changes the splitting tensile strength of RuC [14].

1-2-2-3 Flexural Strength

RuC's flexural strength is on a downward trend that is almost identical to its compressive and split tensile strengths. Similar findings were made by Thomas and Gupta **[15]**, They discovered that adding CR to concrete in place of 20% of the sand caused the flexural strength to drop by 25–27%. One advantage of replacement, according to some research, is that RuC does not suddenly fail when bent like regular concrete **[16][17]**.

1-2-2-4 Compressive stress-strain curves and elastic modulus

Rubber can be added to concrete to improve ductility and strain capacity **[18]**. When combined crumb and chipped rubber took the place of both FA (fine aggregate) and CA (coarse aggregate), the increase in ductility was at its maximum **[14]**. Before failure, there was significant elastic deformation in RuC **[19]**. According to Duarte et al. **[20]**, for every 15% increase in rubber content, the strain ratio of RuC to PC increases by 170 %, making RuC more ductile. Because of the plastic nature of rubber, which prevents brittle failure under compressive stress,

RuC specimens fail similarly way to PC specimens **[19]**. RuC shows a wider stress softening and a greater height stress earlier than failure when in contrast to PC. A everyday stress-strain relationship for RuC is proven in Figure (1-4). **[21]**. The stress-strain conduct of the rubber aspect changed via BS (British standard), no matter having a most price that is 40% decrease than that of PC **[22]**. The findings of earlier research can be summed up as follows: Rubber particles in concrete have a significant impact on the material's pre-peak behavior, and RuC's stress-strain behavior is often more nonlinear than NC's. The elongation at break of RuC increases with increasing RA content and RA size, and it is anticipated that RuC with finer RA will have stronger cracking and plastic deformation resistance than that of coarse RA. When FA is substituted with 15% floor rubber, Zheng et al. [23] The static and dynamic moduli of elasticity have been observed to have diminished through 19% and 5.7%, respectively. An increased discount in modulus of elasticity was once viewed with rubber. Compared to concrete bolstered with CR, concrete strengthened with recycled tire fibers has a greater modulus of elasticity. **[24]**.

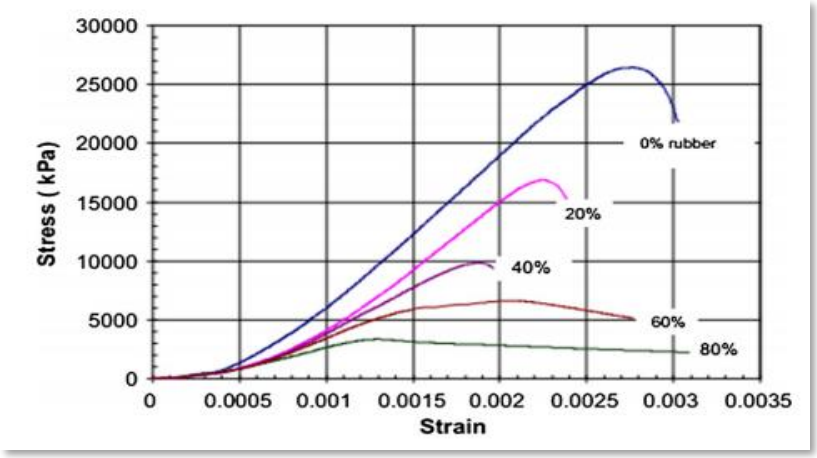

Figure (1-4): "Stress-strain curves of rubber content-varying" [22].

1-2-3 Advantages of Rubberised Concrete

Since the last few decades, rubber is used in asphalt for roads pavement and in concrete by replace aggregate. Particle percentages of rubber crumb are used in several highway surfacing and concrete works, since it has several advantages. Some of these advantages are getting an increase in the resistance of water in the roads, considerable reserving in use of the aggregates, safe disposal of waste or scrap rubber type because rubber can be expensive, difficult to store, and storage of rubber tires required large areas. The successful use of waste rubber was not only by saving the environment, but also it can decrease costs of construction **[25].** The other advantages of using rubber can be outlined as follows**[3]:**

- Lightweight concrete (low unit weight).
- More resistance to abrasion.
- Improved brittleness.
- High resilience, durability and elasticity.
- The rubber work to improve water permeability.
- High ductility.
- High absorbing to the vibration and shocks.
- Improve the cracking, and the shrinkage of concrete.
- Good resistance to chloride material on penetration.

1-2-4 Disadvantage of Rubberised Concrete

Many researches proved that the major disadvantage of using rubber in concrete were reduction in strength of compressive, flexural, and tensile strengths.

1-3 Objective of Thesis

The main purpose of this thesis can be summarized as follows:

- Investigate experimentally, the structural response (such as cracking load, crack pattern, failure mode, ultimate load, and both vertical and lateral deformation) of the rubberised reinforced concrete columns with different percentages of crumb waste tire rubber (5%, 10%, and 15%) as partial volumetric alternative of exceptional aggregates below monotonic loading, with different value of eccentricity, and evaluating the consequences with regular strengthened concrete column samples.
- Researching the have an impact on of rubberized substances on the structural traits of concrete, such as its compressive strength, tensile strength, modulus of rupture, etc., is one of the key goals.
- A numerical analysis using a non-linear three-dimensional finite element program (ABAQUS/Standard 6.14) to track the overall performance of the tested columns and compare the findings to those from experimental investigation.
- A numerical study of many important parameters that was not taken in the experimental program. Display many cases of loading eccentric applied on rectangular columns.

1-4 Problem Statement

In this experimental study, a series of normal and rubberized concrete columns were tested under monotonic loading and with different ratio of rubber (5%, 10%, and 15%), different value of eccentricity (45, 75 mm) to study the performance of this specimens.

1-5 Layout of Thesis

This thesis consists of six chapters as well as two appendices:

Chapter one (Introduction): comprises general information for reinforced concrete columns, rubberized concrete, advantage and disadvantage of rubberized concrete, the effect of rubberized material on structural properties such as compressive strength, tensile strength, …est. Also, the main objectives for the present study.

Chapter two (Literature Review): offers the previous experimental and analytical studies which is related to the subject of rubberized reinforced concrete columns, and some studies about the non-linear finite element methods.

Chapter three (Experimental Program): presents the details of the experimental works and provides information about the properties of the used constriction materials, details of mixes and specimens, and test procedures.

Chapter four (Results and Discussion): offers and discusses the results of the experimental works and deals with the evaluation of experimental results.

Chapter five (Numerical Simulation): summarize numerical results of the finite element modeling which is carried out by a computer program **ABAQUS** and comparing results with those experimental results.

Chapter six (Conclusions and Recommendations): This chapter contains a summary of the current work's conclusions as well as recommendations for future work.

Chapter two

Literature Review

2-1 General

Many of the studies have previously investigated the rubberized concrete columns for various cases of loading, various percentages of rubber and different cross-sections. Based on that, this chapter is dedicated to refer to some of these studies. In addition, employment of finite element method in analyzing rubberized concrete is also reviewed in this chapter.

It is critical to notice that this chapter will additionally take a look at the have an impact on of substituting the mixture with rubber on the mechanical traits of the ensuing concrete (rubberized concrete), due to the fact that this sort of evaluation can assist to higher recognize the conduct of rubberized concrete. In addition, the finite element studies reviewed in this chapter also covered most of the studies investigated rubberized concrete using finite element method due to the limitations of studies investigated the numerical modeling of rubberized concrete columns.

2-2 Review on Mechanical Properties of Rubberized Concrete

A rubberized concrete mixture can be defined as a concrete mix with a partial volumetric or a weight replacement for its natural aggregate (sand and/or gravels) by grains of waste tire rubber. The replacement ratio is usually between 1.5% to 25 % by weight, or between 5% to 50 % by volume **[18].**

Ghedan and Hamza, 2011 [26], examined the concrete's compressive electricity and thermal conductivity after changing the best and coarse particles with rubber. The results were then compared with normal concrete, and how it was affected by using a material a coupling agent such as a SILAN, which was used in this study to treat the rubber particle. The patches were prepared and, each patch consists of three cubic specimens with dimensions (150×150×150) mm and two-disc specimens with dimensions (50×10) cm. The first patch was natural concrete, while the second was rubberized concrete, with waste tire particles replacing 15% of the gravel volume, and the third was modified rubberized concrete with addition and treatment with SILAN around 0.1 percent of water as a coupling agent. The three patches were then tested for thermal conductivity and compressive strength.

The results showed that adding waste tire particles to concrete to make lightweight concrete reduced the compressive strength by about 49.8% compared to the normal concrete. SILAN was used to enhance and treat the surface of rubber particles as a coupling agent, and it was found to be very effective in improving the compressive strength, which was reduced to 12.9% compared to the normal concrete after using SILAN with rubber concrete. In addition, adding rubber particles to the concrete lowered the thermal conductivity of the rubberized concrete by roughly 26.7% compared to the conventional concrete, whereas treating rubberized concrete with SILAN increased thermal conductivity by 17.8% compared to the normal concrete.

Dass et al., 2013 [8], investigated the impact of replacing the aggregate with rubber particles on compressive, flexural, and tensile strength of concrete, where the research's test findings show that there is a large possibility for using scrap tires in concrete mixtures in certain percentages. Fine aggregates were replaced in some concrete mixes with recycled crumb rubber waste material in various percentages

(0, 5%, 10%, 15%, and 20%) in order to make recycled crumb rubber concrete examples. Next, the material's compressive strength, splitting tensile strength, flexural strength, and stress-strain behavior were examined. The results showed that the crumb rubber mixture had a reduction in all categories of strength, while slump values increased as the crumb rubber percentage grew from 0% to 20%. Additionally, lookup proven that the concrete's cut up tensile electricity and compressive electricity each diminished via round 37% and 30%, respectively, when 20% of the sand used to be substituted with rubber. Concrete containing a high amount of crumb rubber will be extremely tough. When 1% to 10% crumb rubber is added to new concrete, the slump increases by roughly 1.08%. The majority of the energy created in fresh concrete is plastic.

NOOR, 2014 [3], investigated physical performance and durability of rubberized concrete. The major goal of this study was to create rubberized concrete with a structural strength that could be achieved with a simple mix design. The simple mix design refers to employing crumb rubber that has been acquired from the plant in its natural state, without being washed or pre-treated. There were several types of durability tests used, including the following: (1) Diffusion of chloride ions, (2) Test for abrasion wear resistance (3) Thawing and freezing.

In another study, two different types of rubber particle samples, ground rubber and crumb rubber, were employed by **Khalid and Hameed (2015) [27]**. The rubber replacement percentages were 5%, 10%, 15%, 20%, 25%, 30%, 35%, and 40% for aggregates that are coarse and excellent. Previously, the mixing process could only last for five minutes. According to the experimental text, adding rubber to concrete reduced the slump, with a 40% replacement rate resulting in zero slump. The concrete mixtures showed lower compressive quality as compared to normal one. It was determined that replacing 5%-10% of concrete

with rubber could be a more acceptable choice for making light-weight concrete without sacrificing compressive strength or slump.

Strukar et al., 2018 [28], To enhance the cloth model, an experimental learn about on the stress-strain conduct of rubberized concrete was once carried out. For rubberized concrete, current constitutive stress-strain fashions are insufficient, and the expanded fashions that are now handy want to be examined in opposition to a larger physique of experimental data. By conducting uniaxial compressive checks on concrete with rubber changing 10%, 20%, 30%, and 40% of the aggregate, it was once viable to learn about and consider the effect of rubber content material on mechanical behavior. Compressive strength, elastic modulus, traces at large stress levels, and failure patterns had been all examined at some stage in the whole stress-strain curve. Previous research on rubberized concrete found that adding rubber aggregate lowered the mechanical qualities of the concrete, such as elastic modulus and compressive strength. However, the produced stress-strain curves revealed advantages, such as (1) reduced softening stiffness in the post-peak area and (2) improved ductility and (3) energy absorption. The following points should be highlighted based on the findings: The inclusion of rubber aggregate lowered compressive strength in a linear relationship, according to testing results. Rubberized concrete stress-strain curves demonstrated that as the rubber component increased, the elastic modulus fell. On the different hand, the pressure at most stress and remaining pressure increased, aiding the concept that rubberized concrete was once extra ductile than regular concrete.

Siddika et al., 2019 [29], An explanation of the characteristics and uses of used tire rubber in concrete. As a result, waste accumulation rises to dangerous levels. Because of the quick rise in and countless variants of current advances around the world, tire trash is one of them that causes major environmental

difficulties. As a result, recycling leftover tire rubber as aggregates as a supplemental construction resource is beneficial. This paper discusses the history of waste tire rubbers and rubberized cementitious composites as well as the properties, uses, and serviceability of these materials. The goal of this lookup is additionally to provide a theoretical framework for comprehending how rubberized concrete (RuC) composite substances can be used to enhance building techniques, inclusive of purposes to enhance the environmental sustainability of concrete buildings in the development industry. By including recycled rubber combination (RA), concrete is made lighter, stronger, greater ductile, and has a longer fatigue life. In each warm and bloodless climate, recycled RA concrete works admirably, with exceptional effects underneath integral publicity and numerous loading scenarios. In general, RuC has a low mechanical strength, then again, this energy can be extended thru desirable processing and the addition of additives. RuC has been extensively explored as a material, although more research on its structural components is needed.

Lv et al., 2020 [30], rubber particles had the ability to improve the fatigue properties of lightweight aggregate concrete (LC) due to their superior deformation and energy absorption capacities. The fatigue properties of LC-containing rubber particles, on the other hand, were not well studied. The influence of rubber particles on the uniaxial compressive fatigue parameters of self-compacting rubber lightweight aggregate concrete was studied in this research (SCRLC). The findings of uniaxial compressive fatigue tests showed that as the percentage of rubber particles substituted grew, so did the fatigue life and strain of SCRLC. The fatigue strain of SCRLC also increased as the number of cycles increased. The analysis' findings reveal that the SCRLC's fatigue life follows a two-parameter Weibull distribution. The double logarithmic fatigue equation is used to establish the

SCRLC fatigue equation based on the experimental results. It was determined from the lgS-lgNf curves of SCRLC that increasing the rubber particles' replacement percentage resulted in a decrease in fatigue limit strength, although the stress level at fatigue life of 2 106 increased first and then declined. Rubber particles' substitution percentage of 30% would result in the greatest stress level of SCRLC. SCRLC has better fatigue properties than LC under the same strength level, according to a complete analysis.

Kadhim and AL-Mutairee, 2020[31], experimentally studied the behavior of rubberized concrete deep beams. This learns about introduced the findings of experiments carried out on concrete deep beam samples made from scrap tire rubber to verify flexural tensile strength, compressive strength, rupture modulus, and have an effect on resistance. four different volumes of coarse and fine filler are swapped out for scrap rubber ("5 %, 10%, 15%, and 20%, respectively"). Nine different structural concrete mixes will be produced as part of the test program, and the novel material will also be tested. Analyze the findings after taking any combination of hardness measurements, such as compressive strength, flexural strength, splitting strength, density, and impact strength. As a result, the results demonstrated that substituting crumb rubber for natural fine and coarse aggregate reduces mechanical qualities such as compressive, flexural, and breaking tensile strength. However, if 20% of the coarse and fine aggregates are replaced with crumb rubber, the impact resistance increases to 426% and 396%, respectively.

Fawzy et al., 2020 [5], studied rubberized concrete properties and its structural engineering applications. This study reviewed rubberized concrete mixtures and their attributes, including toughness, water absorption, ductility, sound absorption, and resistance to sulfates and acids. Additionally, it covered a

discussion of the use of rubberized concrete in structural components and its impact on ductility and compressive strength. Compared to regular concrete mixtures, rubberized concrete mixes showed less strength. Rubberized concrete, on the other hand, exhibited increased ductility and energy-wasting behavior. The findings of this research revealed the following:

- The use of rubber considerably increases the density loss of concrete mixtures as the percentage of rubber particles in the mixture increases. Rubberized concrete can be made in lightweight mixes to satisfy the requirements of a number of applications due to its lower density.
- Rubberized concrete's compressive strength is lower than that of regular concrete mixtures. If the rubber makes up no more than 20% of the total filler content, a reduction in compressive strength is permitted. As can be seen, the compressive strength drastically drops over this ratio. The rubber granules can be treated with any bonding agent to lessen the loss of compressive strength.
- Increasing the rubber content in rubberized concrete mixtures improved abrasion resistance, water absorption, and shrinkage. It improved sound isolation and freezing and thawing resistance.
- It used to be observed that the modulus of elasticity of rubberized concrete used to be decrease than that of traditional concrete mixtures, and that the loss in modulus of elasticity multiplied with the rubber concentration.
- Rubberized concrete was resistant to acid attack well. Additionally, it demonstrated a strong resistance to chloride ion penetration.

2-3 Experimental and Theoretical Studies on Rubberized Concrete Columns

Many of the researches have previously studied the rubberized concrete columns for various cases of loading, various percentages of rubber and different sections. Because of the limited studies on static loads, this section will address the

studies of rubberized concrete columns under other loads such as cyclic, seismic loads…etc. in addition to the static one.

Son et al., 2011 [32], investigated the efficiency of waste tire rubber-filled concrete to improve the deformability and energy absorption capacity of RC columns by considering different concrete compressive strengths, sizes of waste tire rubber particles and rubber contents. Twelve cylindrical specimens were created by combining 0.6- and 1-mm tire rubber particles with concrete that had compressive strengths of 24 and 28 MPa. Each batch of concrete was used to create 27 cubes, which were then tested for performance. The results showed that compared to the same concrete mixture without waste tire particles, the compressive strength of 24 MPa concrete with 0.5% and 1% rubber component was 13% and 22% lower, respectively. Similar outcomes were found for 28 MPa concrete with 12% and 19% and 12% and 1% and 1% reductions in compressive strength, respectively. According to the results, the weight fraction of rubber particles ought to be confined to 0.5 and 1% at 24 and 28 MPa, respectively, in order to manipulate the compressive power of the concrete (i.e., the restriction is decreased by means of 20%). Concrete with waste tire rubber brought has a 90% amplify in flexural elasticity however a minor discount in compressive power and elastic modulus. The great energy dissipation capacity and ductility of this type of concrete make it perfect for earthquake applications.

Xue and Shinozuka, 2013 [33], By combining concrete and recycled rubber waste, rubber-concrete composites will be introduced as a new type of building material with improved seismic performance. Small-scale columns have been built out of rubberized concrete with a range of proportions of rubber crumb to consider structural dynamic performance, which covered free vibration assessments to set up damping ratios and seismic shaking desk checks to seem into structural

responses to floor action added on by using earthquakes. Meanwhile, the compressive power and elastic modulus of concrete-rubberized cylinders had been tested. For the free vibration and seismic shaking desk testing, small-scale concrete columns with lumped hundreds have been created and constructed, even as cylindrical specimens had been created and developed for the compression experiments. Examples of each everyday concrete and rubberized concrete have been used, every with a one-of-a-kind rubber crumb to concrete ratio. Some rubberized concrete cylinders obtained silica fume additions. When in contrast to ordinary concrete, rubberized concrete's damping coefficient increased with the aid of 62%, which decreased the structure's acceleration for the duration of seismic reactions with the aid of 27%. The compressive power of the concrete, however, reduced as rubber crumb was once added. The compressive power of rubberized concrete was once improved by means of including silica fume due to the fact it multiplied the connection between the rubber and the cement. In conclusion, this find out about proved the viability of the usage of environmentally pleasant rubberized concrete as a structural cloth to decorate dynamic overall performance and reduce seismic response of concrete structures.

When making crushed rubber concrete (CRC), leftover tire rubber particles are used to partially replace the natural cement particles **Youssf et al., 2015 [34]**. Rubber can enhance concrete's elasticity, damping coefficient, and energy dissipation qualities, three factors that are crucial for building earthquake-resistant concrete structures, according to earlier material-level studies. However, in contrast to everyday concrete, CRC has a decrease compressive strength. In this research, experimental work that was once performed to see whether or not CRC might also be used for structural columns is described. Figure (2-1) suggests the comparison of a bolstered concrete column with a 240 mm diameter and a 1500

mm shear span below axial compressive stress and a variety of loads. The other two columns are made of regular concrete with varying axial loads, whereas the first column is composed of CRC. A snap-back take a look at used to be carried out on every column to discover its damping capabilities. The use of CRC elevated the columns' hysteretic damping ratio and strength dissipation, respectively, with the aid of 13% and 150%. However, CRC diminished the viscous damping ratio when in contrast to a standard concrete column. CRC columns can stand up to 98.6% extra aspect masses and 91.5% greater remaining flow than normal columns can. Research suggests that CRC is greater environmentally pleasant than usual concrete in structural applications.

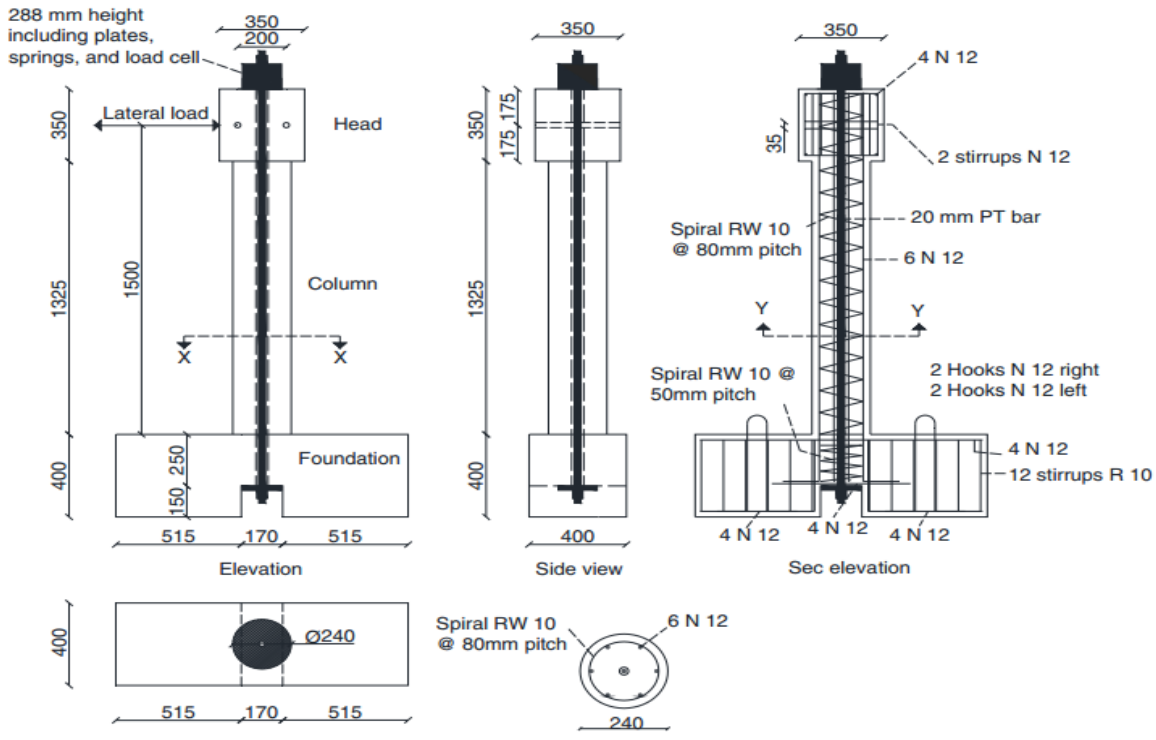

Figure (2-1): "Column dimensions and reinforcement details"[34].

Youssf et al., 2016 [35], presented a study to offset the losses in compressive strength by confining concrete (using fiber reinforced polymer (FRP)). This report outlines research done to see if CRC could be used for structural columns in the

future. Four strengthened concrete columns with a diameter of 240 mm and a shear span of 1500 mm have been assessed below regular axial compression and slowly rising reversed cyclic stress. Two of the four columns were built with CRC and 0 and 2 layers of FRP, while the other two were built with conventional concrete and 0 and 2 layers of FRP. The FRP-encapsulated CRC column carries a lateral load that is 0.93% greater than the FRP-encapsulated conventional concrete column. However, its final drift is decreased by 0.5%. The unconstrained CRC column, on the other hand, can bear 98.6% and 91.5%, respectively, of the lateral load and ultimate deflection of the unconstrained conventional column. Traditional concrete has less environmental impact than CRC in structural applications.

Moustafa et al., 2017[36], inquiry using a vibrating table for rubber concrete columns that use a lot of energy. Crumb rubber was used to replace 20% of the volume of fine aggregate in the rubberized column. The rubberized column's response was compared to that of a traditional bridge column. The sole variation between the two columns was the material utilized in their construction. Both piers have gone through a number of previous surface motions that have been identified by faults from the 1994 Northridge 01 earthquake. A flexible plastic hinge with reinforcement equal to 140% of the design earthquake was generated using the traditional column after 14 thorough test cycles. The rubber column's reinforcing failure after 19 test cycles was equal to 190 percent of the earthquake used as the design foundation. Only 3% less force may be applied to the rubber column than to a standard column. The rubber column's ability to resist lateral drift is also increased by 12.5%. The enclosed pillar loses energy at a rate 16.5% higher than the traditional pillar, on average.

Hassanli et al., 2017 [37], A presentation of an experimental research of reinforced concrete components. This learns about presents experimental statistics

to greater entirely understand the conduct of rubberized concrete in structural purposes and to numerically forecast the conduct of rubberized concrete beams and columns. Four bolstered concrete (RC) beam specimens and 4 RC column specimens have been developed the usage of rubberized concrete with 0%, 6%, 12%, and 18% crumb rubber extent substitute of sand to have a look at the results of rubber content material on structural behavior. To make up for the authentic 0, 6, 12, and 18% of sand in the mixture, rubber particles with a common measurement of 1.18 mm had been added. The span distance between the helps was once 2600 mm, and the beams' width was once a hundred thirty mm, 225 mm in height, and 2800 mm long. Following cyclic loading on beam specimens, the failure mode, pressure displacement behavior, and power dissipation conduct are compared. In order to decrease nearby inaccuracies and facilitate the software of axial masses off-center, the column specimens are prolonged at each end. The middle cross-sectional dimension of the column specimens is eighty x eighty mm, and their universal size is 1420 mm. The conduct of the column specimens used to be in contrast following trying out with eccentric monotonic loading. The check consequences of beam and column specimens that contained more than a few quantities of rubber had been then in contrast in order to reveal how properly these aspects performed. The correctness of the concrete fabric mannequin was once evaluated the usage of finite aspect evaluation (FE) using the LS-DYNA device by way of simulating rubber concrete elements. As rubber content material climbed from 0% to 18%, the material's compressive energy declined by means of round 31%, however the beam and column elements' potential to guide weight solely reduced via about 6% and 12%, respectively (despite being constructed of the identical concrete composition). because of this to this test. As the rubber content grew, the potential for compressive pressure additionally increased. This find out about determined that the addition of rubber to concrete extended the viscous

damping ratio and kinetic strength however diminished the dissipated hysteretic energy.

Hassanli et al., 2017 [38], the seismic performance of granular rubberized concrete columns that are precast, prestressed, segmented, GRP-encapsulated, and unconfined is detailed. The experimental findings of unbonded (PT) prestressed precast concrete columns are presented in this research study. Eight cylinders in total were cycle tested and preloaded. The support is made up of four dry-jointed concrete cylinder segments that are stacked one on top of the other. The PT rod divides at the top and connects to the top and bottom of the column seal at the bottom of the pipe section, passing through a hole in the ground in the middle of the pipe section. The factors in this study include concrete restrictions, concrete material type, and prestressing. The columns are subjected to two separate prestress hundreds of 50 and a hundred kN, ensuing in common axial stresses in the concrete of 2.83 MPa and 5.77 MPa, respectively. To inspect the impact of concrete fabric on the performance of the pipe section, the researchers used ordinary concrete and rubber crumb concrete (CRC). By covering the floor with GRP panels, the effect of concrete encapsulation was investigated. The findings of this study show that FRP-wrapped CRC segmental columns are an environmentally friendly substitute for traditional concrete columns in structural applications. Rubberized concrete had a greater influence of confinement on its strength than regular concrete.

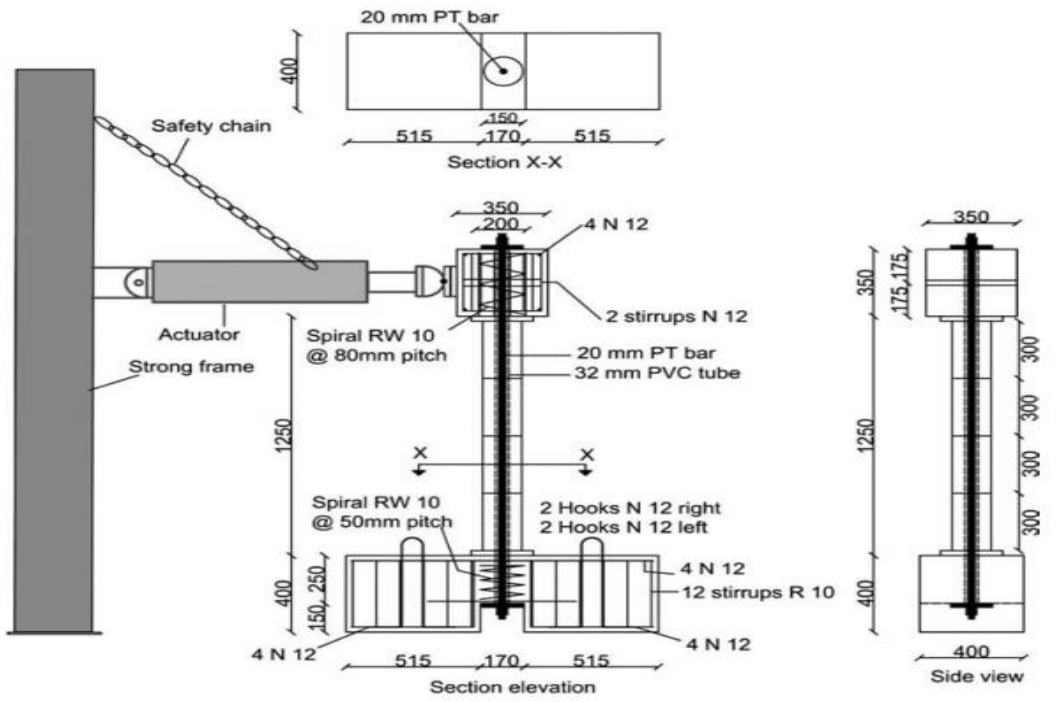

Figure (2-2): Column's geometry and test setup [38].

Li and Li (2017)[39], presented experimental study on performance of rubber particle and steel fiber composite toughening concrete. The mechanical, flexural, compression, and seismic properties of high-strength concrete are examined in this work in relation to steel fibers and rubber particles. Figure depicts a schematic representation of seismic bearing reinforcement (2-3). To test the seismic performance, a low cyclic load with an axial compression ratio of 0.27 was applied. Per experiment, just one sample was examined. Vertical jacks and horizontal hydraulic servo actuators, respectively, apply axial and horizontal loads. The loading mechanism is displacement control, and each step is loaded twice in one cycle until the sample is destroyed, as illustrated in Figure (2-4).

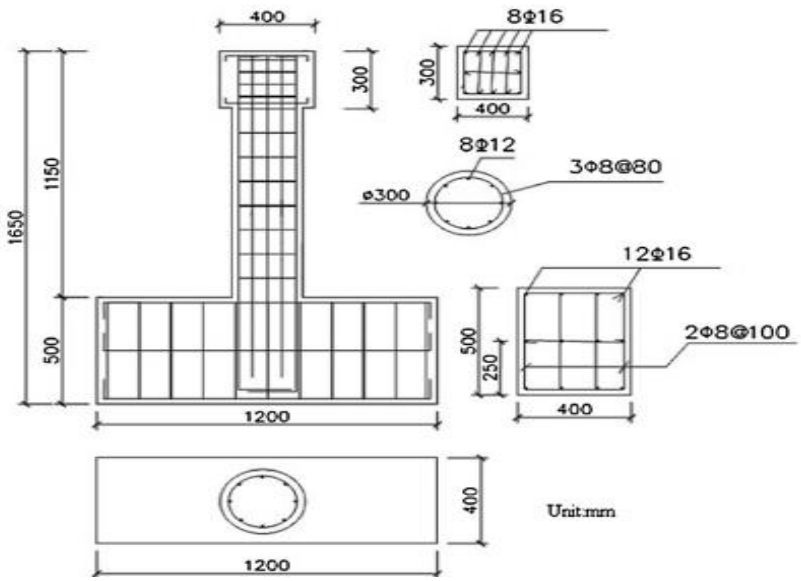

Figure (2-3) Reinforcement diagram of seismic columns [39].

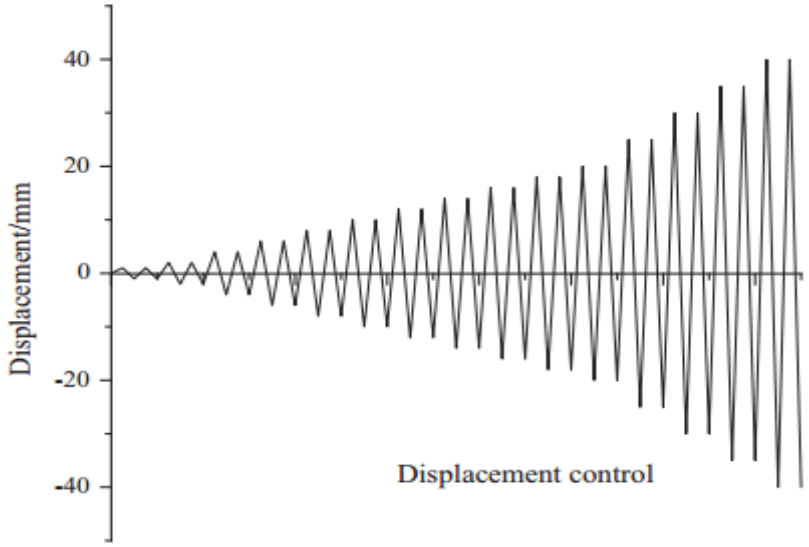

Figure (2-4): Schematic diagram of charging system [39].

The effects exhibit that the concrete's compressive strength, flexural strength, and Young's modulus are all diminished when 5% rubber particles are added. After the addition of 0.9% metal fibers, the flexural electricity drastically rose however the compressive electricity and elastic modulus barely changed. Rubber particles barely have any impact on concrete's flexural strength. Concrete's flexural strength

significantly increased with the addition of 0.9% steel fibers. Repeated cracking causes the load-deflection curve's slope to decrease and the failure mechanism to switch from brittle to ductile fracture. Concrete can be made more flexible and deformable by adding steel or rubber fibers, which also boosts the concrete's compressive strength. Due to the discount in concrete's compressive electricity introduced on with the aid of the addition of metal fibers and rubber particles, the seismic column's bearing ability will barely decrease; however, the hysteresis loop will come to be extra complete, the flexibility and electricity dissipation capacity, as nicely as the stiffness, will be considerably improved. will be reduced. it is brakes.

Hassanli et al., 2017 [40], Study the seismic performance of prefabricated, post-stressed, segmental GRP-fastened and unfastened split rubber-concrete columns. In this work, an experimental study of infinitely prestressed (PT) segmented precast concrete columns is presented. Pretrained and examined with growing alternating masses had been a complete of eight cylindrical supports. With dry joints made of 4 concrete cylinders, the helps are developed one on pinnacle of the other. The PT rod is inserted through a hole drilled in the middle of the segment, released and attached to the upper and lower foundations or column loading heads. Factors in the study included the degree of prestress, the type of concrete used, and the limitations of the concrete. The columns had been subjected to two exclusive stages of prestressing, 50 and a hundred kN, which produced common axial stresses in the concrete of 2.83 and 5.77 MPa. Conventional concrete and rubberized concrete (CRC) had been taken into consideration to determine the effect of concrete fabric on section bearing performance. In order to learn about the confinement, have an effect on of concrete, a fiber-reinforced polymer (FRP) shell masking the flooring used to be used. The findings of this

learn about exhibit that in structural applications, FRP-encapsulated CRC phase columns can provide an environmentally pleasant replacement for everyday concrete columns. The power of rubberized concrete is extra affected via this restrict than traditional concrete is. Rubber particles have a a long way smaller terrible have an impact on on concrete electricity loss than they do on concrete cloth power loss. As the post-column voltage increases, the measured peak load for both unclamped and FRP-clamped samples increases and the final drift decreases. The study also concluded that the axial stress ratio in unconstrained PT struts must be limited to ensure full self-centering behavior.

Hassanli et al., 2018 [41], it is investigated how segmented self-centering rubber concrete columns perform under various loading directions. Segmented self-centering struts are favored in seismic areas because to their minimal or nonexistent residual deflection and cheap maintenance/downtime expenses. This find out about investigates the conduct of segmented rectangular column factors with excessive element ratios below a number loading instructions in order to adapt the thought of segmented self-centering columns to wall factors such as shear partitions and protecting walls. The sorts of bolstered concrete (usually concrete or rubber concrete), the presence (or lack) of reinforcement, and the loading directions in-plane (bending round the sturdy axis) and out-of-plane (bending round the vulnerable axis) are the necessary factors of this find out. Under reverse cyclic shear loading, eight concrete columns with aspect ratios of 2.5, each made up of three concrete segments with intermediate dry joints, were assessed. A preload of 100 kN is applied to the column using unbonded prestressed rebar (PT), causing a stress of 2.8 MPa.

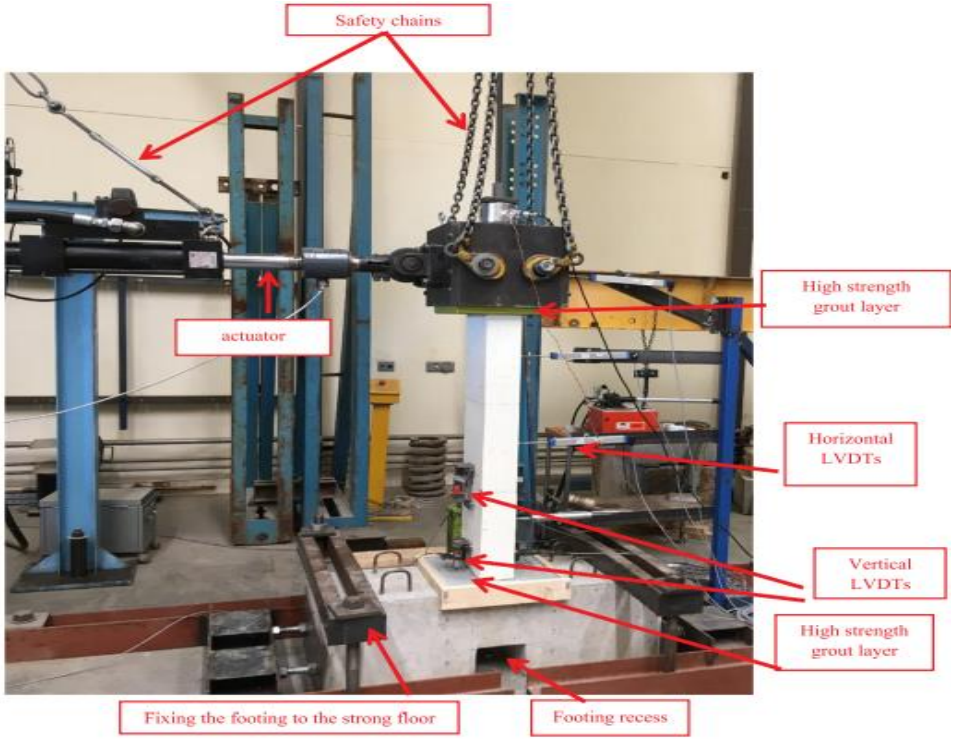

Plate (2-1): Test setup [41].

The results show that in-plane loaded columns have better resistance than out-of-plane loaded columns, but a poorer ductile response, more damage, and a bigger PT force loss. For all examined samples, the total equivalent viscous damping and its fluctuations are incredibly modest, and they only slightly increase with increasing deflection ratio. An empirical equation was developed to describe damping as a function of deflection factor. Additionally, it was shown that reinforcing had little to no impact on the force-displacement behavior in specimens loaded out-of-plane. If the rectangular columns are subjected to a minimal horizontal axial prestress, reinforcement of the structure for out-of-plane loads is not necessary (to prevent shear or sliding failure). Additionally, at the material level, the structural strength loss caused by rubber in concrete is far less pronounced than the structural strength loss caused by rubber in concrete. The

massive element ratio of the take a look at columns approves the consequences of this learn about to be utilized to segmented concrete walls.

Elghazouli and et al., 2017 [42], An investigation of the performance of structures made of rubberized reinforced concrete under cyclic loads is presented. In this study, recycled rubber particles were used in place of mineral aggregates to conduct an experimental investigation of the cyclic behavior of reinforced concrete elements. 13 big pieces with circular cross-sections were evaluated under various axial loads and rubber content ratios, both with and without stirrup restraints. A predefined amount of simultaneous axial force and inelastic lateral cyclic displacement are applied to the specimen. The most significant findings and observations are presented and discussed following a discussion of the experimental design and sample specifics. The test results emphasize flexibility, energy dissipation, and stiffness qualities and strength interactions, enabling a direct comparison of the samples' primary response characteristics. The findings demonstrate that rubber-coated reinforced concrete members, when compared to conventional reinforced concrete members, can offer a fair compromise between flexural stiffness and ductility, particularly under moderate axial stresses. In the presence of relatively high axial loads and the use of a lot of rubber material, external confinement, such as the FRP plates employed in this study, can be used to restore the necessary capacity and give a very steady hysteresis response. The debate also focused on the various approaches for figuring out the primary design criteria and the significance of the findings for the actual use of rubber-coated reinforced concrete parts.

Pham et al., 2019 [43], It is demonstrated how rubberized concrete reinforcement responds dynamically in side collisions with and without FRP limitations. This study used experiments to examine the impact strength of rubber-

concrete columns in side impacts. A pendulum impactor was used to test concrete columns at varied rubber content levels, including 0%, 15%, and 30%. Swap out fine and coarse aggregates for rubber granules with a particle size of 2-5 mm or 5-7 mm. According to test results, rubber concrete supports can dramatically reduce peak impact (27% to 40%) when used as barricades, lowering the danger of injury and even death. Concrete columns made of rubber are also more flexible than those made of regular concrete. The reference columns can be redirected twice before failing. Impact energy absorption is significantly improved by rubberized concrete. In comparison to the control column, the impact energy absorption of the 15% and 30% rubber crumb columns rose by 58% and 63%, respectively. In terms of energy absorption and performance, GRP-coated rubberized concrete supports exceed comparison supports.

2-4 Numerical Studies of Nonlinear–Finite Element in Rubberized Concrete Materials.

Many of the researches have previously studied finite element in rubberized concrete materials for various cases of loading, various percentages of rubber, and different sections. Because of the limited studies on rubberized concrete columns, this section will address the studies of numerical analysis of reinforced concrete members with recycled rubber components**.**

Al-Tayeb et al., 2013 [44], under static and impact stress conditions, the behavior of rubber and mixed rubber concrete structures was investigated. Rubberized concrete samples were created by partially replacing sand with waste crumb rubber (5 %, 10%, and 20% by volume) and evaluated in this learn about underneath influence three-point bending pressure as nicely as static load. With a drop weight impact machine, a weight of 20 N was applied to concrete samples

that were smooth, rubberized, and double-layered with smooth concrete on top and rubberized concrete on the bottom. The static load test was conducted using three additional identical specimens. Each specimen's stress displacement and fracture energy were examined in these two studies. Using the LUSAS V.14 program, finite-element simulations of the samples' dynamic behaviors were also conducted. The predicted impact load vs. displacement behavior was compared with the experimental findings to substantiate the present FE model, which illustrates a good matching. The predicted and experimental displacements of plain concrete at the conclusion of impact response are 1.0 mm and 0.8 mm, respectively, as shown in Figure (2-5) (a). As the amount of sand replaced by fine crumb rubber increases, the respective displacements rise to 2.1 mm and 1.7 mm, respectively, as illustrated in Figure (2-5) (b). The failure mode predicted by the FE model in all the beams is bending, which matches the experimental observations. As a result, it can be concluded that the proposed FE model is excellent at managing the problem at hand.

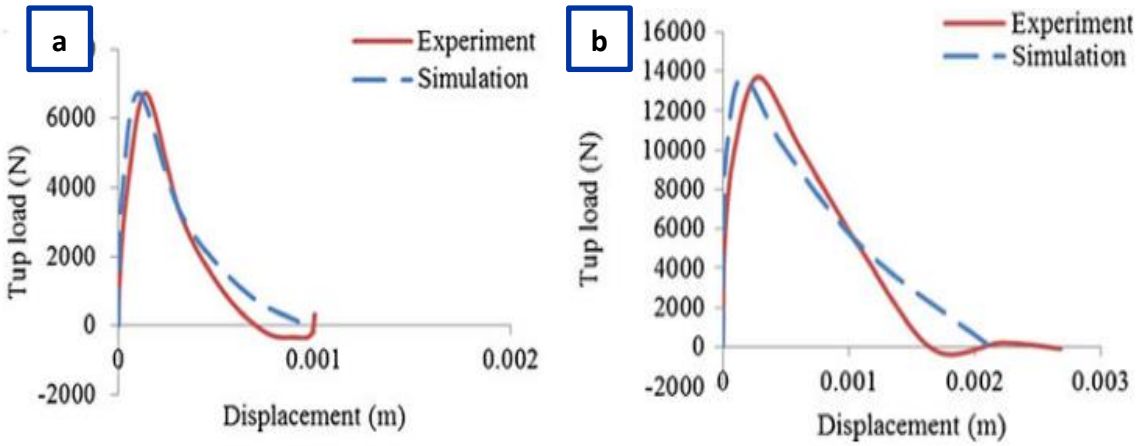

Figure (2-5): Experimental and predicted impact load vs. displacement[44].

Duarte and et al., 2016 [45], presented a finite element modeling of short steel tubes filled with rubberized concrete. In this study, numerical evaluation is used to take a look at the power and failure of quick metal pipes stuffed with

rubberized concrete (RuC), a combine of concrete and rubber particles. This study's essential intention is to expand the ductility and strength absorption of CFST through substituting a RuC core for traditional concrete as the core (NC). First, a succinct precis of the applicable literature is provided. Then, the usage of the business finite factor software program bundle ABAQUS, nonlinear finite factor (FE) fashions for round, square, and rectangular cold-formed metal tubes crammed with three concrete mixes (NC, RuC5, and RuC15) have been described and simulated. The numerical fashions have been made the use of the authors' personal experimental methods. As proven in Figure (2-6), whilst the column is loaded, the decrease inflexible plate is consistently subjected to a longitudinal displacement (along the Z-axis), which totally constrains the greater inflexible plate with regard to this diploma of freedom. The top and decrease strong plates' reference nodes are confined in all three rotations as nicely as in their two lateral orientations (along the X, Y axes), as proven in Figure (2-6).

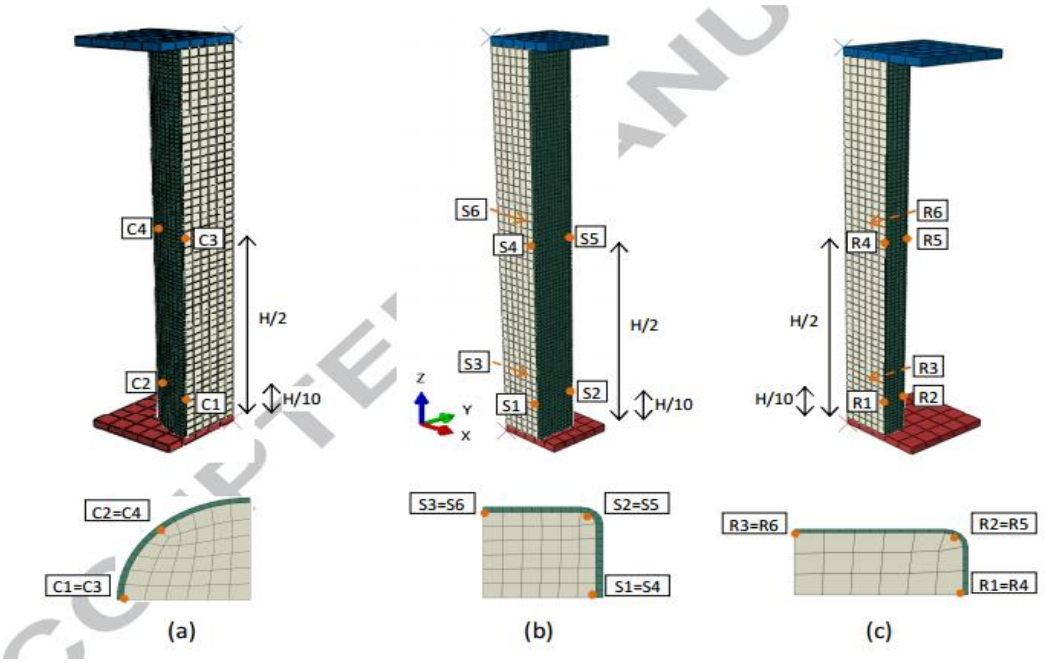

Figure (2-6): "Geometry and meshing of FE models of columns with (a) circular, (b) square, and (c) rectangular cross-sections"[45].

The following are the study's primary findings:

• Due to the model's incorporation of measured elastic and plastic residences of metal and concrete, there is suitable settlement between the numerical and experimental data.

• The model can simulate the inelastic behavior of regular concrete as well as the ultimate strength of the column, the compressive load and axial deflection curves, and the type of crack by comparing numerical and experimental results (NC). The RuCFST column demonstrated higher ductility compared to the CFST column, as was predicted by the experimental results, but lower strength and stiffness.

• The circular section column's concrete core created a compressive stress that is 60% greater than the greatest circular column filled with standard concrete's expected unconstrained concrete strength due to shrinkage effects. The compressive strength of square and rectangular columns is comparable to the concrete compressive stress.

Elghazouli and et al., 2020 [46], It was done to numerically evaluate reinforced concrete buildings that contained recycled rubber. This dissertation examines the inelastic behavior of recycled tire rubber-filled reinforced concrete beam-column members. Utilizing finite element analysis, plastic modeling, and detailed nonlinear numerical 3D simulation and parametric evaluation of concrete damage. According to Figure, tests were conducted on two specimens with a diameter of about 250 mm and six specimens with a circular section with a diameter of about 350 mm, respectively in figure (2-7). A number of experimental results of normal force tests and bending of conventional and rubber-lined concrete serve to confirm the nonlinear finite element method that was chosen. The impact of important factors is then carefully investigated with regard to fundamental

characteristics including concrete strength, rubber content, reinforcing ratio, and axial stress levels.

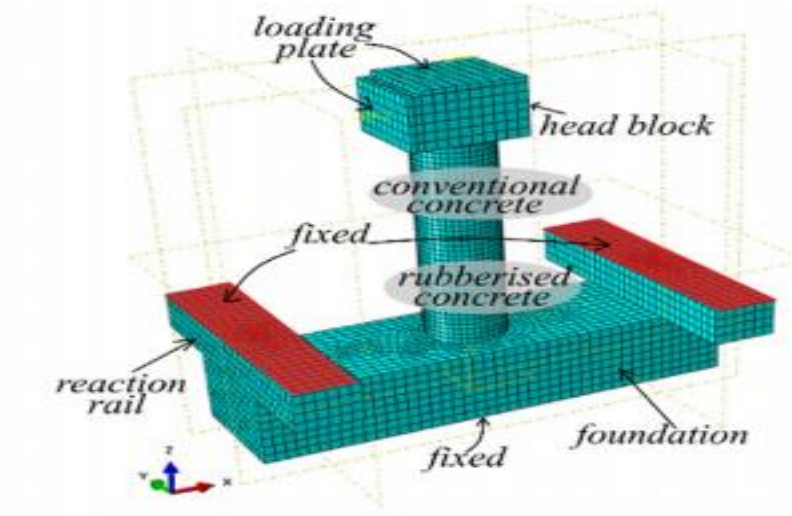

Figure (2-7): 3D numerical representation of Ø350 samples [46].

Based on this, a proposed mathematical model for assessing how the strength and flexibility of reinforced concrete pieces interact is presented. The findings may result in design expressions for rotational flexibility characteristics or a suggested evaluation technique for plastic hinges to ascertain the assembly's maximum rotational capacity. The proposed formulations have proven to be reliable at predicting the strength and ductility of reinforced concrete elements, making them appropriate for codification and practical use.

Alshaikh and et al., 2021 [47], Study was done on the progressive collapse of a reinforced concrete frame using finite element analysis and experimental testing. To create a finite element model for the progressive collapse of a rubber-reinforced concrete frame using ABAQUS is the goal of this work. The FEM findings were compared with the experimental test data in order to validate the suggested numerical model. In order to better comprehend the progressive collapse, ten additional models with various plots and details were added to the numerical

analysis. Four experimentally tested frames were chosen from the study titled "Progressive collapse of reinforced concrete" to validate the finite element model. The concrete elements (beams and columns) in each frame are represented by continuous elements (solid cubes). To shorten the lengthy processing time of the study, the element known as C3D8R can be described as a second-order 3D element with 8 nodes and reduced integration. To represent the reinforcement, truss bars (T3D2 with 3D and 2-node attributes) are employed. Typically, this element is a part of a continuum element or a concrete element (ABAQUS, 2019). The numerical results show that the simulation model performs far better than the experimental test results. Compared to the computational model, compare the sample's measured peak stress (Pmax), maximum displacement (max), and area under the stress-displacement curve (EU). The outcomes demonstrate the numerical model's ability to faithfully reproduce the sample.

Al-ansari et al., 2022 [48], presented study about nonlinear simulation analysis of mechanical behavior of rubberized concrete**.** The main goal is to use a finite element approach with ANSYS V.15 software to simulate the representation of rubber concrete with different percentages of rubber (0, 20, 40, 60, 80, 100 percent) In order to determine the compressive strength, elastic modulus and displacements of the concrete, a preferential cylinder is used to study the consequences with the previous experimental study which published a settlement very close to 5%. Modes were examined for their non-linear behavior by simulating experimental modes from the previous study, the laboratory tests of which were carried out by the researcher. The conclusions also demonstrated that when the elements were regular, or homogeneous, as opposed to irregular, the meshing distribution of the studied elements by ANSYS gave greater values of compressive strength and a decrease in the associated displacements. The mean

and arithmetic mean were found to be acceptable and near when comparing the theoretical and practical outcomes, according to statistical analysis.

Liang and et al., 2022 [49], The damping of recycled rubber concrete has been studied and the damping of its elements has been evaluated by finite element analysis. Concrete structures are always damaged by dynamic loads that cause discomfort and vibration. Concrete damping wants to be superior to passively take in vibration power in order to decrease danger and enlarge comfort. Two problems have to be resolved earlier than the usage of this approach: how to make concrete that can disperse electricity successfully and how to determine out the damping parameters of its components and structures. Experience has validated that recycled rubber combination (RRA) and coarse recycled concrete mixture (RCA) collectively produce recycled rubber concrete (RRAC) with a foremost damping overall performance than herbal aggregate. For herbal aggregates, RCA, and RRA concrete, a generic electricity dissipation and pressure amplitude feature used to be additionally created.

The damping houses of RRAC, NAC, and RAC substances have been investigated via repeated loading and unloading with a vary of stress amplitudes and loading frequencies. Investigated are the influences of stress amplitude, stress amplitude, and stress frequency from the viewpoints of strength dissipation and dissipation factor. Developed were general functions for energy dissipation and strain amplitude based on the findings of material damping tests. Using the finite element approach to examine the nonlinear damping behavior of RRAC beams, a general function was developed to forecast the damping behavior of concrete elements. It is endorsed and proven how to use posted stress electricity distribution features and finite issue evaluation to derive the inside damping ratio of RRAC factors from fabric damping. The cautioned approach used to be used to

numerically consider the influences of load amplitude, load frequency, and load records on the nonlinear damping conduct of RRAC beams. Buildings made of recycled substances are now extra possible in accordance to experimental effects and a counseled method for calculating damping, particularly the place vibration isolation is required.

Gomaa et al., 2020 [50], Short reinforced concrete columns' performance in hot environments was investigated. In this study, experimental and numerical methods are used to evaluate how heated rubber concrete short columns containing brittle steel bars respond to axial compressive stress. The research effort included an analysis of nine pillars. By substituting crumb rubber for fines at indicated replacement levels of 0%, 10%, and 20% of the total volume of fines, mixtures of these columns were created. Three columns served as controls, and the remaining six columns were heated to 400 °C and 600 °C for three hours each. After the heated tower had cooled to room temperature, it was axially loaded until it broke. The finite element model developed using the well-known finite element program ANSYS is validated using the experimental results. According to the experimental findings, as the exposure temperature rises to 400°C and 600°C, the column's residual axial resistance and the percentage loss of secant stiffness are larger. When the rubber content was increased, the amounts of strength and stiffness decreased. However, using crumb rubber significantly improved the ductility. Additionally, the constructed FE models were successful in determining the column's maximum axial load capacity and modeling the distribution of temperature across its cross-section.

2-5 Concluding Remarks.

The following findings can be reached by basing them on the literature review that was previously presented:

1. The compressive strength and elastic modulus of the natural aggregate replacement with rubber content will be reduced (40% rubber content is reduced to 60%).
2. Therefore, the rubber content should be kept at no more than 20-30%. Mechanical properties can be improved by adding additional cementitious materials such as metakaolin, which can increase fly ash compressive strength by up to 20%. Surface modification techniques can also be used to improve adhesion between the colloidal particles and the mortar.
3. As the percentage of rubber increases, the workability slightly improves. This is brought on by the rubber's hydrophobic properties and the lack of a link between the rubber particle and aggregate.
4. The qualities of hardened rubberized concrete at an early age, restricted to 7 days, are not significantly different from those of normal concrete.
5. The stress-strain curves show that rubberized concrete exhibits behavior that is more nonlinear than normal concrete. It was found that the small aggregate concentration affects the rubberized concrete's final stress, whereas the coarse aggregate concentration affects the curve's shape. Both improved deflection and reduced compressive strength are factors that affect how rubber addition affects the maximum compressive load of concrete.
6. When utilized in high proportions, rubber can be employed to create lightweight concrete.

7. According to the results of the axial compressive load test of the column, the compressive strength of the column sample decreases as the rubber content increases. The results show that rubber-coated concrete columns withstand more than twice the lateral deflection before failure than conventional concrete columns. This suggests that the rubberized concrete column can absorb more energy before it fails.
8. Due to the viscoelastic properties of rubber particles, rubberized concrete has higher elasticity, higher energy dissipation, higher degree of hysteresis damping and higher initial stiffness of rubber columns, all of which are related to their cyclic loading. The performance is better than traditional concrete samples. In general, rubber specimens have considerable flexibility, making them more suitable for use in seismic structures.

By using experimental and numerical investigations, this study aims to present the first investigation on rubberized reinforced columns. The experimental investigation concentrated on how much rubber was utilized to replace natural aggregate and how eccentricity affected both the overall size effect and the total load capacity. Instead of fine aggregate, varying volumetric quantities of rubber (5%, 10%, and 15%) will be used (4.75 - 0.15 mm size).

In comparison to previous studies, sieve analysis was done on rubber particles to get the same gradient of sand and gravels within the limits of IQS No. 45/1984. Creating a rubberized concrete mixture with suitable fresh and hardening qualities is a part of the experimental study. Additionally, to provide more straightforward methodologies for load capacity estimations of such elements, numerical research is used.

Chapter three
Experimental Investigation

3-1 Introduction

The experimental research on the structural behavior of rubberized Reinforced concrete columns is described in this chapter. The purpose of the experimental procedure was to study the performance of rubber-lined reinforced concrete columns by determining the effect of rubber size and the amount of rubber used to replace fine aggregates on the performance of rubber-lined reinforced concrete structures.

The specifics of the experimental program are described in this chapter. It provides details on the materials utilized, the mix proportions, the production and testing of column specimens, as well as the research methods employed to achieve the goals outlined in Chapter one.

3-2 Test Program

The current experimental program included a series of tests on a variety of building materials, control specimens (cubes, cylinders, and prisms), and eight reinforced concrete columns, two of which were used as controls. The experiment was carried out in the laboratories, of civil engineering department of university of Babylon. Normal strength concrete was used to construct the tested reinforced columns. Table (3-1) shows the details of all column groups.

Table (3-1): Details of the tested columns.

Group No.	No.	Specimen Symbol	Eccentricity of load	Percentage of replacement (%)	Reinforcement ratio	Dimensions (mm)	Spacing between ties(mm)
Group 1	C1	G1N	e1=45	0	ρ =0.021	120×120	100
	C2	G1F5	e1=45	5	ρ =0.021	120×120	100
	C3	G1F10	e1=45	10	ρ =0.021	120×120	100
	C4	G1F15	e1=45	15	ρ =0.021	120×120	100
Group 2	C5	G2N	e2=75	0	ρ =0.021	120×120	100
	C6	G2F5	e2=75	5	ρ =0.021	120×120	100
	C7	G2F10	e2=75	10	ρ =0.021	120×120	100
	C8	G2F15	e2=75	15	ρ =0.021	120×120	100

3-2-1 Mixes Description

As referred to earlier, one of the principal desires of this study about was once to check out the impact of the quantity of rubber used to exchange fine aggregates on the residences of concrete combos used to produce rubber-based structural concrete. Therefore, four mixes will be investigated, as shown in Table (3-2), the first mix includes only normal concrete (N). The second, third, and fourth mixes (F5, F10, and F15) consist of regular concrete with fine aggregate volume replaced by crumb rubber at variable levels (5, 10, and 15 %, respectively).

Table (3-2): description of the mixes.

No	specify sample	Use fine aggregate as volume rather than rubber particle content (%)
1	N	0
2	F5	5
3	F10	10
4	F15	15

3-2-2 Description of Tested Columns

The shape and outward dimensions of all the column specimens are the same, with a square cross-section of (120×120) mm. The complete length of every specimen is a thousand mm. The distance between the corbels (central part) is 520 mm and the dimensions of the corbels are 120 x 240 x 120 mm. The cause for making the bracket is eccentric load, see figure (3-1). All columns are strengthened with 4 (φ 10 mm) deformed longitudinal bars (ρ=0.021) and obvious concrete cover (15 mm). In addition, the columns have steel ties with a diameter (ø4 mm) and a spacing of 100 mm c/c (or 60 mm c/c). All columns are developed in accordance to ACI Code 318 **[51]** specification proven in **Appendix A**. The reinforcement details for the columns and corbels are shown in Figure (3-2).

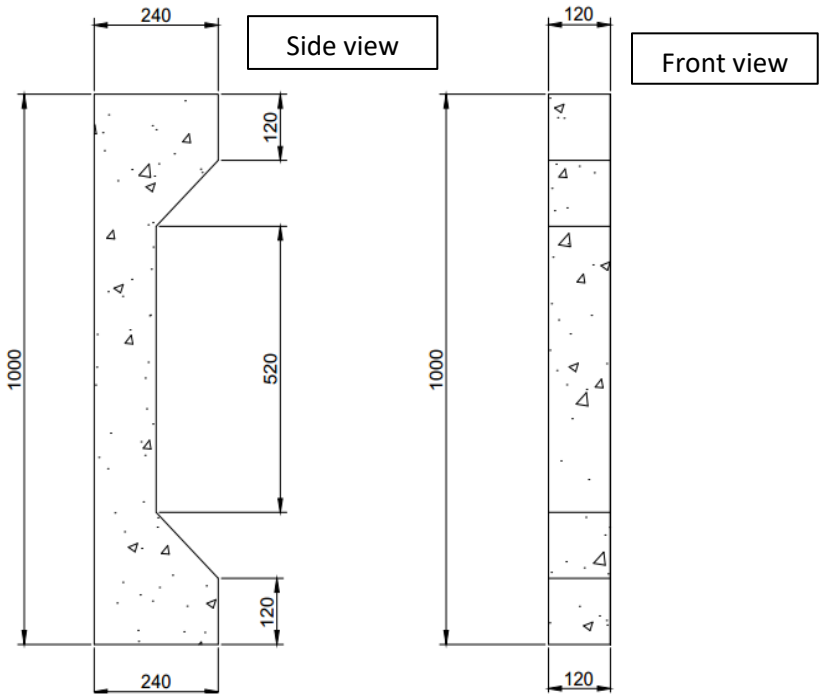

Figure (3-1): Geometry of column (all dimensions in mm).

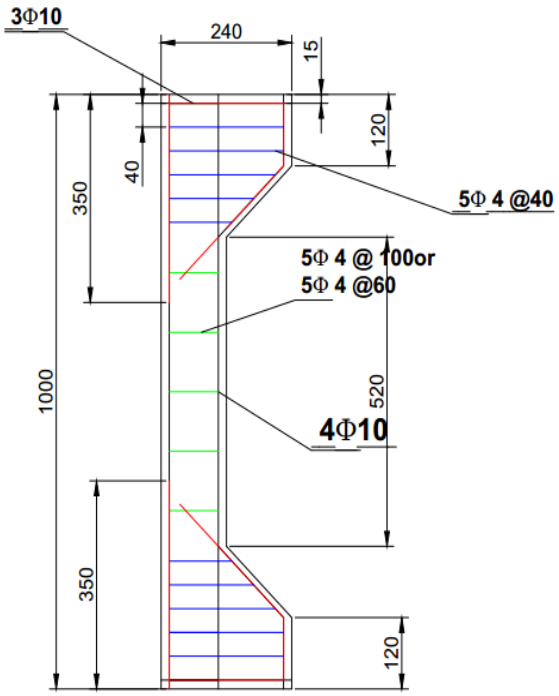

Figure (3-2): Detail of the test column reinforcement (all dimensions in mm).

3-2-3 General Description

The experimental design of the current study involves the analysis of eight column samples, including two control columns:

There are four columns in the first group (C1 to C4). The control of this group is in the first column (C1), and without rubber, rubberized concrete is used for prepared columns (C2, C3, and C4), with rubber crumb substituting 5%, 10%, and 15% of the volume of fine aggregate, accordingly. The columns (C1, C2, C3, and C4) were exposed to load with an eccentricity of (e1=45mm).

There are four columns in the second group as well (C5 to C8). Except the eccentricity value (e2=75mm), this group uses 75 mm, and the second group's test process parameters are the same as those of the first one.

3-2-4 Test Setup.

In this experiment, all specimens were subjected to unidirectional axial loading (other than self-weight) at the age of 28 days. The loading was applied with an electrohydraulic testing machine of 400 kN capacity, as shown in plate (3-1). The columns were tested until failure under load control conditions. The loading setup for the specimens utilized in this study is shown in figure (3-3). For the eccentric loading, a high-strength steel pin attached with a bearing plate (240×120) mm and a thick steel plate of 20 mm was placed at the top and bottom ends of the column to produce combined bending and axial loading effects. A thin layer of plaster of Paris was also applied on all columns to give a smooth and level surface for uniform distribution of load during the test. Two LVDTs with an accuracy of 0.001 mm per deviation were installed vertically on two opposite faces of the column and at the mid-height of the column to measure the lateral deformations of the specimens for each load increment. The axial displacement of the columns was measured by another LVDT of the same specifications at the lower part of the columns along the vertical centerline of specimens, as illustrated in Figure (3-3). For direct and full-field strain of columns, the Digital Image Correlation (DIC) technique is used. To guarantee that the analysis software can realize the positions of relating subsets on the deformed surface (the spacing between both the sample and the camera was 1500 mm), the area of interest must have a high contrast random pattern, while the light intensity must be stable to maintain a reasonable consistent level of overall way of comparison **[53]**.

Plate (3-1): Hydraulic testing Machine: a - Test setup, supports, and load application mechanism; b- Computer recording of the sample's structural behavior at each level of loading; (c and d) - DIC analysis.

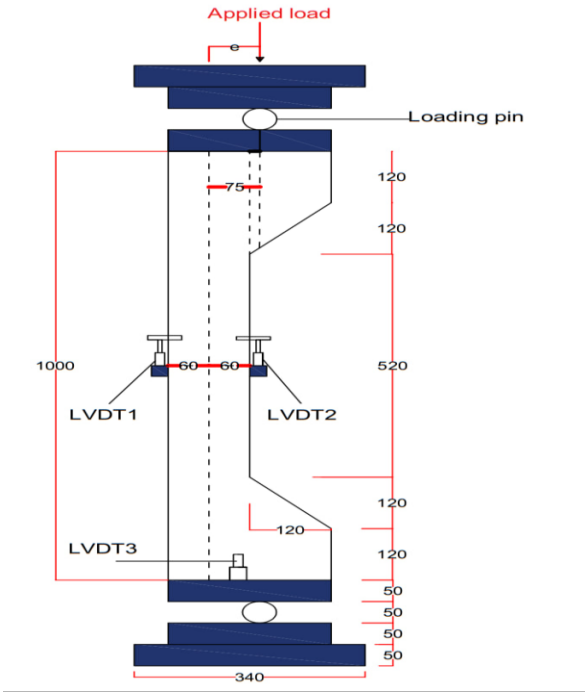

Figure (3-3): The loading setup for eccentric axial loading of columns. The dial gauges 1 and 2 were installed for lateral deformation, and 3 for axial deformation measurements.

3-3 Properties of Construction Materials

Knowing the properties and features of the constituent materials is crucial because concrete is a composite material made up of many individual components, including gravel, sand, water, cement, and admixtures. Strict guidelines were created for the selection of materials, control, and ingredient proportion in order to assure proper production of concrete. The sources of the materials, chemical makeups, and physical characteristics of the materials employed in this experimental study are explained in more detail, as shown in the following subsections. These materials' principal characteristics are as follows:

3-3-1 Cement

All types of concrete for the column models and samples were cast using ordinary Portland cement (type 1) throughout the process of the experiment. Table (3-3) lists the chemical and physical characteristics. The characteristics of normal

Portland cement were tested in accordance with Iraqi specification **[54]**. The chemical and mechanical properties of the cement used were tested at the university of Babylon's construction material and environmental laboratories.

Table (3-3): Chemical properties of cement.

Chemical Test Results			
Oxide		**Test Results**	**Limits of UQS No.5:1984**
Lime	Cao%	62.41	…….
Silica	Soi%	20.88	…….
Alumina	Al2O3%	4.06	……
Iron oxide	Fe2O3%	5.40	……..
Magnesia	MgO%	1.60	≤ 5%
Sulfate	SO3(%)	1.19	if C3A < 5% ≤ 2.5%
Free Lime (%)	Free Cao	0.84	≤ (4.00%)
Loss of Ignition. (%)	L.O. I	2.68	≤ (4.00%)
Insoluble residue. (%)	I.R	0.56	≤ (1.50%)
Lime Saturation Factor	L.S. F	0.91	0.66 to 1.02
	M.S	2.21	
	M.A	0.75	
Main Compounds			
C3S%		53.57	…….
C2S%		19.45	…….
C3S%		1.62	……
C4AF%		16.43	……
Physical Test Results			
Oxide		**Test Results**	**Limits of IQS No,5:1984**
Initial setup time (hours: minutes)		02:23	>00:45(hour: in.)
Fineness (empty) m2/kg		03:25	≤10:00(hour: in.)
Fineness(blain) in m^2/kg		326	>250 m^2/kg
Compressive strength (MPa)	**3 days**		>15.00 MPa
	7 days	20.33	

3-3-2 Fine Aggregate (Sand).

For this investigation's concrete mixtures, natural sand was employed. The nominal maximum size of the fine aggregate used in concrete is 4.75 mm, and it features rounded particles with a fineness modulus about (3.03) and a smooth texture. For fine particles that meet Iraqi requirements, see tables (3-4) [**55]**. Table (3-5) provides a list of the fine aggregate's physical and chemical characteristics. Fine aggregate has been tested at the university of Babylon in the construction material and environmental laboratories of the civil engineering department.

Table (3-4): Sieve analysis of sand.

Sieve size (mm)	Passing %	
	Sand (%)	Limit of IQS No. 45/1984 for Grade No. (2)
10	100	100
4.75	100	90-100
2.36	94.85	75-100
1.18	86.6	55-90
0.6	50.11	35-59
0.3	28.15	8-30
0.15	7.22	0-10

Table (3-5): Physical and chemical properties of fine aggregate.

Property	Test Results	IQS No. 45/1984 for Grade No. (2)
Specific gravity	2.65	--------
Fineness modulus	3.03	--------
Materials finer than sieve 75 μm %	2.7	≤ 5
Sulfate content SO3(%)	0.23	≤ (0.5)

3-3-3 Coarse Aggregate (Gravel)

Concrete was made using gravel that was well-graded, rounded, and no larger than 12.5 mm in size. The gravel was passed through a sieve (12.5 mm) to remove the oversize, washed with water several times, and then allowed to dry. The sieve analysis of aggregate satisfied the requirements of Iraqi specification **[55]** as

presented in table (3-6). The physical and chemical properties matched the Iraqi standard **[55]** are shown in table (3-7).

Table (3-6): Sieve analysis of gravel.

Sieve size (mm)	Passing ratio %	
	Gravel (%)	Limit of IQS No. 45/1984 for Grade No. (2)
12.5	100	90-100
10	94.44	90-100
9.5	94.44	75-100
4.75	4.04	0-10

Table (3-7): Physical and chemical properties of coarse aggregate.

Property	Test Results	IQS No. 45/1984 for Grade No. (2)
Specific gravity	2.65	--------
Absorption %	0.75	≤ 5
Sulfate content SO3(%)	0.23	≤ (0.5)

3-3-4 Waste Tires Rubber

Rubber industry and tire company / Al-Najaf tire rubber is free of steel wires and rubber fibers, with different size of (0.15-0.18) mm, (1.8-2.36) mm, (2.36-4.75) mm, the crumb rubber grade from 0.15 mm to 4.75 mm was used instead of fine aggregate. Figure (3-4) shows the different size of rubbers. The chemical composition and physical characteristics are presented in table (3–8). The general company for rubber industries and tires/Al-Najaf conducted physical and chemical analyses.

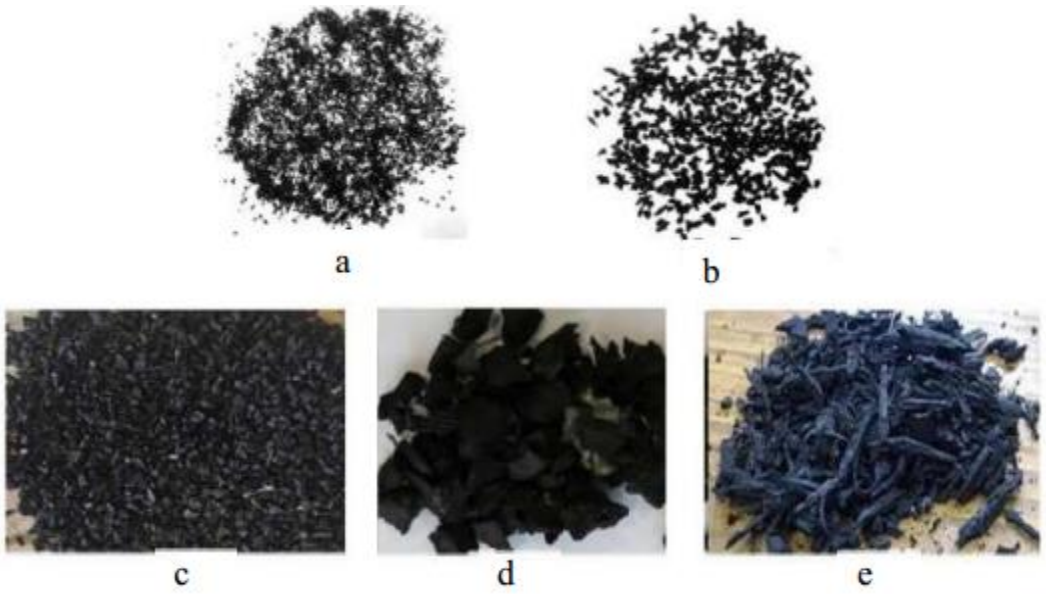

Figure (3-4): Available waste tire rubber in Iraq: a-Ground crumb rubber (0.15-.18) mm; b-Crumb rubber (1-2.36) mm; c-Crumb rubber (2.36- 4.75) mm; d-Chip rubber (4.75-10) mm; e-Rubber fibers.

Table (3-8): Chemical and physical properties of waste tires.

Chemical composition		Physical properties	
Major rubber components	Results	Properties	Results
Acetone extract	10	Fines modulus	3.15
Rubber hydrocarbon	25	Specific gravity	1.78
Carbon black content	30	Water absorption	2%
Natural rubber content	31		
Ash content	4		

The grading of crumb rubber is shown in Tables (3-9). After eliminating all rubber fibers, sieve test of the rubber particles was undertaken to guarantee that the same gradation of fine aggregates is used within the limitations of **IQS [55]**. Sieve analysis was conducted in the civil engineering laboratory at university of Babylon.

Table (3-9): Grading of the crumb rubber and fine aggregate used for rubberized concrete.

Sieves size (mm)	Passing Percentage of crumb rubber.	Passing Percentage of fine aggregate%	Limits of (IQS. No. 45/1984) (zone 2)	
			Max. Limit	Min. Limit
10	100	100	100	100
4.75	94	100	100	90
2.36	82	94.85	100	75
1.18	66	86.6	90	55
0.6	52	50.11	59	35
0.3	20	28.15	30	8
0.15	5	7.22	10	0

3-3-5 Water

Washing rubber and coarse aggregate, casting, and curing concrete samples were all undertaken with tap water.

3-3-6 Steel Reinforcing Bars

In this investigation, two sizes of steel reinforcement deformed bars (ø10mm and ø4mm) produced in Ukraine were used10 mm diameter reinforcing bars are utilized as the primary reinforcement, while 4 mm diameter bars are used as ties. Details of the reinforcement of columns is shown in Plate (3-2). The outcomes of tensile testing on steel bars conducted in accordance with the **ASTM Code [56]** are displayed in table (3-10). As stated in plate (3-3), tensile testing was performed in the laboratory of the collage of Materials Engineering at the University of Babylon.

Plate (3-2): Steel reinforcement.

Table (3-10): Details of steel bars.

Nominal diameters (mm)	Measured diameters (mm)	Yield strength f_y, (MPa)	Ultimate strength f_u, (MPa)
4	4.22	575	602
10	9.94	590	632

Plate (3-3): Tensile tests are carried out on steel bars.

3-4 Concrete Mix Design

3-4-1 Mix Proportion of Concrete

Concrete mixes are designed in accordance with **ACI-211.1 [57]**. To get this goal of compression resistance, the main reference mix (NC) with a compression resistance **(fc') of (30 MPa)** was selected and designed. The designed mixture provides a smooth concrete mixing without segregation and good workability for casting. Table (3-11) shows the mix proportions that prepared by Ammar Abd Alammer.

Table (3-11): Details of mixture proportions for the selected concrete mix.

Mix No.	Mix Symbol	Cement (kg/m^3)	Sand (kg/m^3)	Gravel (kg/m^3)	Rubber (kg/m^3)	(w/c) ratio
1	NC	400	700	1056	0	0.52
2	R5	400	665	1056	10.61	0.52
3	R10	400	630	1056	21.21	0.52
4	R15	400	595	1056	31.82	0.52

NC: Normal Concrete, R5: Rubber Concrete with replacing of 5%, R10: Rubber Concrete with replacing of 10%, R15: Rubber Concrete with replacing of 15%.

3-5 Preparation of Test Specimens

3-5-1 Molds Preparation

All the columns' models used in this investigation were cast in steel molds to obtain a column specimen having a cross-section of (120×120 mm) in the middle and a total length of 520 mm. However, the column molds had top and bottom corbel with cross-section (240 mm × 120 mm) to accommodate eccentric loads during test, as shown in Plate (3-4).

Plate (3-4): Preparation of steel Molds.

3-5-2 Casting Equipment

As indicated in table (3-5), the concrete is mixed in this project using a rotary mixer with a capacity of (0.3 m^3). The mixer needs to be maintained clean, moist, and water-free before beginning to mix concrete. Use the mixing technique described below. Put the coarse and fine aggregate and around 20% combined water in a pan mixer. Add the cement and the remaining water after a few revolutions. Finally, rubber was added to mix. The concrete was mixed well when all materials were in the mixer, for 5 min. Groups of cylinders, prisms, and cubes were made for each batch of concrete throughout the casting process in order to test the concrete's strength and other mechanical parameters as shown in plate (3-6).

Plate (3-5): Mixing equipment's.

Plate (3-6): Groups of cylinders, prism and cubes for each batch.

3-5-3 Casting of Specimens

Eight steel molds that were devised and made for casting the specimens required the preparation and weighing of the chosen materials before the casting. The internal surfaces of the cubes and cylinders should be properly cleaned and oiled to avoid the concrete adhering once it has dried. The steel formwork is then horizontally positioned inside the lattice assemblies, each steel cage (for support),

and secured. Make sure the main rod of the column is covered by inserting the plastic spacers as illustrated in plate (3-7).

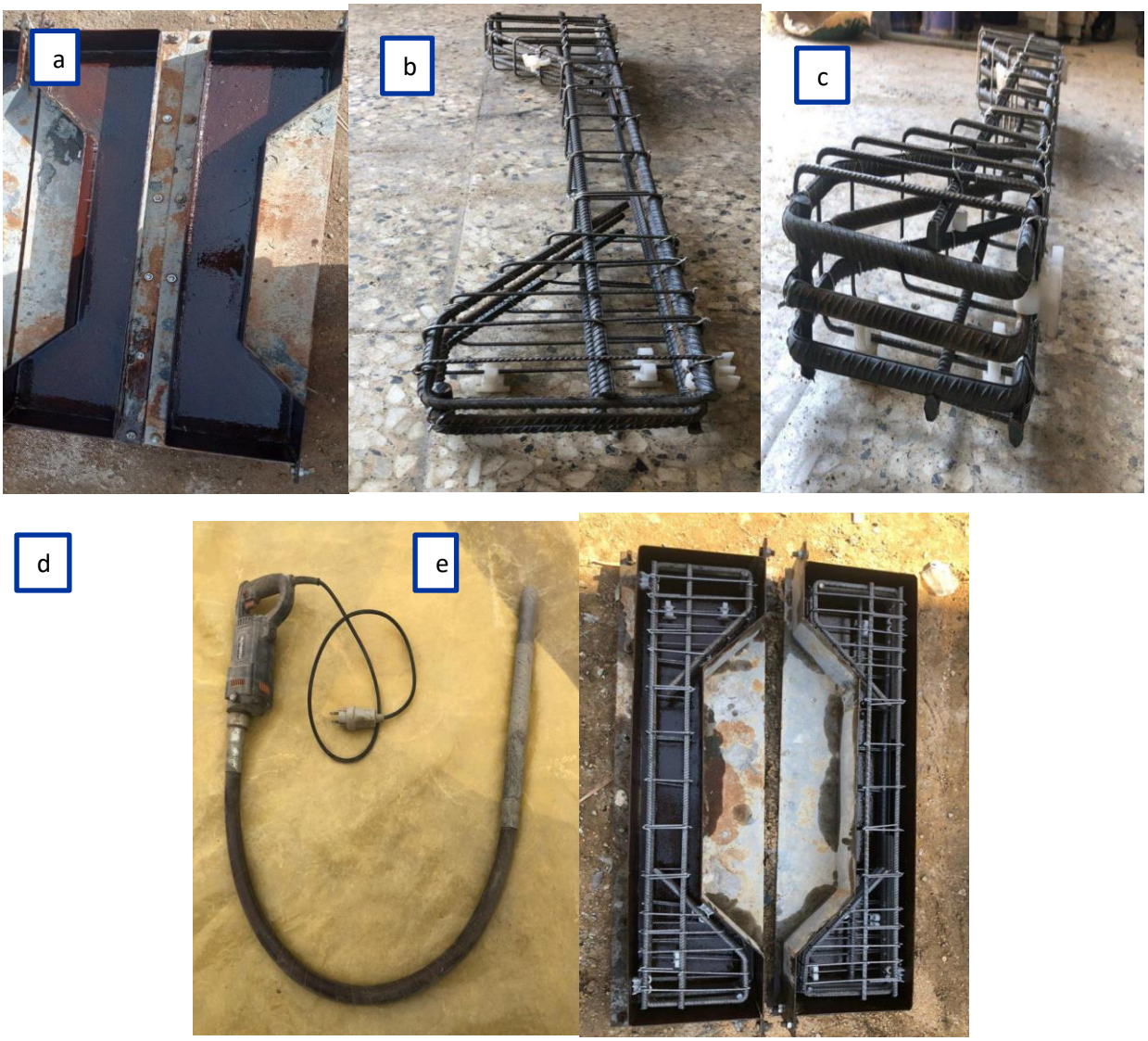

Plate (3-7): Preparation of test specimens. (a)Preparation of steel molds. (b) Preparation of reinforcing steel. (c) Spacer's configuration. (d) Vibration apparatus. (e) Assemblage the molds with reinforcement mesh

3-5-4 Casting Procedure

The structures laboratory of the civil engineering department at Babylon university was where the samples were cast. Before putting the reinforcement cage inside the formwork, the inner faces of the steel formwork were oiled to ensure

ease of demolding. The concrete was put into each mold in a single layer, compacted, and vibrated with an internal vibrator. The number of mix was four with four steel molds.

Following casting, the samples were made up of three 150 x 150 x 150 mm cubes, three 100 mm diameter by 200 mm long cylindrical blocks, and three hybrid prisms with size 100 mm x 400 mm. Depending on the number of layers and rebars, standard methods are used to compact normal concrete with cubic and cylindrical formwork. Use a hand trowel to smooth the standard concrete surface after it has been poured, as shown in plate (3-8).

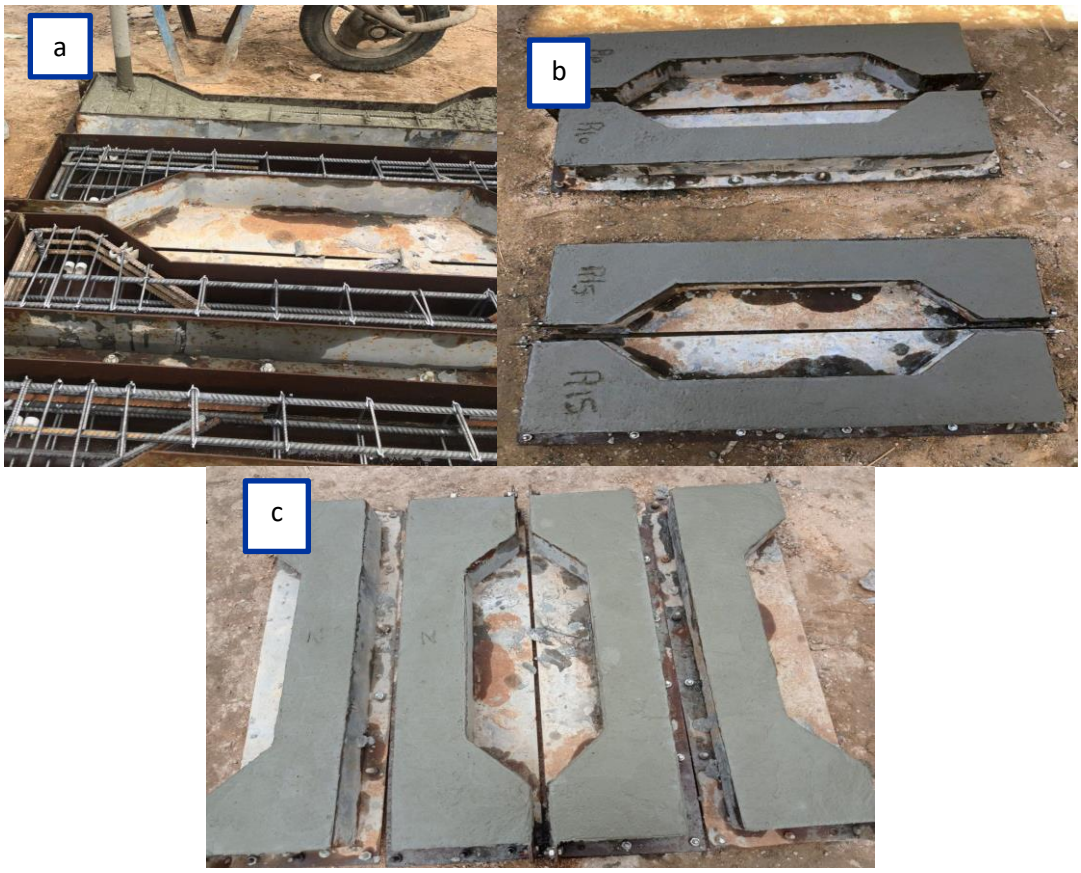

Plate (3-8): The different stages of the casting process. (a) Vibrating concrete. (b) Casting specimens. (C) Specimens after demolding.

3-5-5 Curing

Then, all samples covered by nylon sheets to avoid water evaporation and lifted until they were removed from their mold after one day, and kept saturated in water tanks until the age of 28 days according to the age of the test. After curing time, the samples were removed from the water and prepared for testing according to the specifications of each test, as specified in section 3.6. The curing of test specimens is depicted in Plate (3-9).

Plate (3-9): Curing of column specimens.

3-6 Fresh and Hardened Tests

3-6-1 Workability (Slump Tests)

The following test was used to measure the workability of normal and rubberized concrete in accordance with American specification **[56]**, as shown in plate (3-10).

Plate (3-10): Slump test for normal concrete according to Iraqi specification.

3-6-2 Compressive Strength Test

The test was carried out at the ages of 7 and 28 days via cubic samples of 150× 150× 150 mm for each mixture, according to British specification **[59]**. As shown in plate (3-11), the experiment was conducted by using a 400 kN capacity compressive machine. A constant rate of 18 MPa per minute of load is applied constantly, gradually increasing, and maintained until failure. Compressive strength was assessed using the average of three specimens and the following equations, **[59]:**

$fc' = 0.8 * fc$ …… (3.1)

$fc = P/A$ …… (3.2)

Where:

"fc': Compression resistance (MPa) according to American Standard."

"fc: Compression resistance (MPa) according to British Standard."

"P: Applied force (N); A: Area (mm^2)"

Plate (3-11): Hydraulic compression machine.

3-6-3 Splitting Tensile Strength Test

This test was undertaken in accordance with ASTM standard **[60]** at 28 days via cylinder (200×100) mm. As shown in Plate (3-12), distribute the press's weight evenly across the cylinder's top and bottom, it was necessary to position the cylinder horizontally between two wooden plates. The average of three cylinders samples is used to evaluate the splitting tensile resistance and was calculated by using equation (3.3), **[60]**:

"$ft = 2P/\pi LD$" … (3.3)

Where:

"ft = Tensile stress (MPa)".

"P = Total failure load (N)".

"D = Section diameter (m)".

"L = Section height of(m)".

Plate (3-12): Splitting tensile test.

3-6-4 Modulus of Rupture

The test of flexural stress was carried out according to ASTM standard **[61]** at 28 days using a prism with dimensions of (100×100×400) mm, as shown in Plate (3-13). The test was conducted using a flexural machine with a 150 kN capacity and two-point loads. the average of three samples used to calculate the rupture modulus in equation (3.4), **[61]**:

"$fr = 2PL/bd^2$ " … (3.4)

"fr = Flexural stress (MPa)".

"P = Failure load (N)".

"L = Supports distance (m)".

"b = Section width (m)".

"d = Section depth (m)".

Plate (3-13): Flexural strength test.

Chapter four
Results and Discussions

4-1 Introduction

This chapter, which is divided into two parts, will show the results and discussions from the experimental test performed on reinforced concrete column samples (normal and rubberized). The first part is concerned with generating successful structural mixtures including various percentages of scrap tire rubber by inspecting and assessing fresh properties as well as hardened characteristics (the resistance of compression, splitting tensile, and flexural).

The results of six rubberized reinforced concrete rectangular columns specimens and two ordinary reinforced concrete rectangular columns specimens are provided in the second part. Results are discussed in terms of crack modes, failure loads and modes, deflection relationships, ductility, specimen stiffness and strain distribution.

4-2 Fresh Concrete Properties

4-2-1 Workability (Slump Test)

When compared to normal concrete, RuC has a more workability. The slump value of RuC increases as the percentage of aggregates replaced by rubber increases. The workability of four concrete mixtures was assessed in this study by examining the average result of standard slump test values, as shown in Table (4-1) and Plate (4-1). All of the mixes were easy to deal with, and the differences between them were small. According to the results, increasing the volumetric ratio

of rubber replacement with natural aggregate increased the workability. Where the result of the mix F10 shows a 10% increment in slump value. Although the poor slump may be related to the small particle size of RA, the reason for the poor processability can be explained by the higher water absorption of rubber compared to sand.

Table (4-1): The slump values for different mixes.

Items	Mix type	Slump Value (cm)	%Difference.
1	N	9	0
2	F5	9	0
3	F10	10	10
4	F15	10	10
Notes: The Slump test was performed according to (ASTM 143M-12).			

Plate (4-1): The slump test.

4-3 Hardened Concrete Properties

To predict the characteristics of normal and rubberized concrete requires a thorough understanding of mechanical characteristics. As a result, hardened characteristic tests such as compression resistance, tensile splitting, and rupture modules have been carried out. As a result, after the curing period, various tests are performed on control samples (cubes, cylinders, and prisms) to determine the mechanical properties of hardened normal and rubberized concrete for all specimens. Each value is calculated using the mean of three samples to reduce prediction error within each observation, as listed in Table (4-2). In addition, the cylinder compressive strength (fć) predicted according to the formula (BS 8110-1:1997) is shown in Table (4-3):

$$f\acute{c}\ (NSC) = 0.8 * f\ cu \qquad \ldots\ldots (4.1)$$

Table (4-2): Hardened characteristic test.

Mix type	Compressive strength fcu (MPa)			Splitting Tensile Strength fsp (MPa)			Modules of rupture fr (MPa)		
	Sample 1	Sample 2	Sample 3	Sample 1	Sample 2	Sample 3	Sample 1	Sample 2	Sample 3
N	47.15	47.09	50.09	2.32	3.72	3.14	4.03	4.39	4.12
R5	48.53	47.68	49.94	2.90	3.90	3.30	4.94	4.59	4.02
R10	36.59	38.19	37.96	2.53	2.99	1.55	4.28	4.08	4.30
R15	31.39	32.25	32.32	1.79	2.09	2.71	3.82	4.39	4.09

4-3-1 Compressive Strength

Table (4-3) summarizes the average unidirectional compressive strengths of smooth and rubberized concrete calculated from the three test cubes shown in Figure (4-1) and Table (4-2). The results in Table (4-3) show that increasing the rubber replacement rate significantly decreases the compressive strength value of the rubber-concrete mixture. The one-sided compressive strength of rubberized concrete decreases as the number of rubber particles in the mixture increases, according to previous studies **[6][7]**. Compared with the normal concrete mix (N), the compressive strength value of the sample with 15% rubber chips instead of fine aggregate (F15) decreased by about 33.49%. The size, shape, mechanical properties and replacement percentage of aggregates affect the overall strength of rubberized concrete **[9]**. In some studies, the reason why the compressive strength of rubberized concrete tends to decrease with increasing rubber content has been proposed in different ways. One of the main reasons for this type of degradation is the very weak adhesion between rubber and mortar in concrete, which act as voids in the concrete matrix, reducing its density **[9][10]**. The smooth surface of the rubber ensures limited adhesion of the mortar. Another reason for the strength reduction is that when RuC is compressed, tensile stress builds up along the surface rubber particles and associated cement slurries, leading to early cracking of RuC. **[11]**.

Table (4-3): The average of three compressive strength results for the tested mixes at 28 days.

item	Mix type	Compressive strength (fc') (MPa)	
		At 28 Days	% Difference
1	N	38.48	…..
2	F5	38.96	1.23
3	F10	30.06	-21.88
4	F15	25.59	-33.49

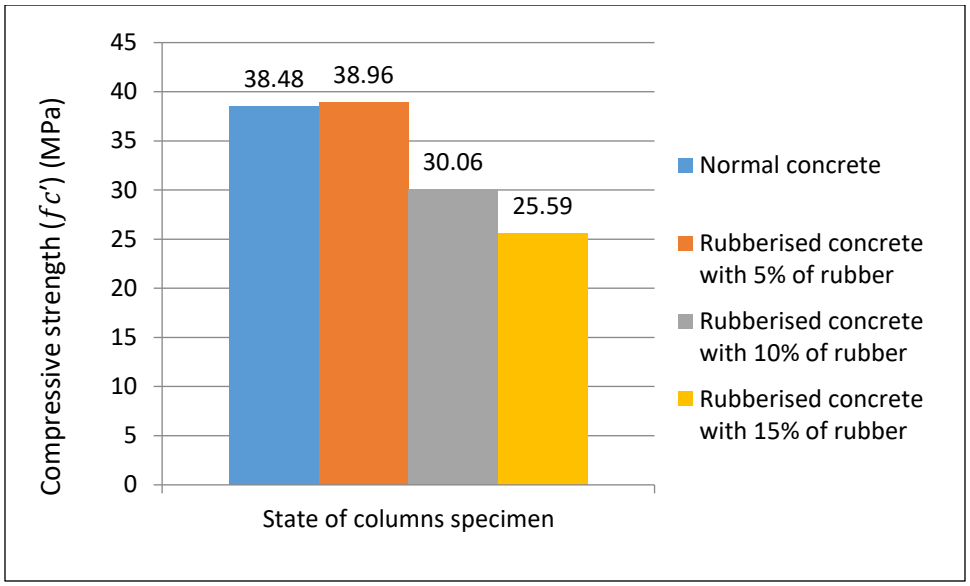

Figure (4-1): Compressive strength results of the mixes.

Plate (4-2): Test of concrete cubes (Cube of R10 mixture).

4-3-2 Splitting Tensile Strength

In general, the results of the four mixtures in Table (4-4) and Figure (4-2) revealed that as the rubber replacement ratio increased, the tensile resistance values decreased. A real split of the specimen occurred in the failure mode of the reference mix (N), when the cylinder was split into two halves (brittle failure). This failure mode is also seen in other rubber-based mixtures (crumb rubber). Instead of being brittle, rubberized concrete mixes failed gradually, as shown in Plate (4-3). The tensile resistance values of samples containing 15% crumb rubber instead of crumb aggregate (F15) decreased by about 28.10 % compared to normal concrete mixes (N), where the F10 samples showed a reduction of 23.20 % in tensile resistance. These findings are in line with earlier research. Akinyele et al. **[13]** used 4% crumb rubber as fine aggregate replacement in concrete and found a 41% loss in tensile strength and a 58% reduction when 16% crumb rubber was used. As a result, increased RA resulted in decreased strength. Researchers have previously proposed several explanations for this phenomenon. The overall tensile strength of RuC is lower than that of NC because the surface where RA and mortar contact act as microcracks and RA as voids **[9]**.

Table (4-4): The average of three splitting tensile strength results.

item	Specimens	Splitting tensile stress (ft) (MPa)	%Difference
1	N	3.06	…..
2	F5	3.37	9.19
3	F10	2.35	-23.20
4	F15	2.20	-28.10

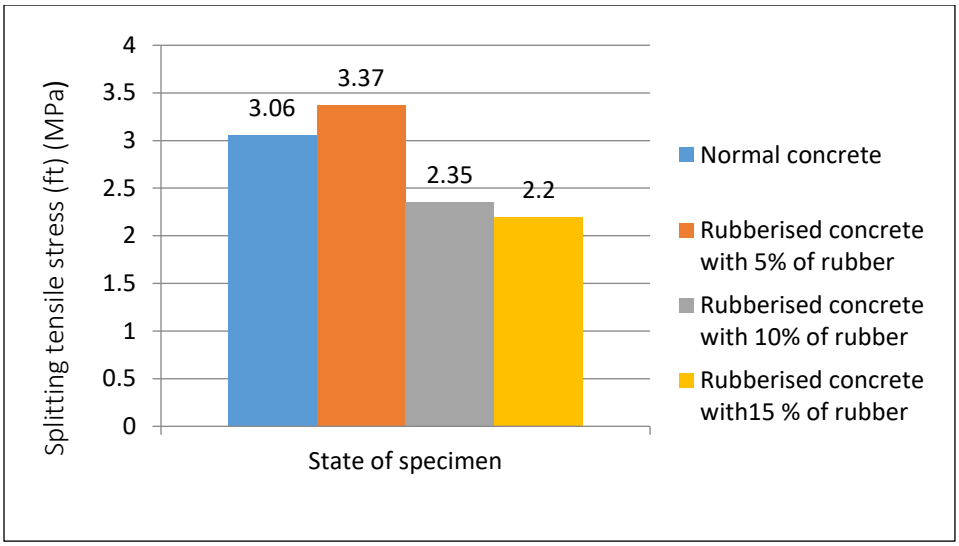

Figure (4-2): Tensile strength results of the mixes.

Plate (4-3): Splitting tensile test samples R15 after failure.

4-3-3 Modulus of Rupture

The result of the flexural strength test for four various concrete mixtures are shown in Table (4-5) and Figure (4-3). This test was performed in accordance with **ASTM C78**, utilizing a prism (10x10x40) cm. Rubber particles were added, which lowered the flexural strength. The reference mix's (N) failure mode indicates that the prism failed in the specimen in the center. This related to the mix's uniformity. Because of the non-uniform distribution of rubber in the mixes including rubber particles, failure mode occurred in the range of internal one third of the specimen, especially in F15 as indicated in Plate (4-4). The flexural resistance values of samples contain 5% crumb rubber instead of fine aggregate (F5) increased about 7.52% than normal concrete mixes (N), where the result of the F15 samples shows reduction of the flexural resistance value of 1.91% and this reduction is more than other mixes contain rubber instead of fine aggregate.

Table (4-5): Result of flexural tensile strength at 28 days.

item	Specimens	Modulus of rupture (fr) (MPa)	%Difference
1	N	4.18	0.00
2	F5	4.52	7.52
3	F10	4.22	0.95
4	F15	4.10	-1.91

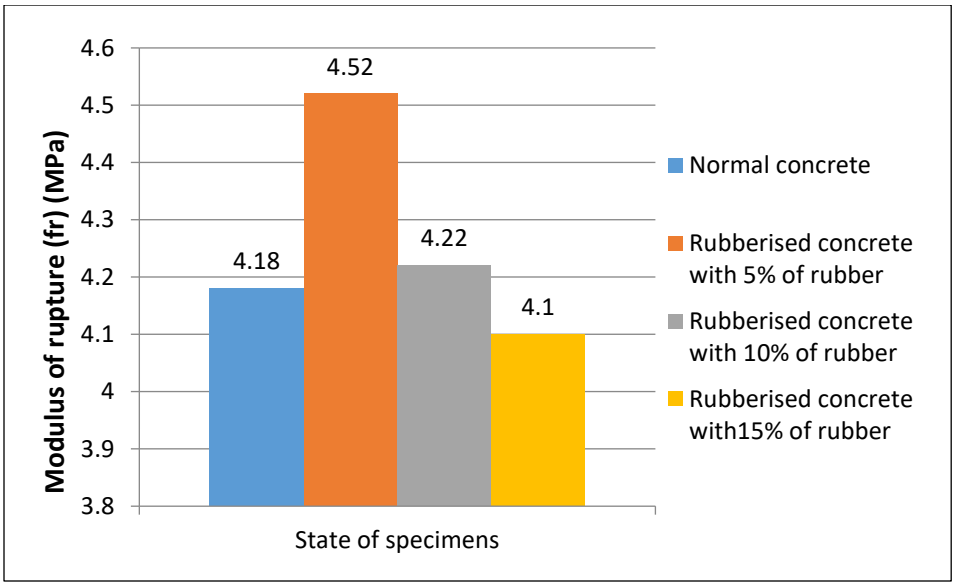

Figure (4-3): Flexural Strength Results for Mixtures.

Plate (4-4): Modulus of rupture result of specimens.

4-4 Column Test Results

The behaviors of eight reinforced concrete columns are represented and discussed in this section. All columns have the same cross-sectional area and steel reinforcement. The results of six rubberized reinforced normal concrete square columns specimens and two ordinary reinforced concrete square columns specimens are provided in this study. To evaluate the effect of rubber addition and the effect of applied load, the results for each column group were compared. Each group was then compared to the other to analyze the effect of increasing eccentricity. The fracture mode of the column, the bearing capacity of the fracture load, the initial crack load, the relationship between the load and the lateral deflection, the axial deformation and the test results of the specimen are shown in Table (4-6).

Table (4-6): Results of all tested Columns in the experiments.

Group No.	Symbol.	Specimen Symbol	Cracking Load Pcr(kN)	Ultimate Load Pu(kN)	Displacement at Ultimate Load Δ**s***(mm)	
					Axial	Lateral
Group1	C1	G1N	90	274.36	6.32	6.78
	C2	G1F5	90	258.06	6.82	5.95
	C3	G1F10	120	217.48	6.23	6.33
	C4	G1F15	92	204.53	5.34	6.64
Group2	C5	G2N	25	159.07	6.78	7.64
	C6	G2F5	38	153.76	6.78	6.79
	C7	G2F10	26	138.06	7.33	7.61
	C8	G2F15	31	138.58	7.76	8.59

4-4-1 Cracking and Ultimate Loads and Failure Modes

The same cracks pattern and failure mode were exhibited for the two samples' faces of each tested columns. The initial crack started halfway through the specimen and then broke again at almost (33–45) % of the maximum load in the contact area between the corbel and the column. On the other hand, the crack length and width increased with the increase of bending and oblique cracks and the stress applied to the specimen during the test. In the end, it failed unexpectedly through a diagonal crack. Tables (4-6) summarize the 8-column test results and breaking loads for each sample provided in the next subsection.

❖ *Control Column G1N*

The specimen consisted of ordinary reinforced concrete without rubber, loaded with eccentricity (e=45 mm). Under axial load (90 kN), the first visible crack is a horizontal crack on the tension side, which occurs halfway through the column. Under axial load (93 kN), the second visible crack appeared at 10 mm from the column height. Under axial load (95 kN), a third visible crack formed 5 mm from the end of the corbel. As shown in Table (4-5), the compression side rapidly fails under load (274.36 kN), the shell is delaminated, and the longitudinal reinforcement is buckled.

Plate (4-5): Failure mode and crack mode of column specimen G1N.

❖ *Specimen G1F5*

This specimen was made from rubberized reinforced concrete with 5% rubber replaced by fine aggregate with the load eccentricity (e=45mm). At axial load (90 kN), the first apparent crack appeared as a horizontal crack 10 mm from mid-height. The steel reinforcement then crashed and buckled under axial stress (193 kN). At load (258.06 kN), the failure occurred progressively on the compression side, as shown in Plate (4-6). There was no reduction in cracking load as compared to the control specimen C1(G1N), but there was a 5.94% reduction in the ultimate capacity.

Plate (4-6): Column specimen G1F5 failure mode and crack mode.

❖ *Specimen G1F10*

This specimen was made from rubberized reinforced concrete with 10% rubber replacement and the load eccentricity (e=45 mm). At axial load (120 kN), the first noticeable cracking appeared as a horizontally crack at the column's mid-height. Under the axial load (131kN), the second obvious crack is a horizontal crack that appears on the half-tension side of the column. When loaded (217.48 kN), the thrust side gradually failed, as shown in plate (4-7). Compared to the control samples C1 (G1N) and C2 (G1F5), the cracking load was increased by about (25%), while the ultimate load was decreased by about 20.73% and 15.72%, respectively.

Plate (4-7): Failure mode and crack mode of column sample G1F10.

❖ *Specimen G1F15*

This specimen was made from rubberized reinforced concrete with 15 % of the rubber replacement and the load eccentricity (e=45mm). Under an axial force (92 kN), the first visible cracks appeared in the horizontal cracks in the middle of the column. Under axial stress (100 kN), the second visible crack is a horizontal crack that occurs on the tension side 15mm from the center of the column. Under the axial load (148 KN), a third obvious crack appeared in the middle of the bracket. When loaded (204.5 kN), the compression side gradually fails, as shown in plate (4-8). Compared with samples C1 (G1N) and C2 (C1F5), the crack load increased by about 2.17%; but compared with sample C3 (G1F10), the crack load decreased by about 23.33%. Compared to the other modes (C1, C2, and C3), the ultimate capacity is smaller because this mode has a higher exchange rate.

Plate (4-8): Failure Mode and Crack Mode of Column G1F15.

❖ Control Column G2N

This specimen has a load eccentricity of (e=75mm) and is composed of normal concrete. The column's tension side experienced a horizontal crack that initially became obvious at around mid-height when an axial force was applied (25 kN). The second visible crack is a horizontal crack 10 mm from the top and bottom of the first crack under axial load (31 kN). The third visible crack occurred 60 mm from the end corbel with an axial load (48 kN). As shown in plate (4-9), the compression side failed under load (159.07 kN), and increasing the load in the final stage resulted in more cracks and displacements than in the earlier stage. Compared to control sample C1 (G1N), cracking and ultimate strength were reduced by approximately 72.22% and 42.02%, respectively.

Plate (4-9): Failure mode and crack mode of column specimen G2N.

❖ Specimen G2F5

This specimen was rubberized reinforced concrete column with 5% of rubber replacement by fine aggregate with load eccentricity (e=75mm). The axial load (38 kN) caused the first crack to become visible. The second visible crack is a horizontal crack that appears on the tension side at 10 mm from the center of the column under axial load (41 kN), while the third visible crack appears at the end of the corbel below. Axial load (41 kN), failure gradually occurred on the compression side, as shown in plate (4-10). The initial crack and ultimate load capacity of Group 1 specimen G1F5 decreased by about 57.77% and 40.41%, respectively. Compared with the control sample of the C5 group (G2N), the cracking load increased by 34.21%, although the ultimate load decreased by about 3.34%.

Plate (4-10): Failure Mode and Crack Mode of Column G2F5.

❖ Specimen G2F10

This specimen was rubberized reinforced concrete column with 10% of rubber replacement by fine aggregate with load eccentricity (e=75mm). At an axial load (26 kN), the first crack became visible at the column's midpoint. The second apparent crack is a horizontal crack that occurred at an axial load (31 kN) 15 mm away from the column's midpoint on the tension side. At the end of the corbel under axial load (41 kN), the third obvious crack occurred. Expansion, of the cracks at axial load (52). Under the load (138.06 kN), the center of the compression column fractured, and then the steel bar buckled, as shown in plate (4-11). The initial crack and ultimate strength of Group 1 sample C3 (G1F10) decreased by about 78.33% and 36.52%, respectively. The ultimate capacity of this group was reduced by 13.21% and 10.21% compared to the control group (G2N and G2F5) of C5 and C6, respectively. The crack load for C5 also increased by

about (3.84) %, and the crack load for C6 decreased by about (31.58) %.

Plate (4-11): Failure Mode and Crack Mode of Column G2F10.

❖ Specimen G2F15

This specimen was rubberized reinforced concrete column with 15% of rubber replacement by fine aggregate with load eccentricity (e=75mm). A horizontal crack that was caused by an axial load (31 kN) first became obvious at the column's midpoint. The column's second apparent crack, a horizontal one, was caused by an axial stress (34 kN) and occurred at mid-height. According to plate (4-12), the failure happened on the compression side in the middle of the column, although under stress (138.29 kN). The initial crack and ultimate load capacity are decreased by around (66.30 % and 32.39 %) compared to specimen C4 (G1F15) for group 1. Compared with the C5, C6, C7 (G2N, G2F5, G2F10) control groups, the cracking load in this group increased by about (19.35, 18.42, 16.13) %, and the ultimate load decreased by about (13, 10), 10.10 and 0.16) %.

Plate (4-12): Column specimen failure mode and crack mode G2F15.

4-4-2 Load-Lateral Displacement

The load and lateral displacement curve of the specimen is shown in Figure (4-4). Four tested column specimens with an eccentricity of (45 mm) included in group G1, which is the first group. For this group, G1N is used as the reference column. It is made of normal concrete (NC). In the construction of the G1F5, G1F10 and G1F15 columns, rubber replaced 5%, 10% and 15% of the volume of ordinary fine aggregate concrete, respectively. The second group (G2), contains four test columns with an eccentricity of 75 mm. Column (G2N) is the reference column for the group. It is made of normal concrete and contains no rubber. The G2F5, G2F10, and G2F15 columns were made of rubberized concrete, with rubber replacing 5%, 10%, and 15% of the fine aggregate volume, respectively. The major goal of this group was to find out how increased eccentricity affects the behavior of rubber-insulated bearings under axial load. As previously stated, the rubber

content was the most important factor in determining the total loading capability of a rubberized concrete column. Figure (4-4) illustrates the load-lateral displacement measured using two LVDTs which were located at both side in the mid-height. The reading of these LVDTs show positive and negative values to refer to in-ward and out-ward deformations. The values of mid-height lateral displacement corresponding to the ultimate load are 6.78mm, 5.95mm, 6.33 mm, 6.64 mm, 7.64 mm, 6.79 mm, 7.61 mm, and 8.59 mm for specimens G1N, G1F5, G1F10, G1F15, G2N, G2F5, G2F10, and G2F15 respectively. Figures (4-5) and (4-6), demonstrate load-lateral displacement for all tested specimens to compare the results of each specimen clearly. It can be seen from this figures that the replacement of fine aggregate with rubber makes a significant influence on the stiffness of specimens, in addition to its effects on the ultimate load.

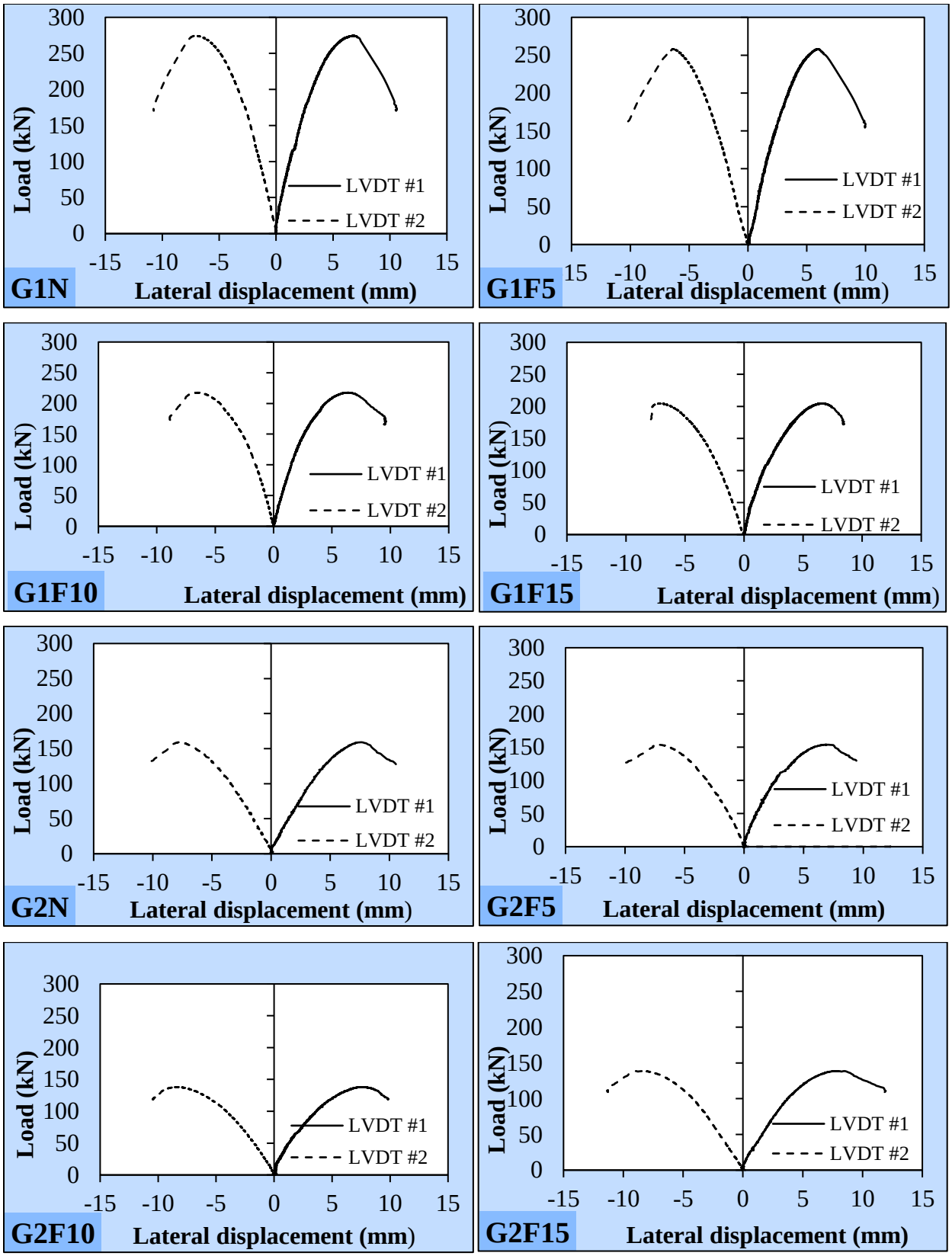

Figure (4-4): Load-Lateral displacement curves for columns C1 to C8.

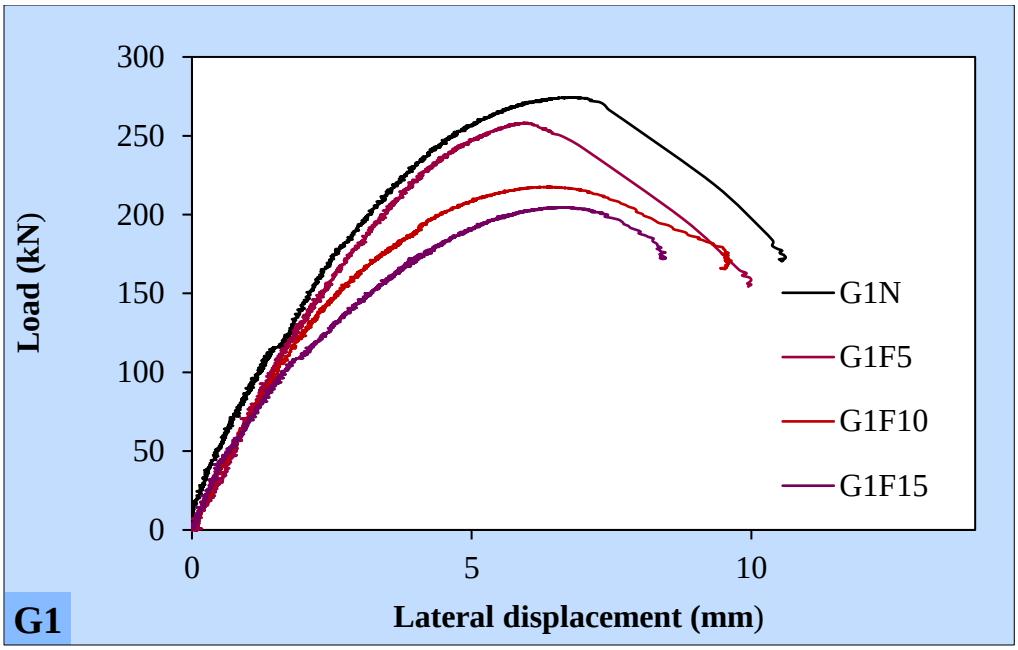

Figure (4-5): Load-Lateral displacement curves for columns Group 1.

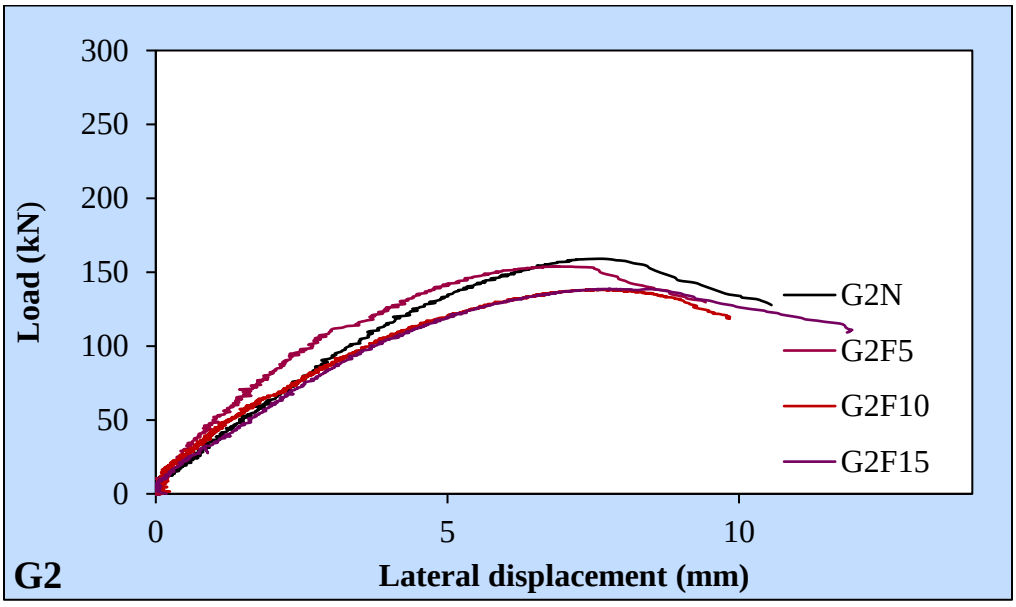

Figure (4-6): Load-Lateral displacement curves for columns Group 2.

4-4-3 Load-Axial Displacement

According to the load-axial displacement curves in Figure (4-7), it can be seen that the general trend was almost the same, with minor differences in the ultimate load and corresponding axial displacement values. These values of axial deflection are 6.32 mm, 6.82 mm, 6.23 mm, and 5.34 mm, 6.78 mm, 6.78 mm, 7.33 mm, and

7.37mm for specimens G1N, G1F5, G1F10, G1F15, G2N, G2F5, G2F10, and G2F15 respectively. Changing the percentage of crushed glue from 0% to 15% causes the axial displacement value to vary according to the breaking load and causes some expansion of the trend.

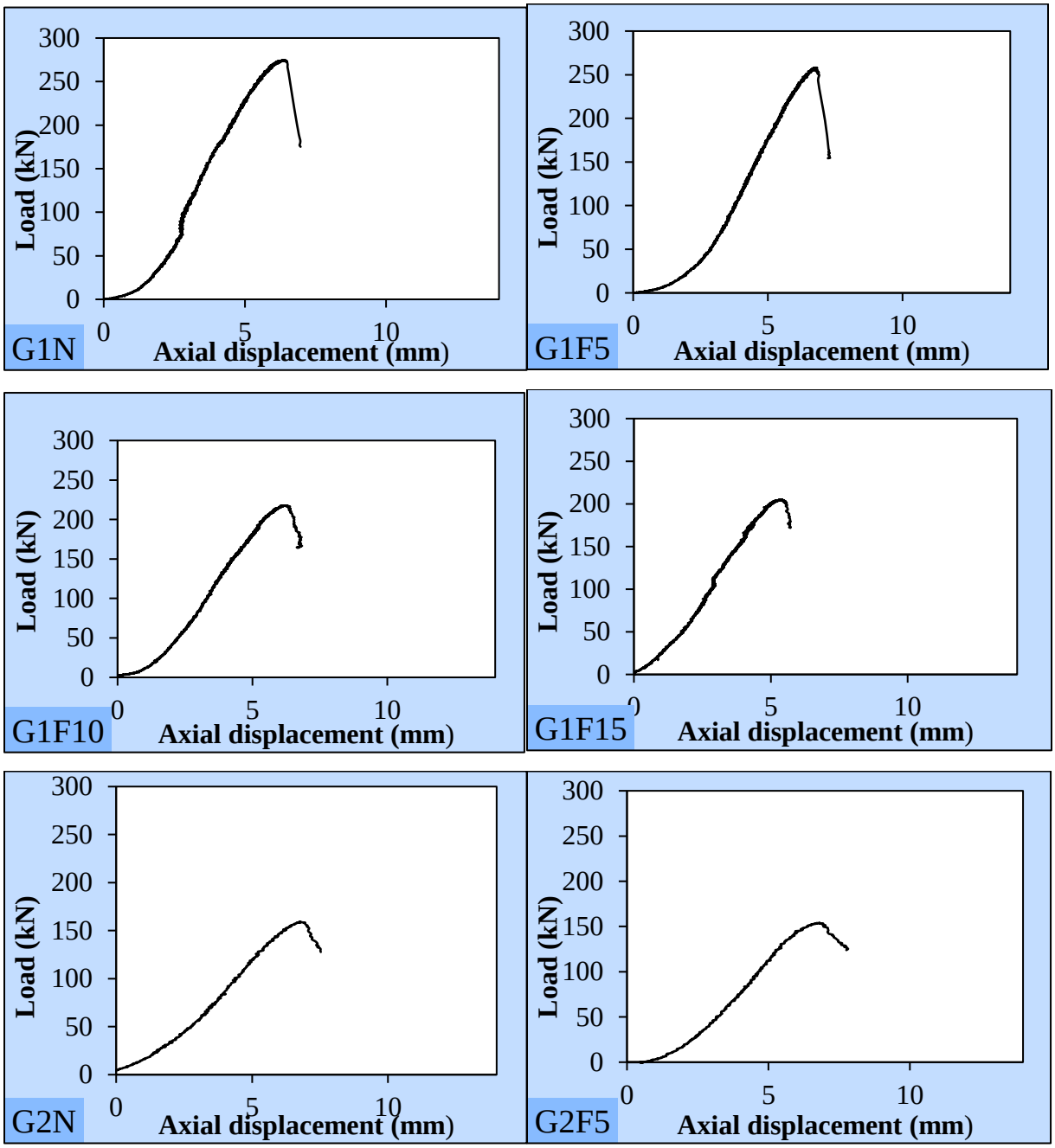

Figure (4-7): Load Axial Displacement Curves for Columns C1 to C8.

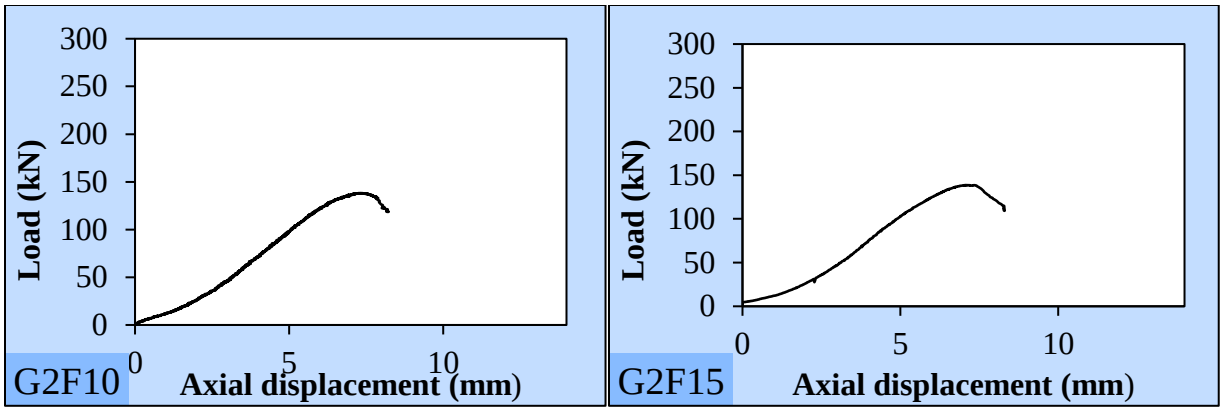

Figure (4-7): Continued.

4-4-4 Ductility

Many researchers have previously looked at the ductility of normal concrete columns, but there have only been a few studies specifically about the ductility of rubberized concrete columns. Elasticity is defined as the energy absorbed by a material before failure. In this study, the vertical or lateral position with the maximum load was removed to use the vertical or lateral displacement during loading to calculate the elastic factor (about 65% of the maximum load) **(Jeffrey, 2003)[77]**.

Table (4-7): Ductility index of tested columns.

Group No.	Specimen Symbol	Service displacement Δs (mm) *		Ultimate displacement Δu (mm)		Ductility ratio **μ**=(Δu/Δs)	
		Axial	Lateral	Axial	Lateral	Axial	Lateral
Group 1	G1N	4.09	2.63	6.32	6.78	1.55	2.57
	G1F5	4.85	2.65	6.82	5.95	1.41	2.24
	G1F10	4.06	2.36	6.23	6.33	1.57	2.68
	G1F15	3.41	2.61	5.34	6.64	1.56	2.54
Group 2	G2N	4.52	3.48	6.78	7.64	1.5	2.19
	G2F5	4.63	2.68	6.78	6.79	1.46	2.53
	G2F10	4.69	3.1	7.33	7.61	1.56	2.45
	G2F15	4.5	3.25	7.37	8.59	1.64	2.64

***Δs== displacement at service load (Ps =0.65 Pu) (Jeffrey, 2003).**

In general, the results of Table (4-7), show a modification in ductility ratio in (axial or lateral) displacement with a percentage of crumb rubber of 5% by around (9.03 and 2.66) % or (12.84 and 13.44) % for specimens (G1F5, and G2F5) with eccentricities of (45 and 75) mm, respectively. For specimens (G1F10, and G2F10) with eccentricity (45 and 75) mm, ductility ratio in (axial or lateral) displacement is increased by about (1.3 and 3.8) % or (4.1 and 10.6) % for specimens loaded with 10% crumb rubber, whereas for specimens loaded with 15% crumb rubber, ductility ratio in (axial or lateral) displacement is increased by about (0.64 and 8.53) % or (4.1 and 10.6) % for specimens (G1F15, and G2F15) with eccentricity (45 and 75) mm, respectively. The ductility index (percentage of specimens ductility/control specimen ductility) for all investigated columns, as given in figure (4-7) and figure (4-8), also reveal that the eccentricity value and rubber content are the most important criteria that influence column ductility behaviour. Ductility of rubber concrete specimens (G2F15) and ductility of conventional concrete specimens (G2N) that used was estimated in the above Table (4-7). As a result, section ductility (G2F15) has improved by 17 % for lateral load at eccentricity 75 mm, and rubber concrete may now be deemed more ductile than normal concrete.

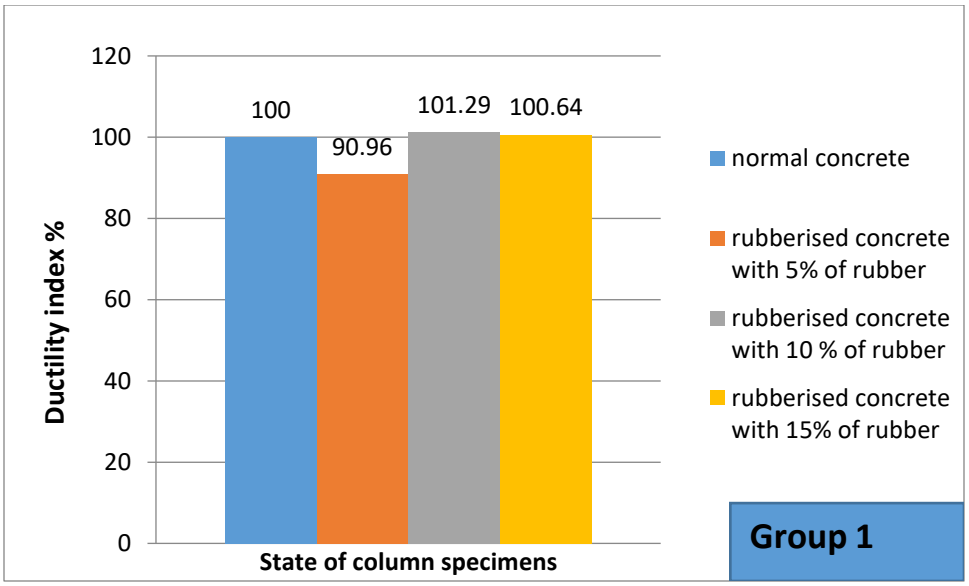

Figure (4-8): Ductility index of tested specimens (G1N, G1F5, G1F10, and G1F15).

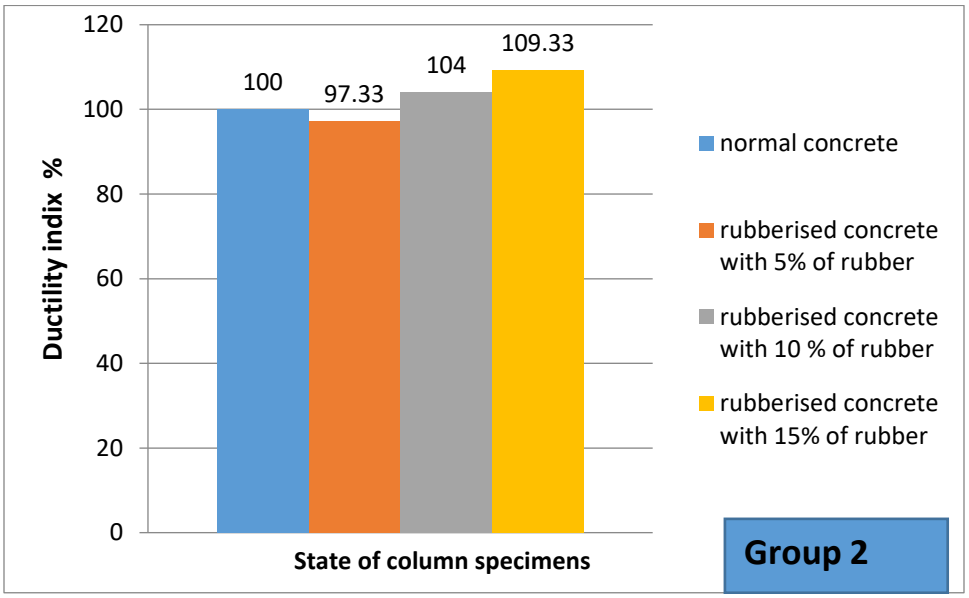

Figure (4-9): Ductility index of tested specimens (G2N, G2F5, G2F10, and G2F15).

The rubberized members generated a relatively soft post-peak response, indicating a more ductile reaction as compared to conventional RC, according to the test results. As a result, determining the effect of this local material behaviour on the overall ductility of members is essential.

4-4-5 Stiffness

The load required to produce a unit of deformation in a part is defined as stiffness. At loads equal to 0.75 times the maximum load, the slope of the secant line plotted on the load-deflection curve can be used as a stiffness criterion **(Muthuswamy and Thirugnanam, 2014)[78]**. as shown in the table (4-8), stiffness is calculated and compared to each group's reference column.

Table (4-8): Stiffness parameter of tested columns.

Group No.	Specimen Symbol (Ci)	0.75 Pu (kN)	Deflection at 0.75Pu (mm)		Stiffness *K* (kN/mm)	
			Axial	Lateral	Axial	Lateral
Group 1	G1N	205.77	4.59	3.13	44.83	65.74
	G1F5	193.545	5.24	3.25	36.94	59.55
	G1F10	163.11	4.59	3.00	35.53	54.37
	G1F15	153.39	3.90	3.30	39.33	46.48
Group 2	G2N	119.30	4.99	4.12	23.91	28.95
	G2F5	115.32	5.08	3.48	22.70	33.14
	G2F10	103.545	5.18	3.75	19.98	27.612
	G2F15	103.94	5.05	3.92	20.58	26.51

"*Δs== displacement at service load (Ps =0.75 Pu) (Jeffrey, 2003)".

The envelope curves shown in Figures (4-10) and (4-11) illustrate the varying stiffness with rubber content and axial load. The stiffness of the rubber surrogate column samples after different loading levels decreased sharply with the increase of loading level, and this decrease in stiffness was accompanied by a decrease in load-bearing capacity. As shown in Table (4-8) and Figures (4-10) and (4-11), stiffness (percentage of specimens stiffness/control specimen stiffness) also decreases with increasing percentage of crumb rubber. After replacement rubber

with fine aggregate specimens with eccentricity (45 and 75 mm), the stiffness in (axial or lateral) displacement of column specimens (G1F5, and G2F5) loaded with a percentage of crumb rubber of 5% fell from (44.83 and 23.91 kN/m) or (65.74 and 28.95 kN/m) of normal concrete specimens (G1N, and G2N) to virtually (36.94 and 22.70 kN/m) or (59.55 and 33.14 kN/m), respectively. While for specimens loaded with 10% of crumb rubber (G1F10, and G2F10), the stiffness in (axial or lateral) displacement decreased with increase in load from (44.83 and 23.91 kN/m) or (65.74 and 28.95 kN/m) of normal concrete specimens (G1N, and G2N) to virtually (35.53 and 19.98 kN/m) or (54.37 and 27.61 kN/m), respectively. For specimens loaded with 15% of crumb rubber (G1F15, and G2F15), the stiffness in (axial or lateral) displacement decreased with increase load and increasing rubber content from (44.83 and 23.91 kN/m) or (65.74 and 28.95 kN/m) of normal 1concrete specimens (G1N, and G2N) to virtually (39.33 and 20.58 kN/m) or (46.48 and 26.51 kN/m), respectively. A comparison of the experimentally determined stiffness of components showed that, as expected, components with higher rubber content had lower stiffness. It can be seen that at different stress levels, the stiffness of the rubber replacement column samples decreases significantly with increasing stress levels. This is believed to be due to the deterioration of the mechanical properties of concrete and rebar, including stress-strain ratio and Young's modulus, as well as chemical changes that increase the permeability and porosity of concrete, mainly resulting in microcracks. material internal structure.

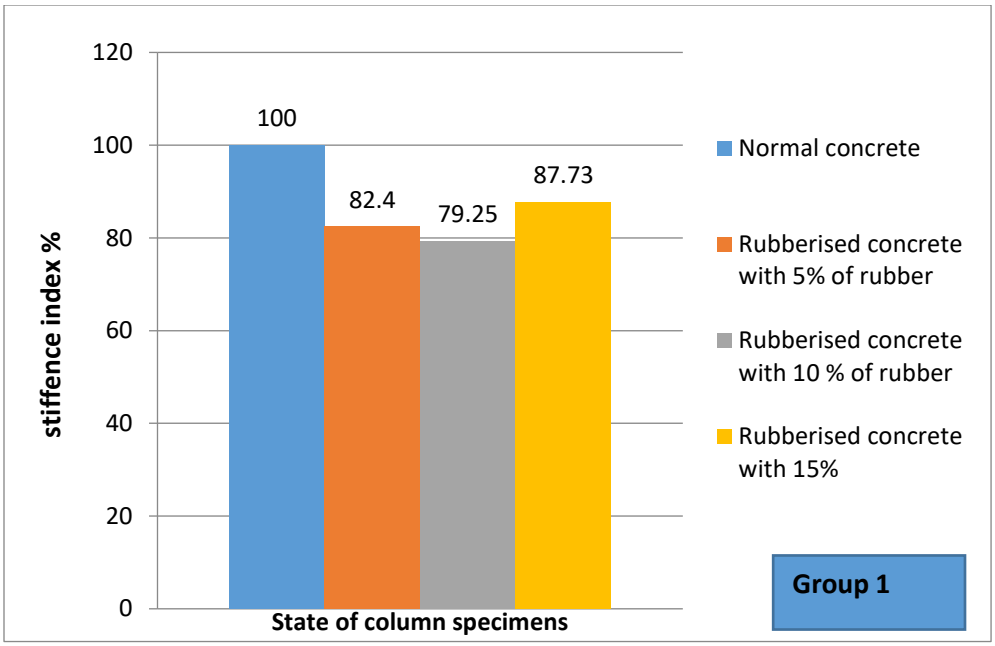

Figure (4-10): Stiffness parameter of tested specimens (G1N, G1F5, G1F10, and G1F15).

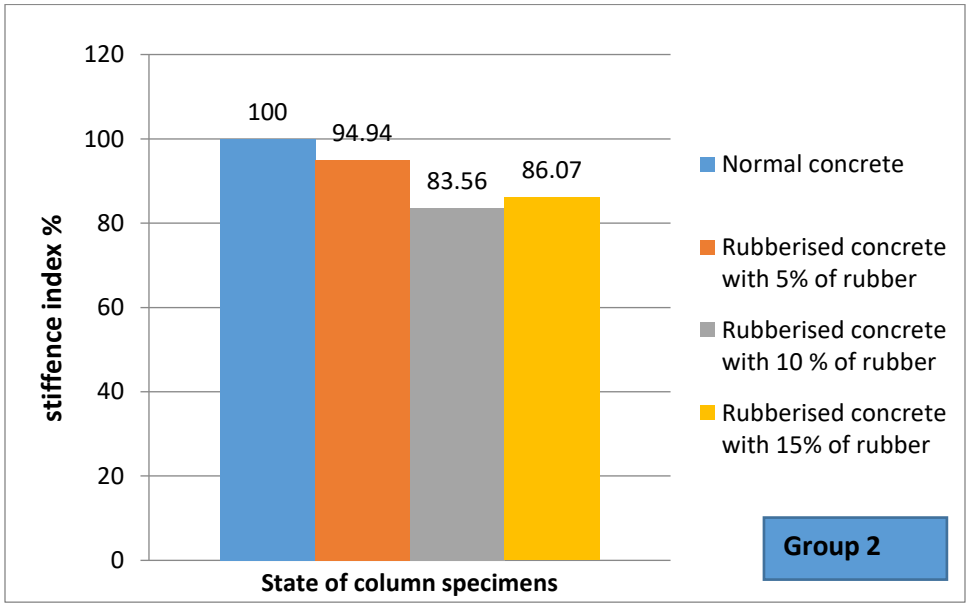

Figure (4-11): Stiffness parameter of tested specimens (G2N, G2F5, G2F10, and G2F15).

4-4-6 Cracking Behaviour

Control reinforced concrete columns and rubberised columns are clear of cracks during the early stages of loading. The crack width was measured using the DIC (Digital Image Correlation) method, and the first crack was identified using natural vision, followed by the measurement of the corresponding load. For eccentrically loaded column specimens, transverse flexural cracks usually start in the tension zone and propagate in the compression zone, while longitudinal cracks start as shear cracks at the corbel.

All DIC analyses were performed using the commercial DIC software GOM Correlate. When working with GOM, the creation of a surface component offers the possibility to evaluate the pattern quality, where the reference image is matched to the deformed image. The measured crack widths and corresponding corrections are shown in Table (4-9) for columns. The findings indicate that, when compared to the reference columns constructed with normal concrete, increasing the rubber replacement ratio causes a minor drop in the width of the specimen's ultimate failure cracks as well as an increase in their quantity. The final failure crack width of the rubberized concrete column decreased from (2.14) mm to (1.20) mm when crumb rubber was replaced with a range of 0% to 15% of the volume of the sand aggregate in standard concrete mixtures. However, the number of cracks increase following rubber replacement. The effect of rubber on compressive strength and failure load can be attributed to the reduction in failure of the rubber column. Both reduced with increasing rubber concentration in rubberized samples. The increased number of cracks in rubberized specimens can be related to rubber's elastic characteristics, which have lower Young's modulus and greater Poisson's ratio values than conventional fillers. During the loading phase, this raises the differential stress rate between the rubber component and the mortar.

Table (4-9): Measured crack widths at crack detection-column.

Column No.	Columns Symbol	Flexural crack width(mm)	Difference in flexural crack width %
C1	G1N	2.14	…..
C2	G1F5	2.125	-0.7
C3	G1F10	1.84	-14
C4	G1F15	1.20	-43.92
C5	G2N	3.05	…..
C6	G2F5	2.1	-31.14
C7	G2F10	1.87	-38.68
C8	G2F15	1.90	-37.7

4-4-7 Strain in Concrete

Digital Image Correlation (DIC) involves calculating displacement and material strain by tracking the motion of features in successive images. Figures (4-12) to (4-19) show the strains of the minor and major strains of the specimens (G1N, G1F5, G1F10, G1F15, G2N, G2F5, G2F10 and G2F15) at 50, 100 and 150 kN result. As the load and longitudinal strain increase, the local strain changes due to cable crimping become more pronounced in the DIC strain field. The correlation between the results recorded using DIC supports the use of DIC to measure strain in a direction parallel to the specimen. In addition, the extension fields shown in Figures (4-12) to (4-19) indicate the ability of DIC to satisfactorily measure local strain variations. The effect of the rubber on the strains can be seen in the strain fields. The strain fields in the minor, and major strain obtained where testing specimen are reported for the different steps, with the strains linearly increasing as the load increased. The use of DIC confirmed the damage observed in full-scale

case study testing. This result could be used to be able to predict where the damage will occur before it actually happens.

Due to the increased flexure effect, the strain value at the column's tension and compression faces generally rises with increasing eccentricity. Additionally, the strain value that initiated the first crack rises with an increase in the tensile stress of the shell's concrete.

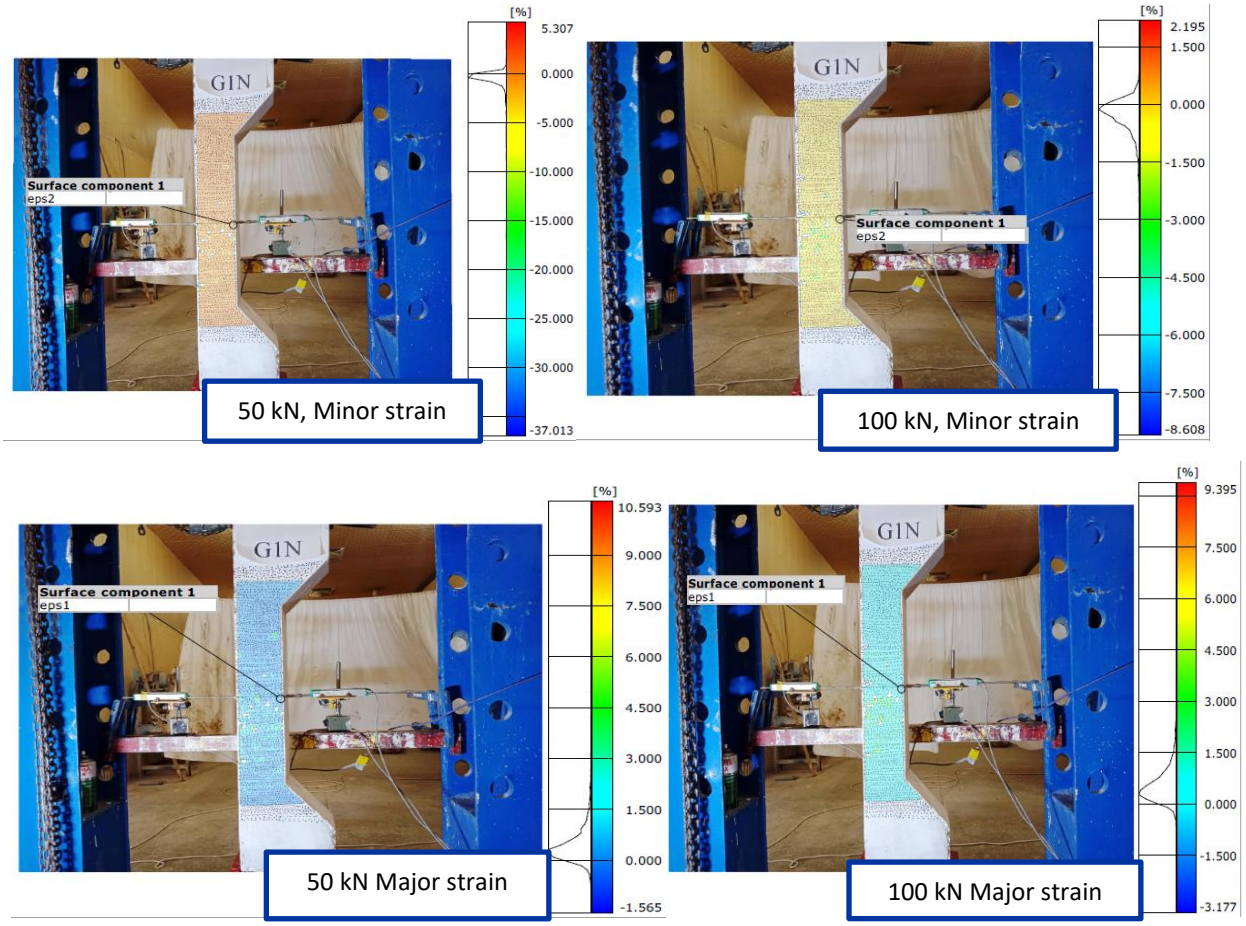

Figure (4-12): Strain results for coupon specimens G1N for minor, and major strains in 50, and 100 KN.

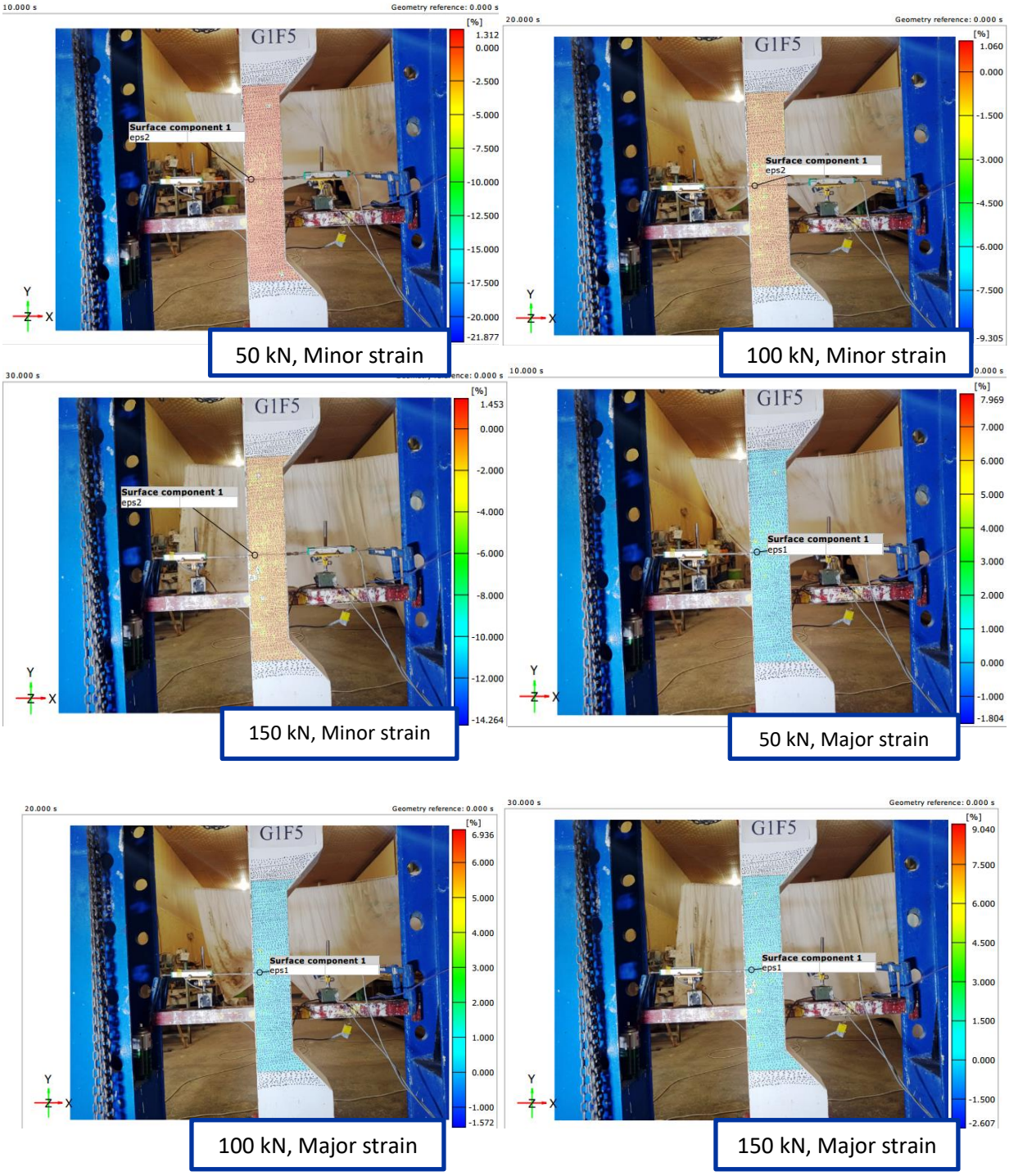

Figure (4-13): Strain results for coupon specimens G1F5 for minor, and major strains in 50, 100, 150, 200, and 250 KN.

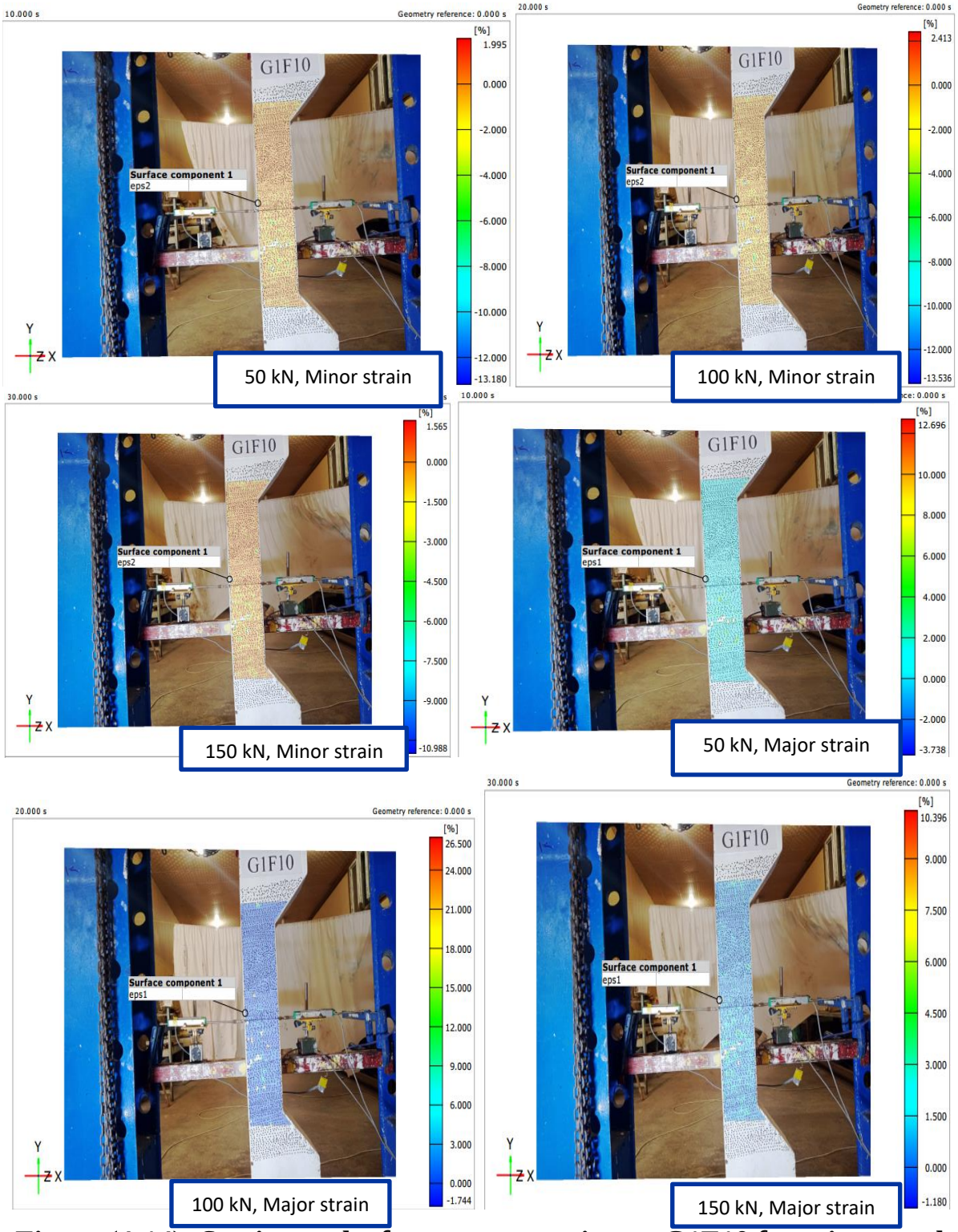

Figure (4-14): Strain results for coupon specimens G1F10 for minor, and major strains in 50, 100, and 150KN.

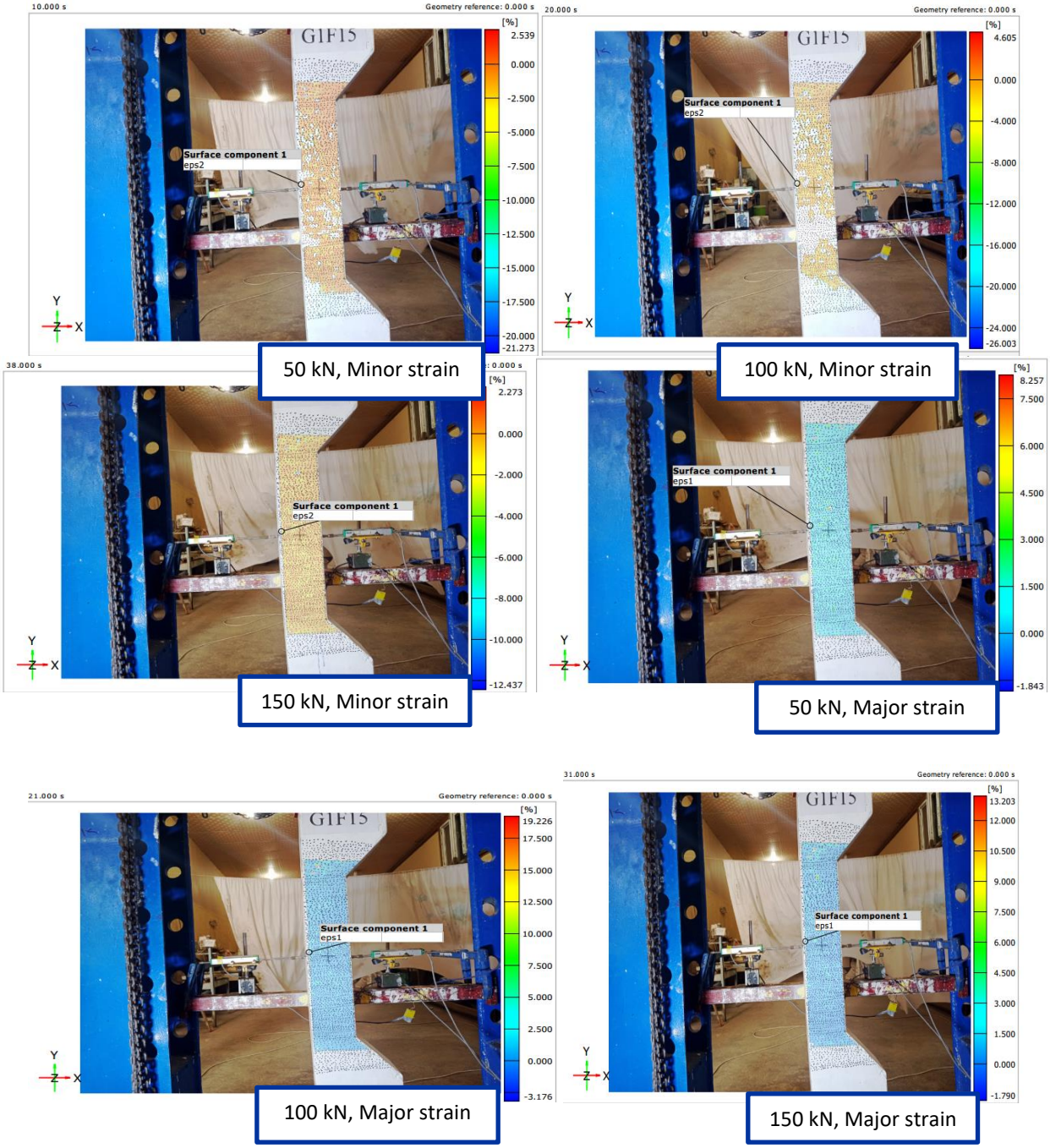

Figure (4-15): Strain results for coupon specimens G1F15 for minor, and major strains in 50, 100, and 150 KN.

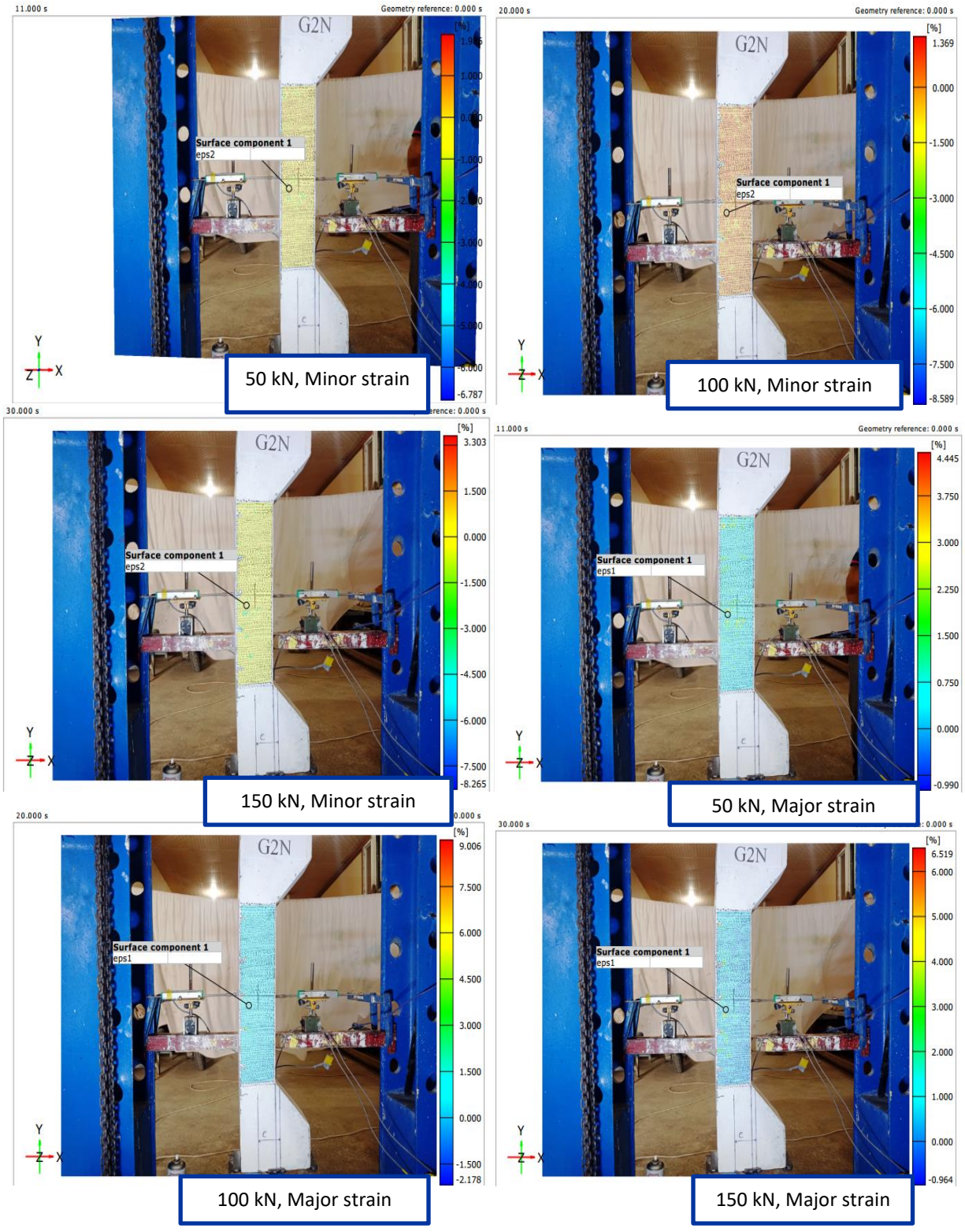

Figure (4-16): Strain results for coupon specimens G2N for minor, and major strains in 50, 100, and 150 KN.

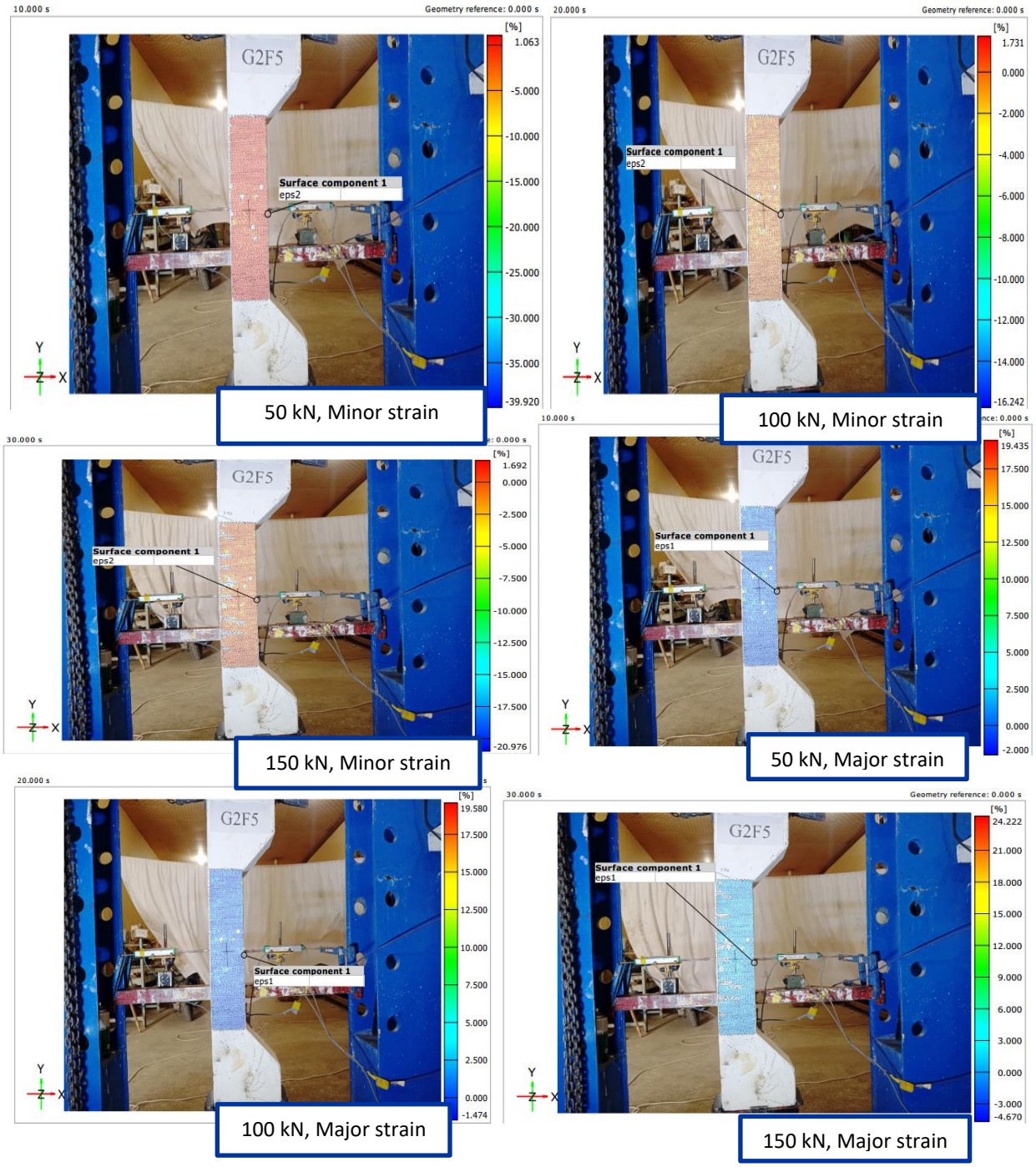

Figure (4-17): Strain results for coupon specimens G2F5 for minor, and major strains in 50, 100, and 150 KN.

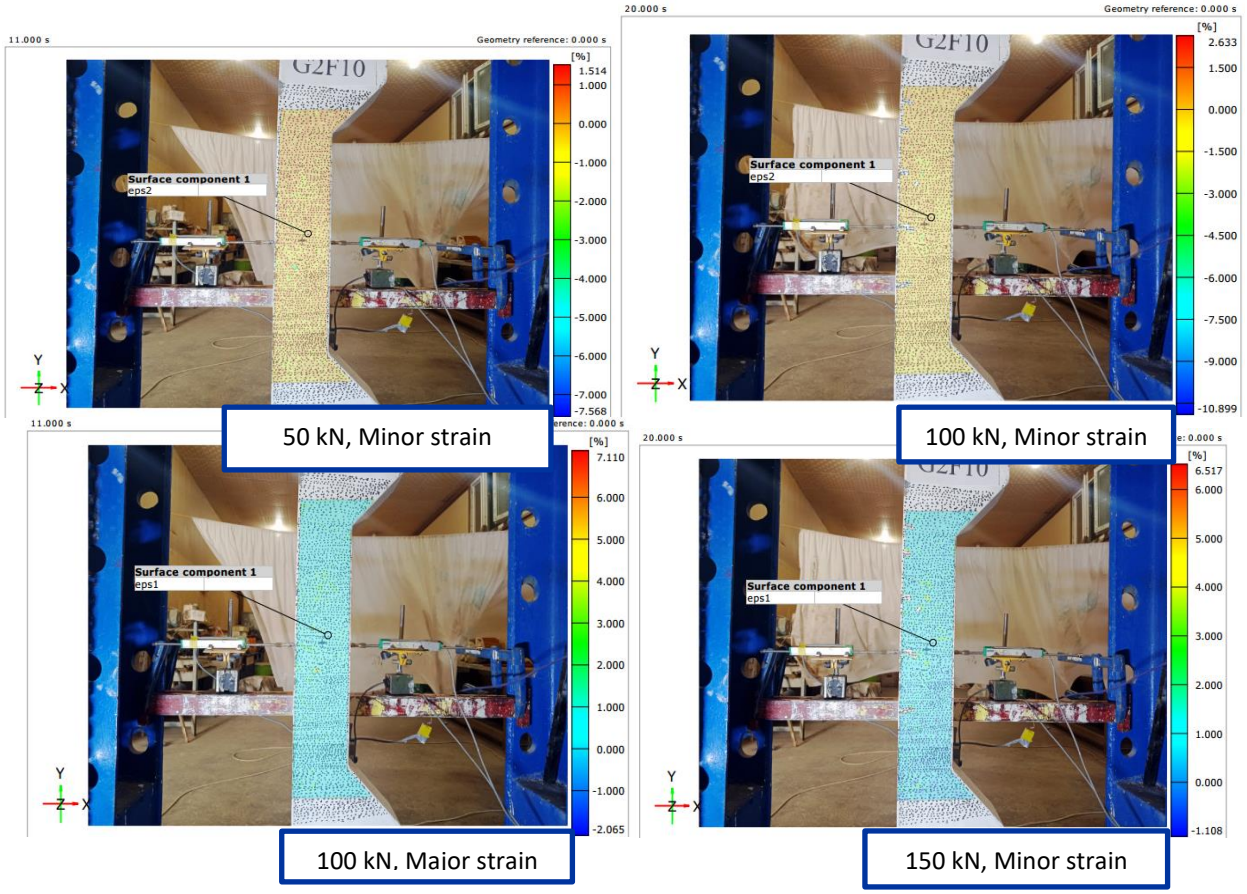

Figure (4-18): Strain results for coupon specimens G2F10 for minor, and major strains in 50, 100, and 150 KN.

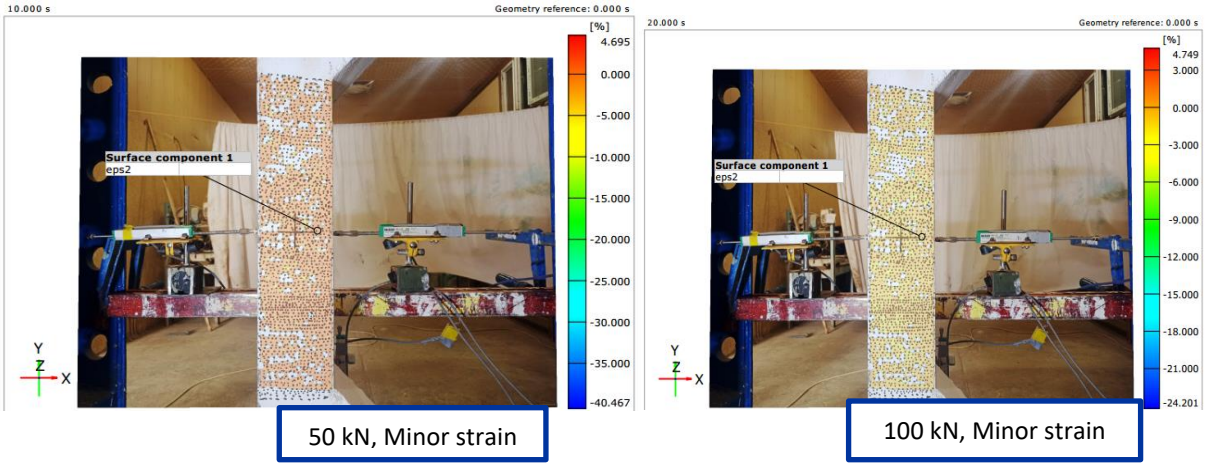

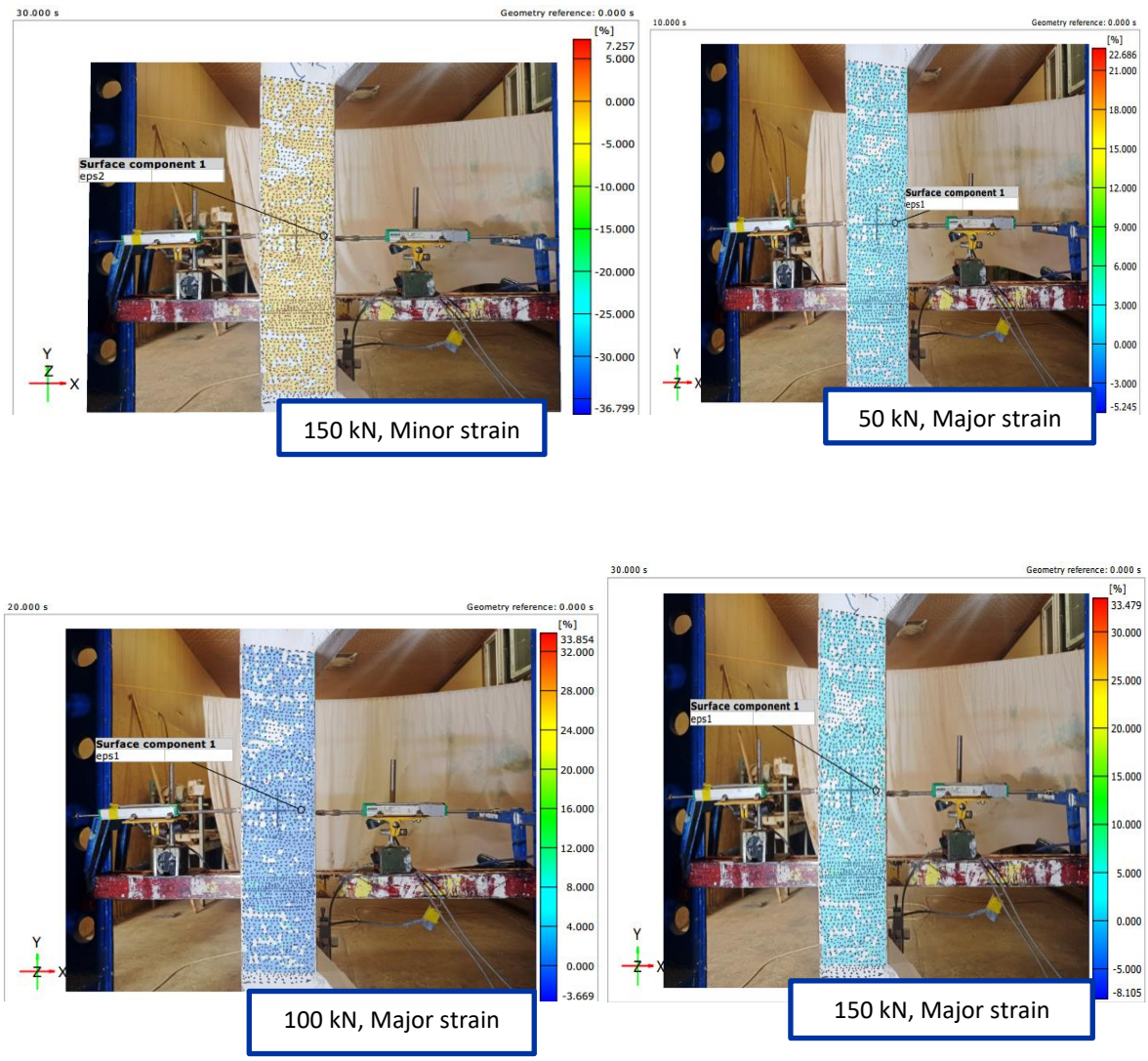

Figure (4-19): Strain results for coupon specimens G2F15 for minor, and major strains in 50, 100, and 150 KN.

Chapter Five

Finite Element Analysis

5-1 Introduction

Finite element analysis (FEA) is a strong and affordable method for assessing the complicated behavior of any construction component, especially those with complex non-linear structural behavior. For studying structural mechanisms and conducting parametric analyses, ABAQUS is one of the most widely used commercial finite element analysis software. The current study presents a comparison of experimental and numerical data to show that modeling of the rubberized column is sufficient, which includes: element type, material attributes, real constant, boundary conditions, and convergence studies. Rubberized reinforced rectangular columns were studied using a nonlinear finite element analysis. The analysis of the columns evaluated in chapter 4 as well as other key parametric investigations utilizing the nonlinear finite element method package ABAQUS/Standard 6.14 are included in this chapter.

5-2 Finite Element Mesh

To investigate the effect of replacing fine aggregate with a varied ratio of rubber, eight columns were modelled. A convergence analysis on the column model to identify an acceptable mesh density is a key step in finite element modelling. When the structure is separated into a manageable number of elements, the results can be assembled. This is practically realized when a reduction in mesh size has no influence on the results, because the complexity of the analysis is proportional to the processing time. As shown in Figure (5-1), the columns with the same material (normal concrete with eccentricity 75 mm) attributes and loading

were modelled with smaller element sizes (raising the number of elements in each direction X, Y, and Z) (50, 35, 30, 25, 15, and 10 mm). For the same applied stress level of 200 kN, the axial displacement for all columns was observed. The discrepancy can be ignored when the mesh size is reduced from (25) mm to (10) mm, according to the convergence research illustrated in Figure (5-2). As a result, for all of the evaluated columns, a mesh size of (30) mm was used, ensuring a satisfactory fit between the element size and the numerical solution's stability.

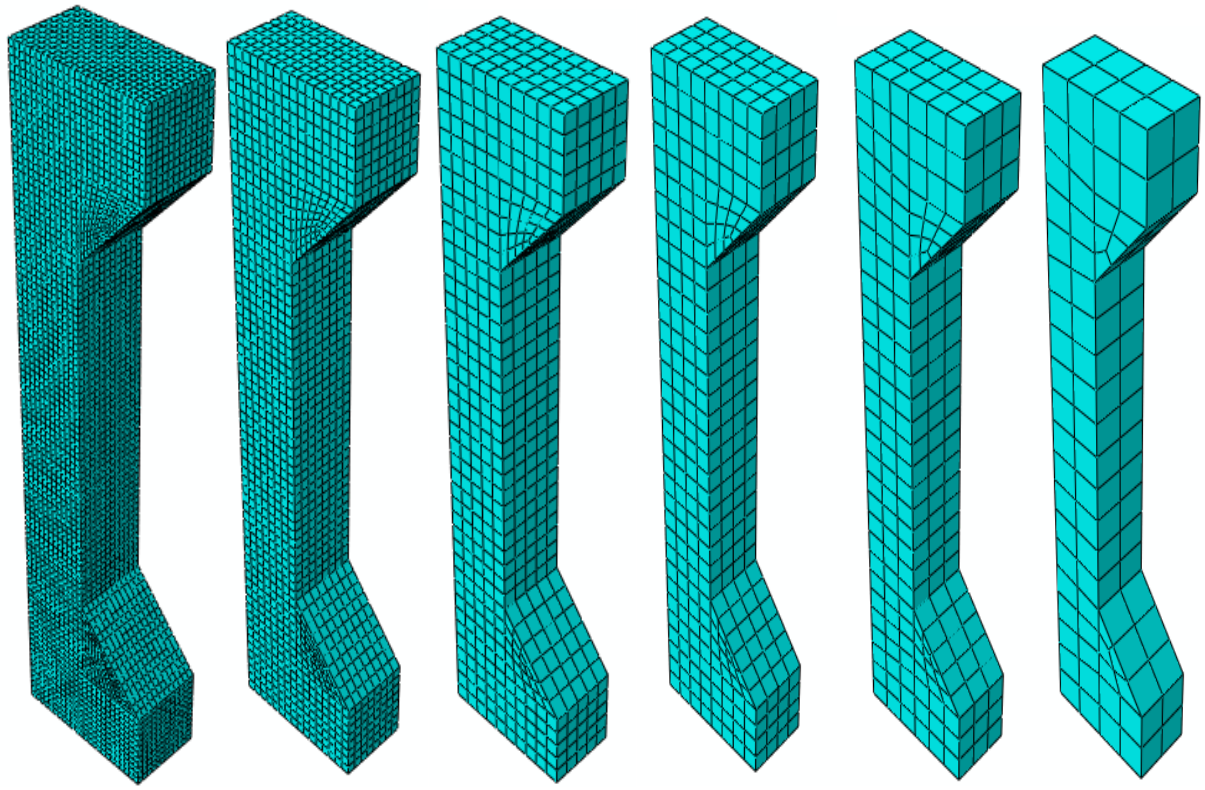

Figure (5-1): The meshes that have been considered for the column specimen

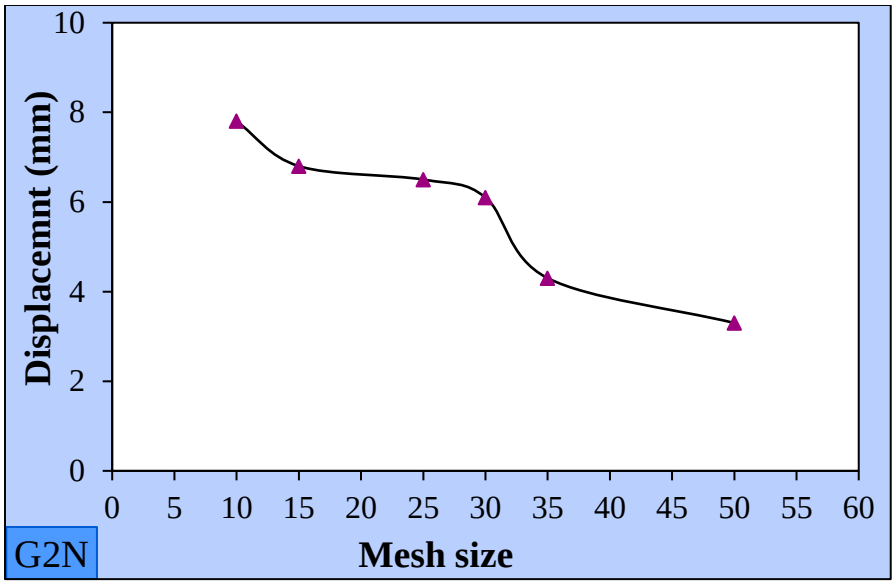

Figure (5-2): Convergence study.

5-3 Types of Elements

To forecast the intricate behaviour of the NC and RuC structures, the nonlinear FE software, ABAQUS, has provided many types of 3D elements. However, the following 3D elements are widely employed for modelling concrete materials NC and RuC:

- C3D20
- C3D8

The C3D8 element is a simple linear solid brick element with 8 integration points (2 x 2 x 2). As illustrated in Figure (5-3a), the C3D8 element was used to model the concrete material of the NC and RuC construction, as well as the bearing and loading plate, on the other hand, ABAQUS, provides a width range of two nodded link elements, such as the T3D2 truss element. As illustrated in Figure (5-3b), the T3D2 element was used to model reinforcement of RuC and NC structure in this work.

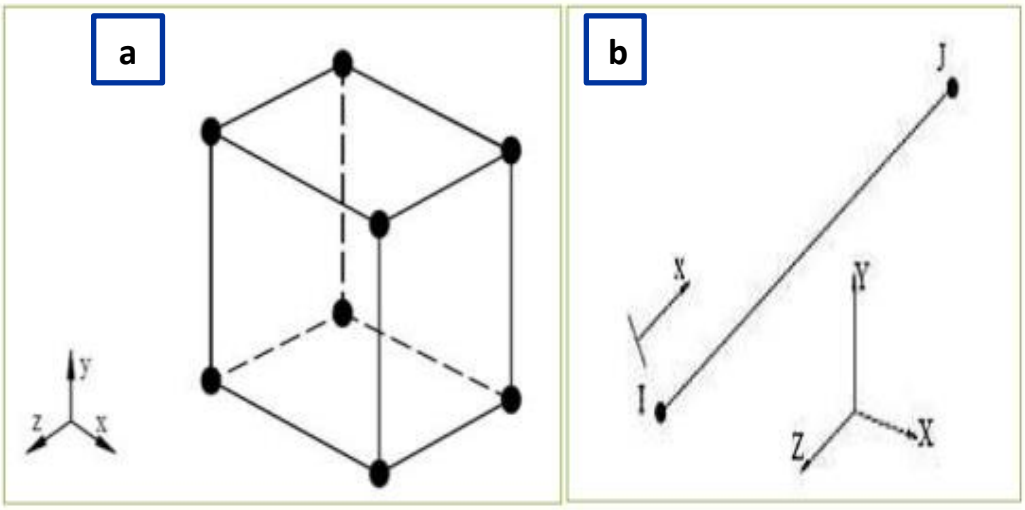

Figure (5-3): C3D8, and T3D2 elements used to model by ABAQUS.

5-4 Material Properties

Many material models for representing concrete have been integrated into commercial software to simulate loaded concrete structures. For example, the most popular modeling models for concrete materials in ABAQUS are the concrete damage plasticity model (CDP), the concrete smear cracking model, and the modified DruckerPrager/Cap model. **Appendix B** shows specifics of the CDP model, including the behavior and characteristics of the rubberized concrete and other materials employed in this study.

5-5 Modeling of Specimens

The column's parts and assembly, component interactions, load conditions, and boundary conditions applied in this study are covered in this section.

5-5-1 Parts and Assembly

The components of each specimen in this study made up: a column corbel, a bearing plate, stirrups, and a longitudinal reinforcing bar. Figure (5-4) displays the part assembly used to create specimen models. The modeling of material properties for ordinary concrete, rubberized concrete, and steel reinforcement are also included in **(Appendix B)**.

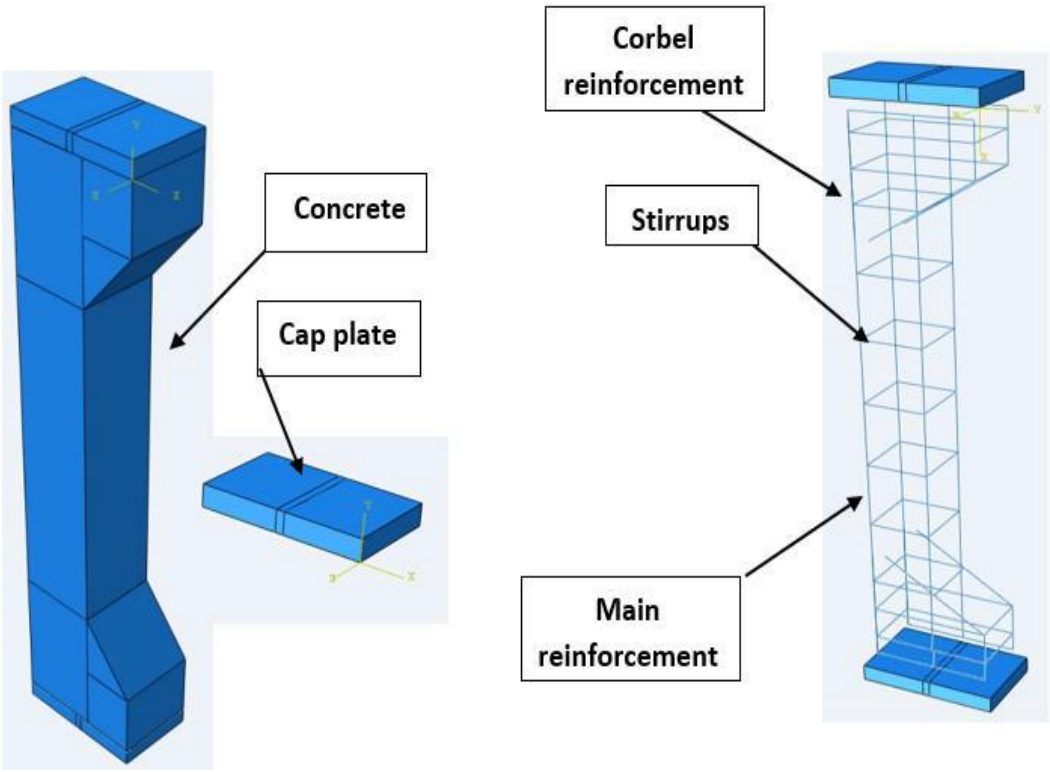

Figure (5-4): the column's assembled components.

5-5-2 Loading and Boundary Conditions

The same locations in the experimental work for all columns are used to load the finite element model, and the load is represented as a uniformly applied pressure by dividing the total applied load on the area in the center of the bearing plate, which is equivalent to the area of applied load in the experimental work as shown in Figure (5-5). The mechanism of representing any column was done by jointing at top and bottom by the hinge, in bottom surface (surface of load) it was restrained the rotation about x and y-axis, in addition, it was restrained the displacement in the direction x and z-axis and free displacement are assumed in the direction y-axis (vertical displacement) and rotation about (z). At the top support of the column, the top surface the part has restrained the displacement in the direction x, y and z-axis, and rotation in the direction x and y-axis, and free rotation about (z).

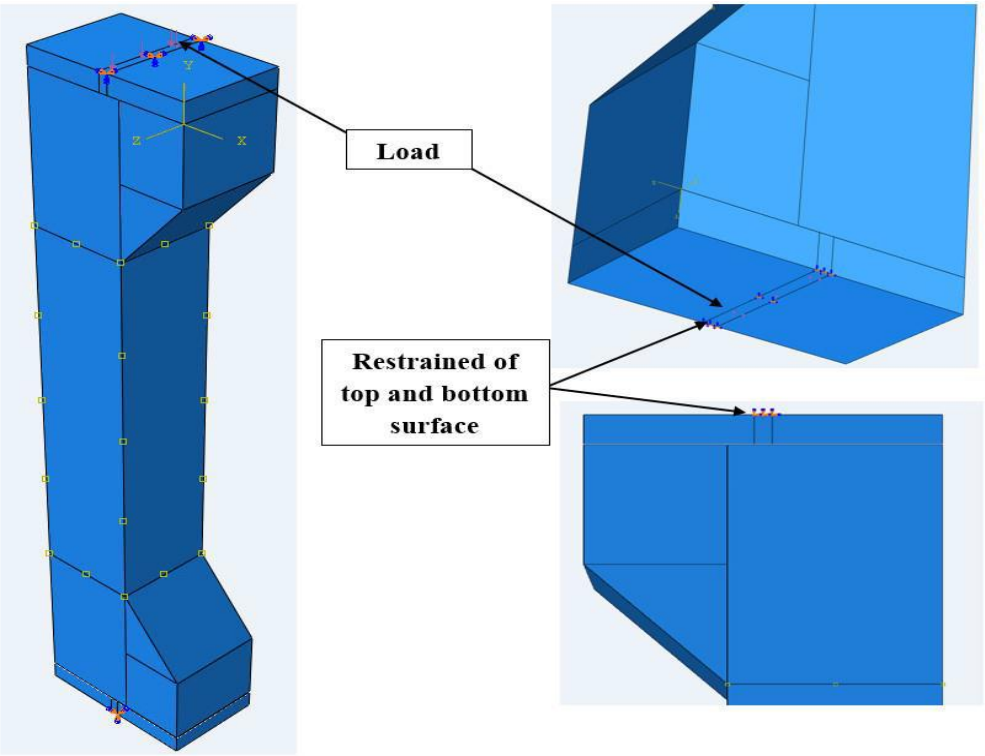

Figure (5-5): Representation (simulation) of applied loads and boundary conditions of modeled column.

5-5-3 Static Analysis Model

The structural analysis was completed utilizing a one-step process for the reference (without rubber) and rubberized specimens (static general analysis step). When modelling concrete with 8 node brick elements, all columns are modelled with 3D solid elements (C3D8). A 3D truss element with two nodes (T3D2) is used as reinforcement.

5-6 Finite Element Analysis Results and Discussion

For all tested column (normal and rubberised concrete), the experimental findings and the results of the finite element analysis performed using the ABAQUS program are compared in this section. Based on this comparison, which takes into account the load-deflection response, ultimate load support, service displacement, cracking pattern, plastic strain, and failure modes, the validity of the numerical model is established. The numerical results for ultimate load support and service deflection are shown in Table (5-1).

Table (5-1): Experimental and numerical results for all tested columns.

Specimens		Ultimate loads Pu (kN)	Percentage difference Pu%	Service axial displacement Δsv(mm)**	Percentage difference Δsv%***	Service lateral displacement Δsh(mm)**	Percentage difference Δsh%***
G1N	FEM	261.348	-4.743	2.60	36.43	2.35	-10.646
	EXP	274.36		4.09		2.63	
G1F5	FEM	269.106	4.280	2.40	-50.51	3.22	21.509
	EXP	258.06		4.85		2.65	
G1F10	FEM	204.428	-6.00	3.00	-25	2.75	16.52
	EXP	217.48		4.06		2.36	
G1F15	FEM	200.167	-2.133	3.20	-6.15	2.10	-19.54
	EXP	204.53		3.41		2.61	
G2N	FEM	168.146	5.705	2.50	-44.69	3.75	7.758
	EXP	159.07		4.52		3.48	
G2F5	FEM	163.274	6.185	3.25	-29.81	2.81	4.85
	EXP	153.76		4.63		2.68	
G2F10	FEM	143.764	4.132	2.30	-50.95	3.20	3.225
	EXP	138.06		4.69		3.1	
G2F15	FEM	140.807	1.607	2.75	-38.88	3.00	-7.692
	EXP	138.58		4.50		3.25	

* $\frac{P_{u(FE)}-P_{u(EXP)}}{P_{u(EXP)}} \times 100\%$

"**Δsv or Δsh = displacement at service load (Ps =0.65 Pu) (Jeffrey2003)."

*** $\frac{\Delta_{s(FE)}-\Delta_{s(EXP)}}{\Delta_{s(EXP)}} \times 100\%$

Table (5-2): The ductility index of Columns' numerical results.

Specimens		Ultimate displacement Δu (mm)*		Service displacement Δs (mm)*		Ductility index, μ**		Percentage difference % μ ***	
		Axial	Lateral	Axial	Lateral	Axial	Lateral	Axial	Lateral
G1N	FEM	6.328	7.836	2.60	2.35	2.433	3.334	-5.33	29.72
	EXP	6.32	6.78	4.09	2.63	1.55	2.57		
G1F5	FEM	4.840	6.456	2.40	3.22	2.016	2.005	42.5	-11.45
	EXP	6.82	5.95	4.85	2.65	1.41	2.24		
G1F10	FEM	6.246	5.640	3.00	2.75	2.082	2.051	32.61	-17.09
	EXP	6.23	6.33	4.06	2.36	1.57	2.68		
G1F15	FEM	4.868	5.400	3.20	2.10	1.52	2.57	-2.56	1.18
	EXP	5.34	6.64	3.41	2.61	1.56	2.54		
G2N	FEM	6.1705	7.488	2.50	3.75	2.468	1.99	64.5	-9.13
	EXP	6.78	7.64	4.52	3.48	1.5	2.19		
G2F5	FEM	7.010	8.141	3.25	2.81	2.15	2.89	47.26	14.22
	EXP	6.78	6.79	4.63	2.68	1.46	2.53		
G2F10	FEM	5.090	7.53678	2.30	3.20	2.17	2.343	39.10	-4.36
	EXP	7.33	7.61	4.69	3.1	1.56	2.45		
G2F15	FEM	6.152	6.58526	2.75	3.00	2.23	2.19	35.97	-17.045
	EXP	7.76	8.59	4.50	3.25	1.64	2.64		

"*Δs = displacement at service load (Ps =0.65 Pu) (Jeffrey2003)".

** $\mu = \frac{\Delta u}{\Delta s}$

*** $\frac{\mu_{FEM} - \mu_{EXP}}{\mu_{EXP}} * 100\%$

5-6-1 Analytical Results of Control Columns (Without Rubber)

Table (5-1) compares numerical values from finite element analysis to the ultimate load, service axial displacement, and lateral displacement of reference column specimens evaluated experimentally. Also, in Figure (5-6 to 5-9) finite element results of displacement are compared with experimental data for control column specimens of each group (1, and 2) with different eccentricity (45, and 75) mm, respectively. The proposed model is consistent and may be employed with

confidence, according to the test and analysis' strong agreement. The result of the control column (G1N) from the group (1), shows the ultimate load (261.348 kN) from the FE model is close with the ultimate load of (274.36) kN from the experimental data. It should be observed that the experimental values for (G1N) is outperformed by (4.743) % from the numerical values of ultimate load of the control column specimens. The service lateral displacement of this model was less than that of the experimental column by (10.646) %, while the service axial displacement of this model was more than that of the experimental column by (36.43%). However, the reference column (G2N) result from group two shows that the ultimate load of (168.146 kN) from the FE model and the ultimate load of (159.07) kN from the experimental data with different assumptions are extremely similar (5.705) %. The service lateral displacement of this model was more than that of the experimental column by (7.758 %), while the service axial displacement of this model was less than that of the experimental column by (44.69) %. Additionally, as indicated in Table (5-2), the numerical values of the ductility in the (axial or lateral) displacement of the control column specimens are (5.33, and 64.5%) or (29.72, and 9.13 %) higher than the experimental values for G1N and G2N, respectively.

We can assume that the experimental test and the FE analysis are reasonably in agreement based on the aforementioned arguments. This proved that the suggested model is trustworthy and consistent as a result. The failure modes for all reference column specimens from groups 1 and 2 that came from FEA produced from plastic strain are shown in Figures (5-10) and (5-11), and they are depicted to be close to the failure in the experimental test.

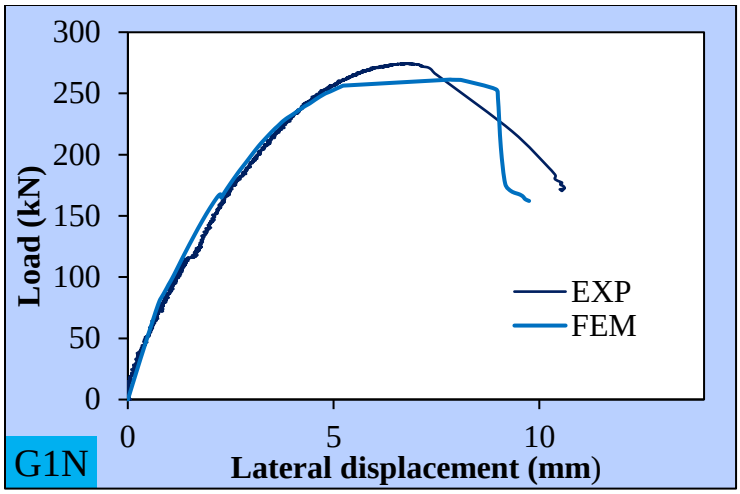

Figure (5-6): Load-lateral displacement relationship for G1N samples.

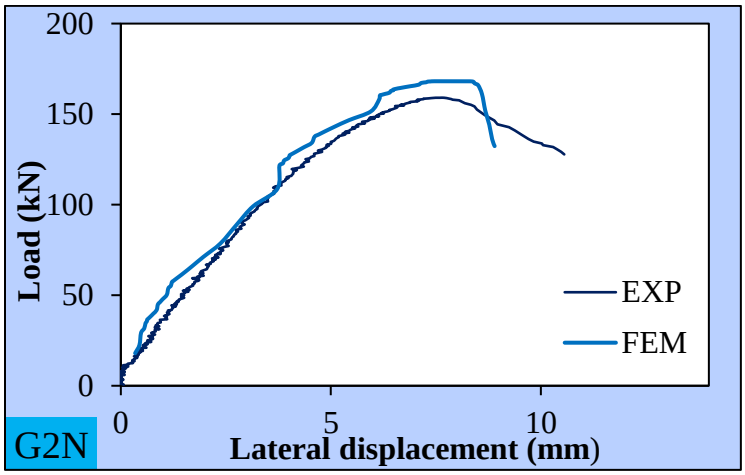

Figure (5-7): Load-lateral displacement relationship for G2N specimens.

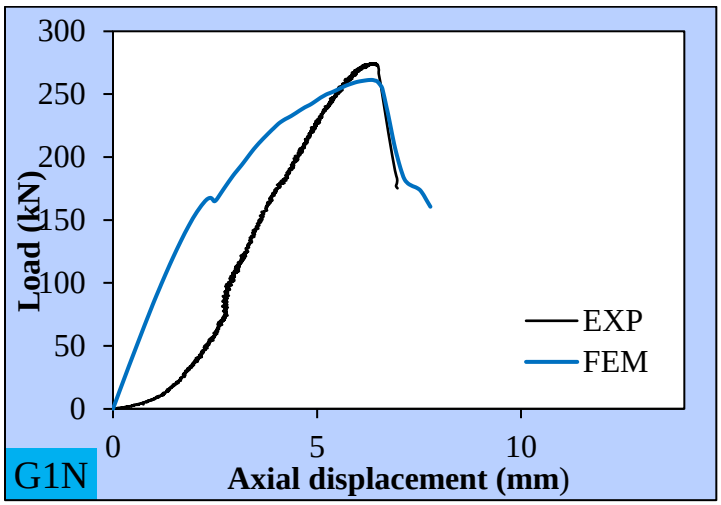

Figure (5-8): Load-axial deformation relationship for G1N specimens.

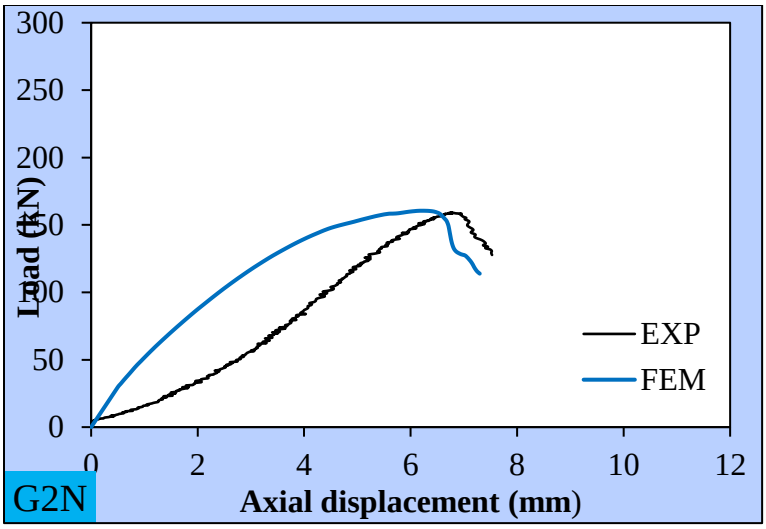

Figure (5-9): Load- axial deformation relationship for G2N specimens

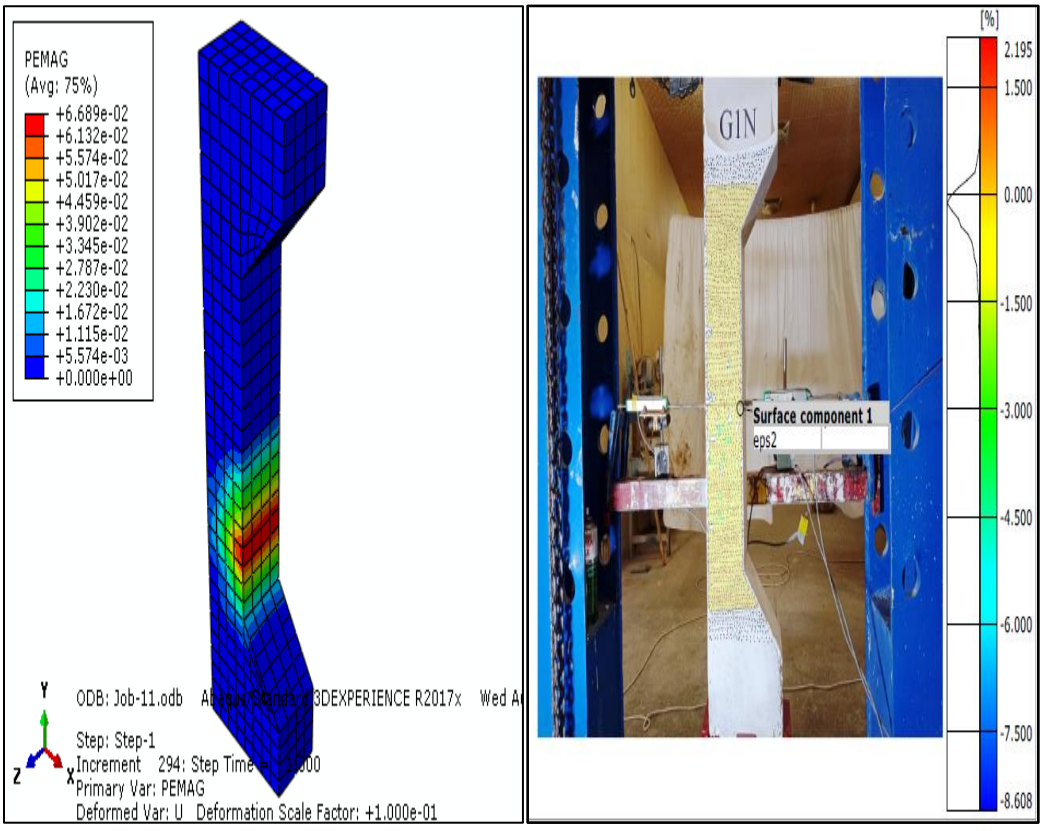

Figure (5-10): Plastic strain distribution of G1N column.

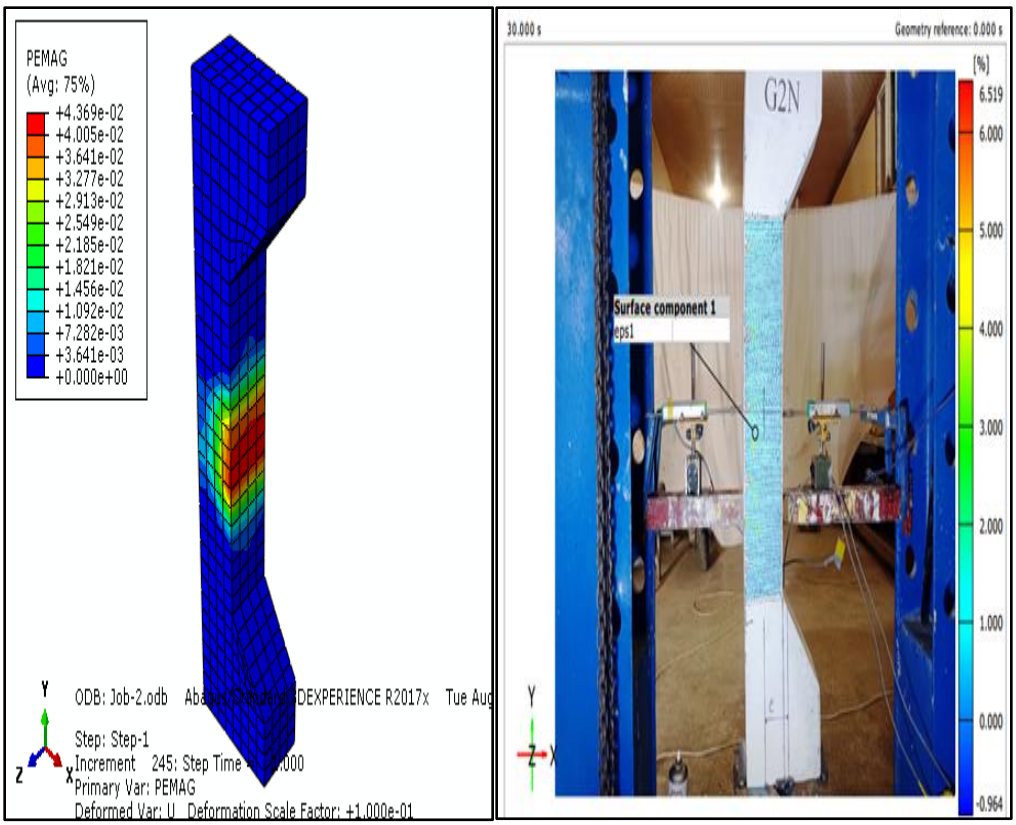

Figure (5-11): Plastic strain distribution of G2N column.

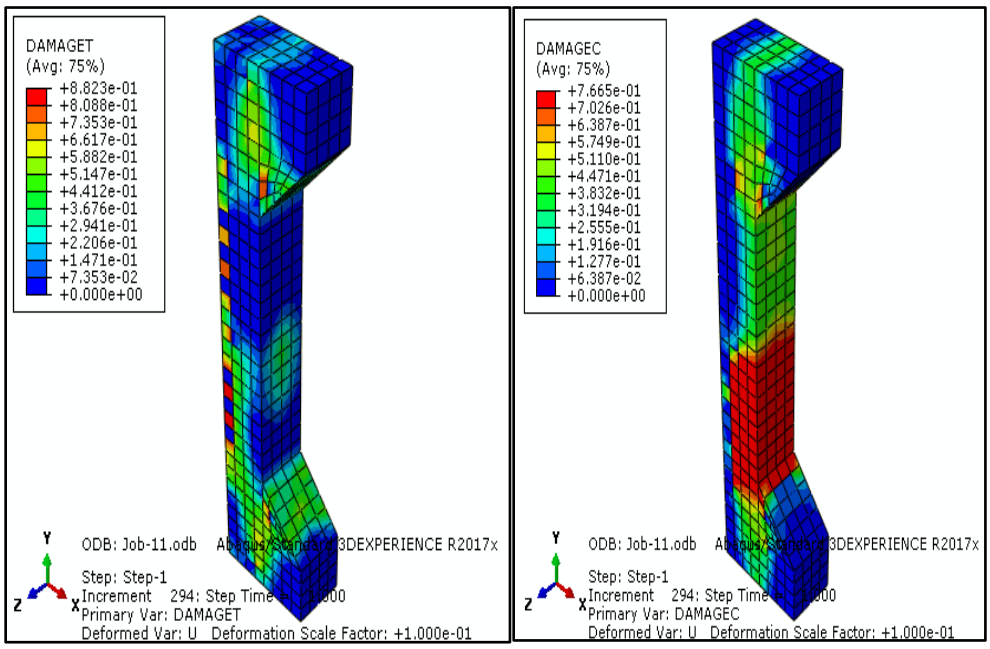

Figure (5-12): Concrete damage plasticity distribution (tensile and compressive damage variable) of G1N column.

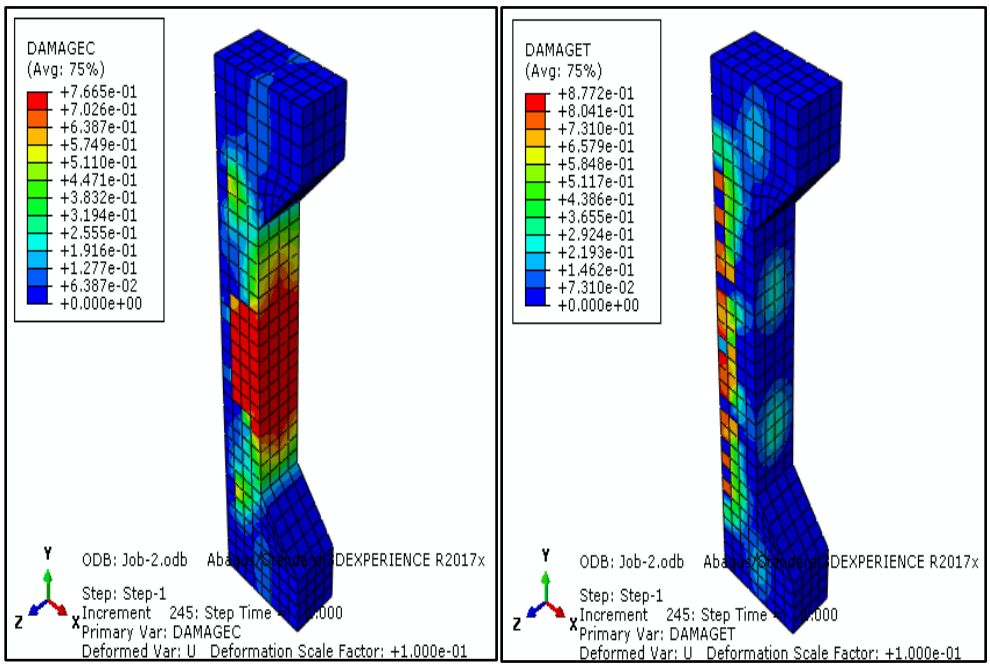

Figure (5-13): Concrete damage plasticity distribution (tensile and compressive damage variable) of G2N column.

5-6-2 Analytical Results of Rubberised Concrete Specimens (With 5% of Rubber)

This section compares numerical values from finite element analysis to the ultimate loads, axial displacement, and lateral displacement of the tested column specimens that were replaced by 5% crumb rubber with different eccentricity (45, and 75) mm for two groups (1, and 2) respectively, and as shown in Table (5-1).

The ultimate load from the FE model, which was 269.106 kN, was higher than the final load from the experimental data, which was 258.06 kN by (4.280%), according to the results of column (G1F5) from group (1) with eccentricity 45mm. Table (5-1) shows that the service lateral displacement of this model was more than that of the experimental column by (21.509%), while the service axial displacement of this model was less than that of the experimental column by

(50.51) %. Whereas the result of the column (G2F5) from the group (2) with eccentricity 75mm, the ultimate load from the FE model, which was 163.274 kN, was higher than the final load from the experimental data, which was 138.06 kN by (6.185%).

The service lateral displacement of this model was more than that of the experimental column by (4.85%), while the service axial displacement of this model was less than that of the experimental column by (29.81) %.

The load-displacement relationships of columns with 5% crumb rubber were depicted in Figures (5-14 to 5-17), which created the impression that experimental columns were stiffer than numerical analytical columns. From these Figures, the increase in rubber content led to decrease the ultimate load of columns, leading to most damage in RuC column, thus reduced the capacity of tested columns. Numerical models and experimental results generally agreed on the ultimate load, lateral, and axial displacements. Figures (5-18) and (5-19), show the failure mode and Plastic strain of the exposed column. The maximum strain was in the middle third of the column, and this failure approximated that of the tested column when spalling occurred in the center of the RuC column's compression face. As was the case in the tested column where the shape of failure varied from column to column depending on its case of replacement of rubber, this strain was spread on the column by various percentages.

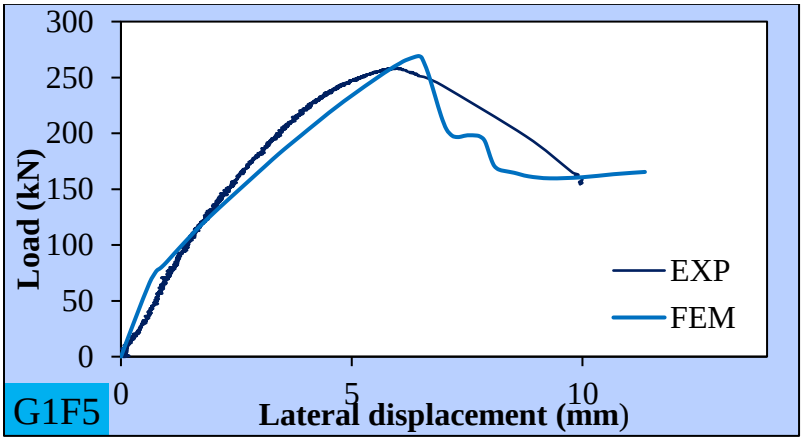

Figure (5-14): Load-lateral displacement relationship for G1F5 specimens.

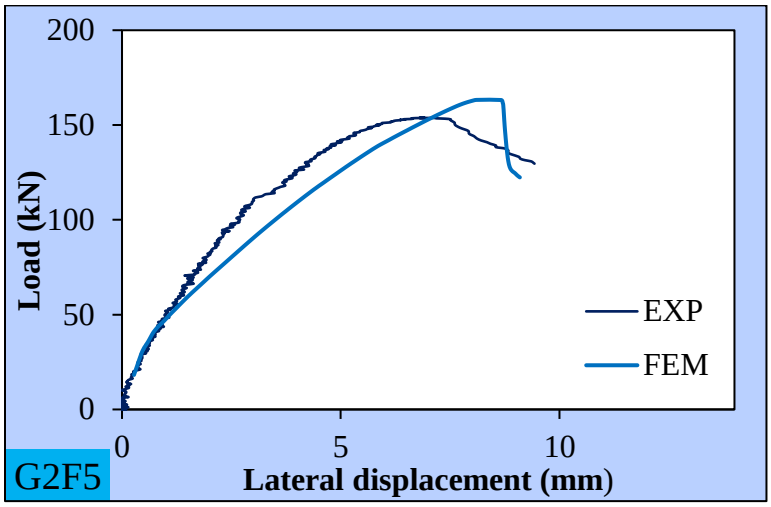

Figure (5-15): Load-lateral displacement relationship for G2F5 specimens.

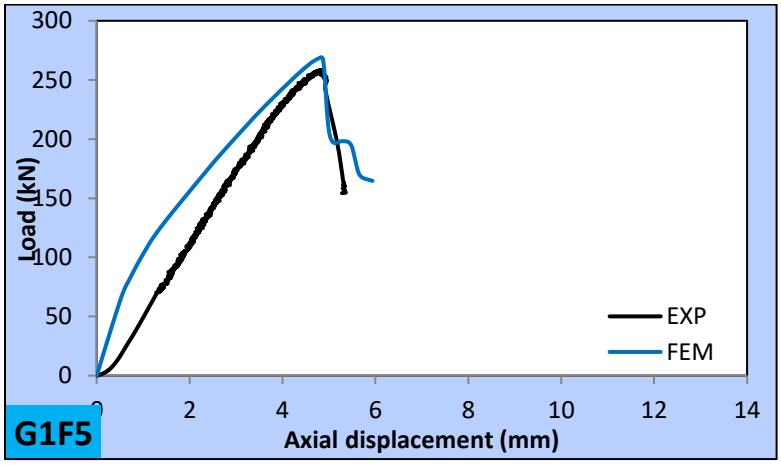

Figure (5-16): Load-axial displacement relationship for G1F5 specimens.

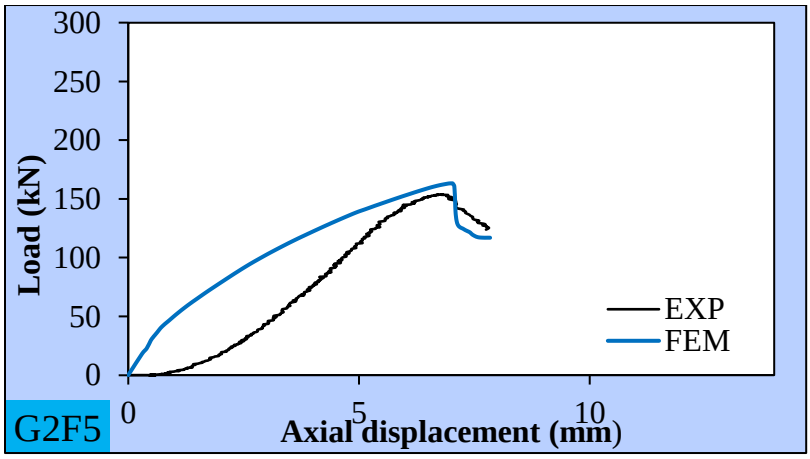

Figure (5-17): Load-axial displacement relationship for G2F5 specimens.

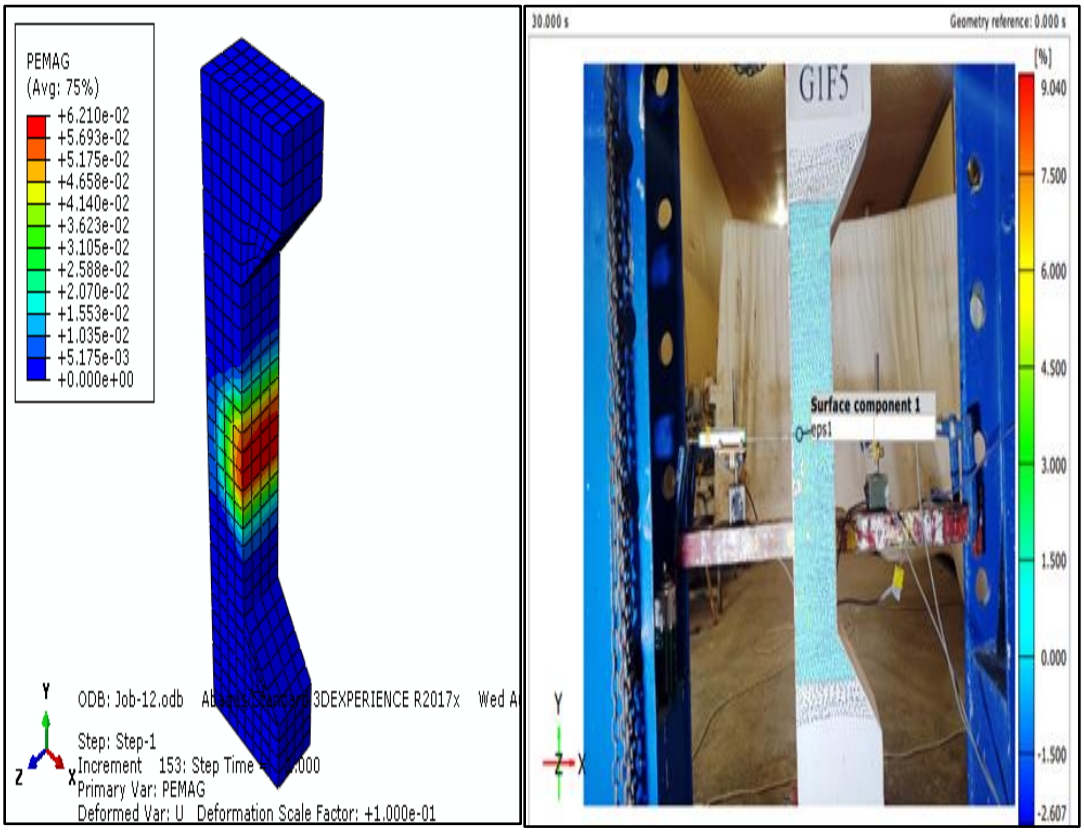

Figure (5-18): Plastic strain distribution of G1F5 column.

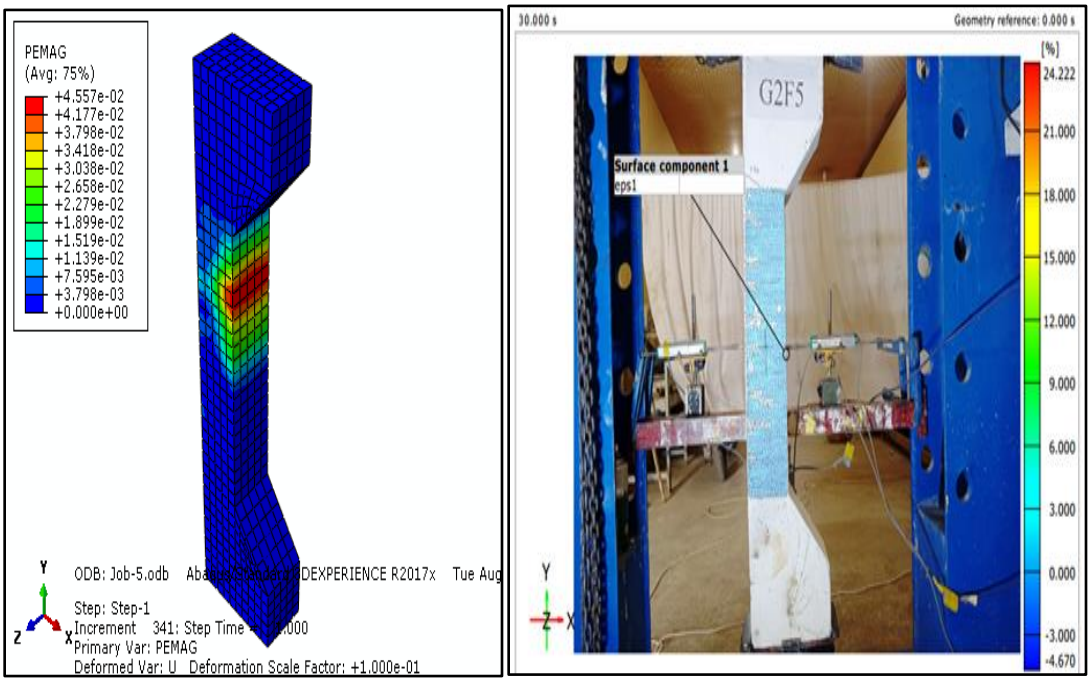

Figure (5-19): Plastic strain distribution of G2F5 column.

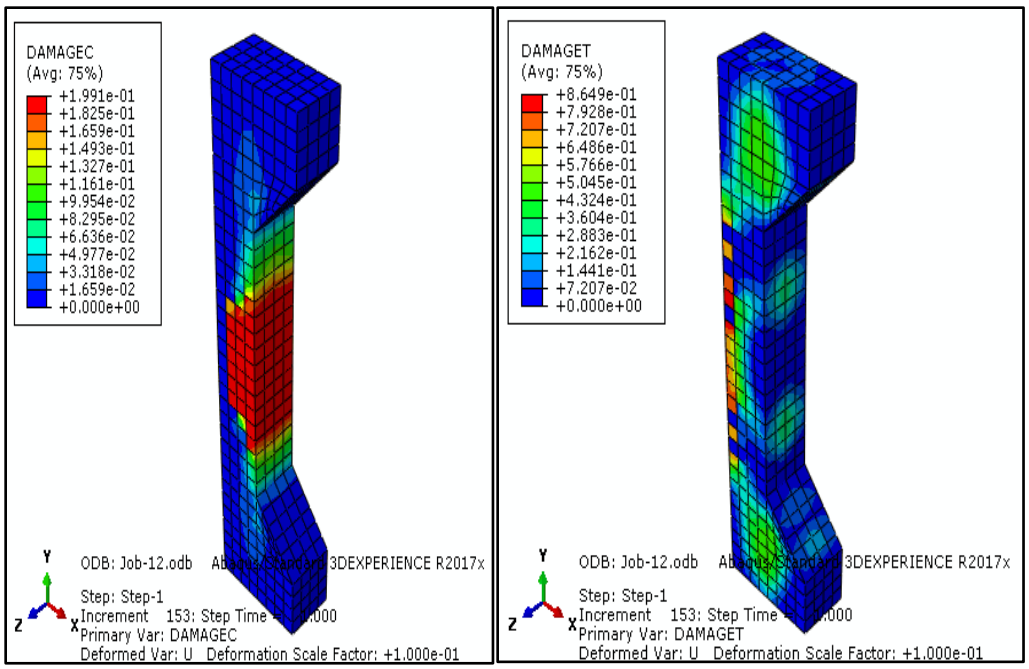

Figure (5-20): Concrete damage plasticity distribution of G1F5 column.

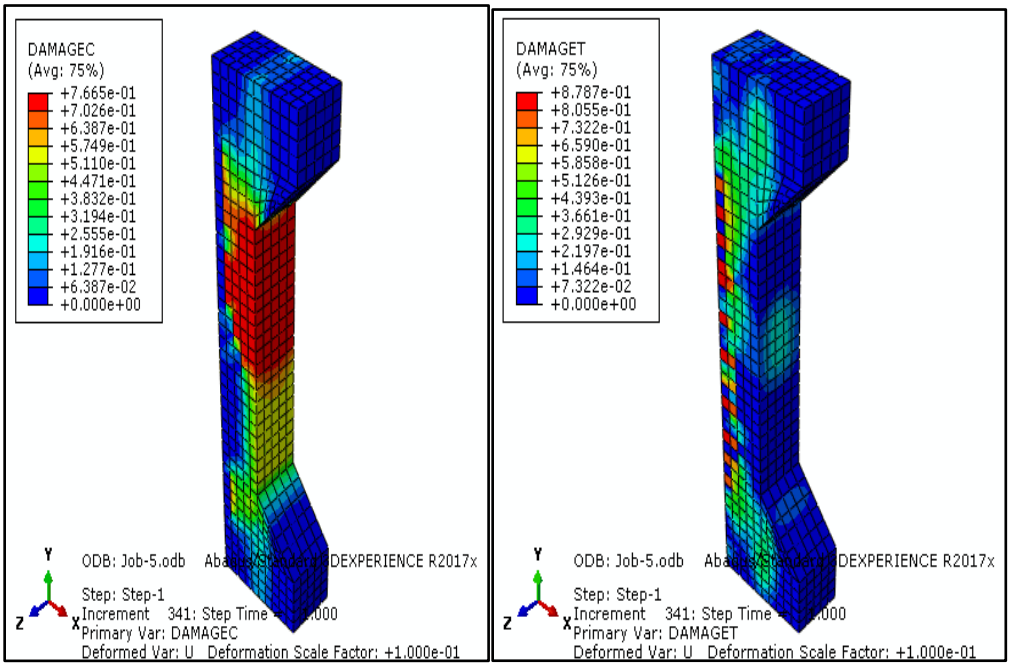

Figure (5-21): Concrete damage plasticity distribution of G2F5 column.

5-6-3 Analytical Results of Rubberised Concrete Specimens (With 10% of Rubber)

This section consists of two columns (G1F10, and G2F10), were replaced the fine aggregate by 10% of rubber with different eccentricity (45, and 75) mm,

respectively. Table (5-1) shows the results ultimate load, axial displacement, and lateral displacement of these columns. The ultimate load from the FE model, which was 204.42 kN, was less than the final load from the experimental data, which was 217.48 kN by (6 %), according to the results of column (G1F10) from group (1) with eccentricity 45mm. Table (5-1) shows that the service lateral displacement of this model was more than that of the experimental column by (16.52) %. The service axial displacement of this model was less than that of the experimental column by (25) %. Whereas the result of the column (G2F10) from the group (2) with eccentricity 75mm, the ultimate load from the FE model, which was 143.76 kN, was higher than the final load from the experimental data, which was 138.06 kN by (4.132%). The model's service lateral displacement was more than that of the experimental column by (3.225) %. While the service axial displacement of this model was less than that of the experimental column by (50.95) %.

It should also be mentioned that, as indicated in Table (5-2), the numerical values of the ductility in the (axial or lateral) displacement of these column specimens differ from the experimental values by (32.61, and 39.10) % or (17.09, and 4.36) % for G1F10, and G2F10, respectively. For column specimens from all groups (1, and 2), the load displacement findings using finite elements are compared with experimental data in Figures (5-22) to (5-25), respectively. Figures (5-26) and (5-27), exhibit the failure modes and plastic strain for columns specimens of groups (1, and 2) resulting from FEA generated from plastic strain.

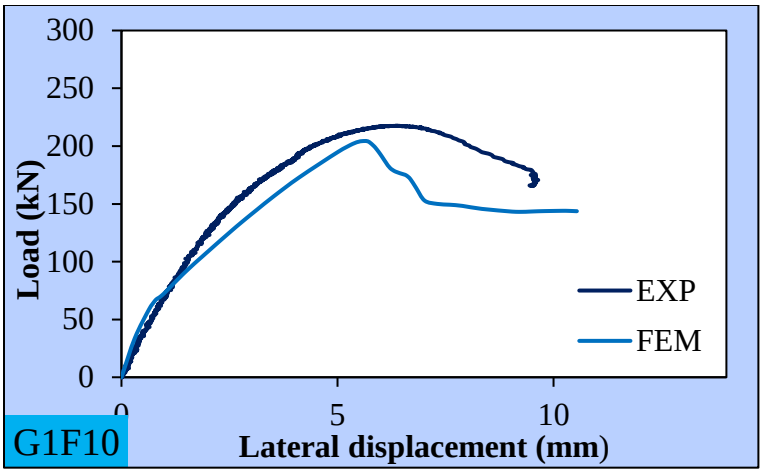

Figure (5-22): Load-lateral displacement relationship for G1F10 specimens.

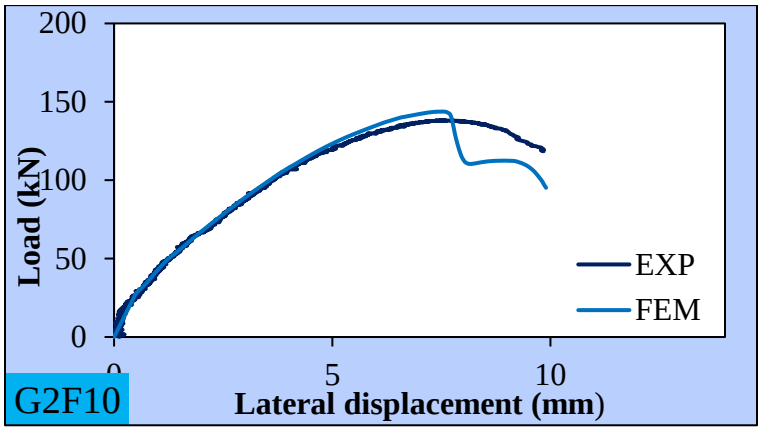

Figure (5-23): Load-lateral displacement relationship for G2F10 specimens.

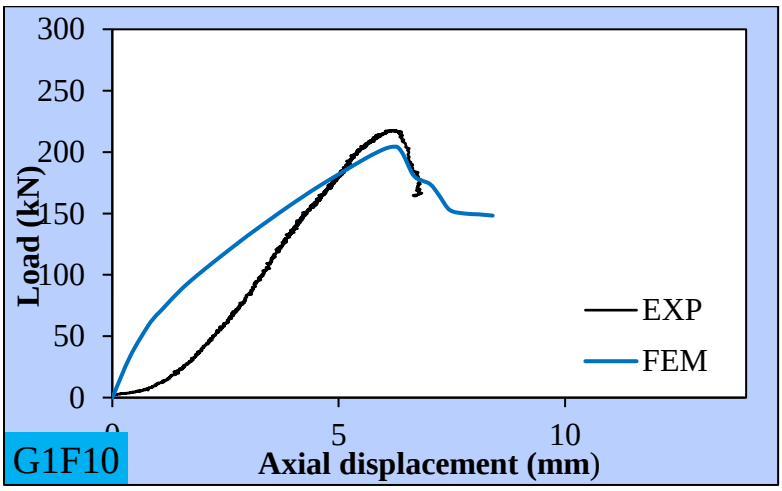

Figure (5-24): Load-axial displacement relationship for G1F10 specimens.

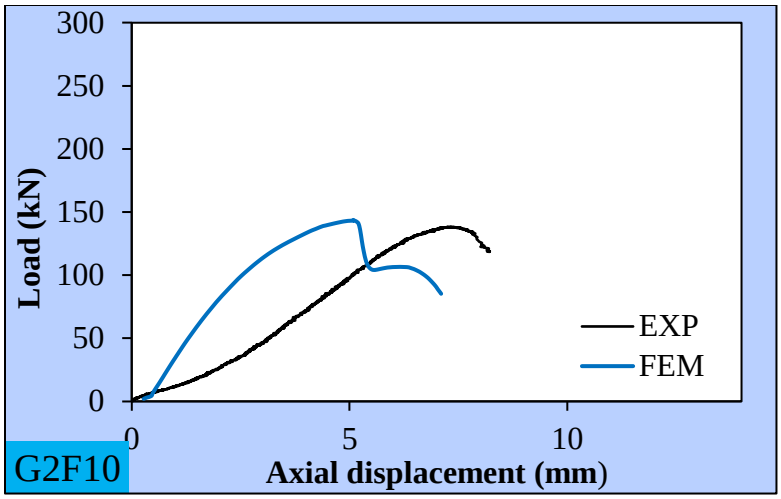

Figure (5-25): Load-axial displacement relationship for G2F10 specimens.

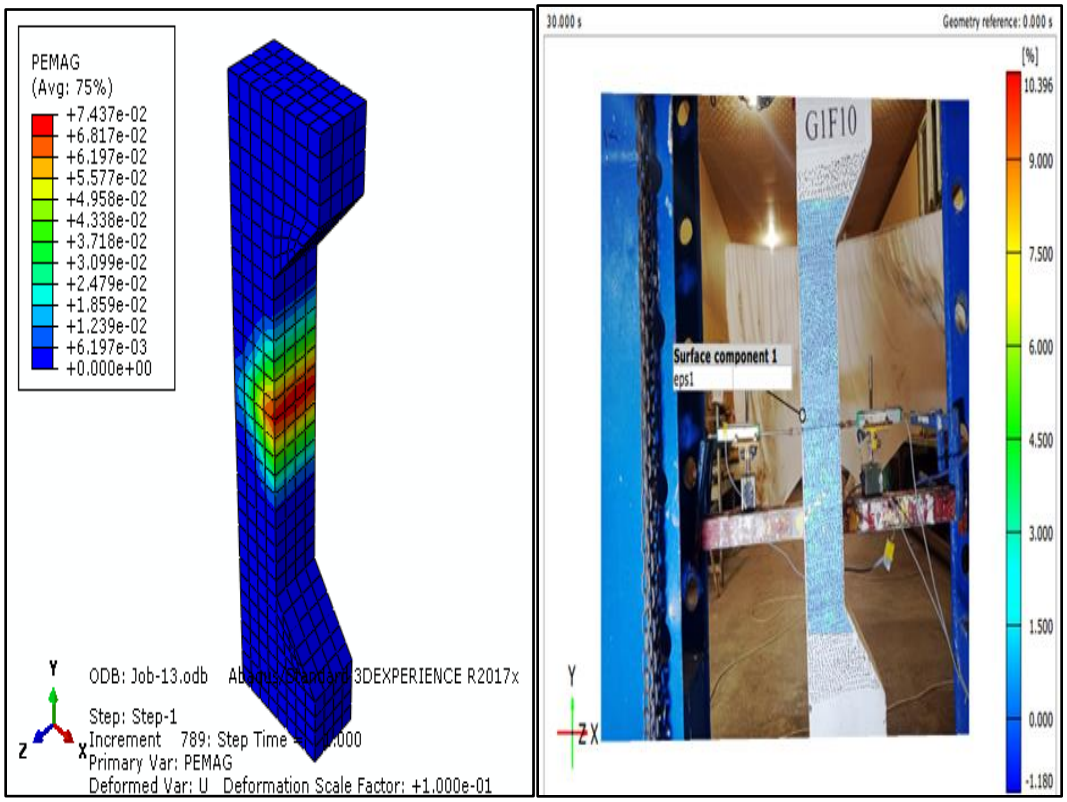

Figure (5-26): "Plastic strain distribution of G1F10 column".

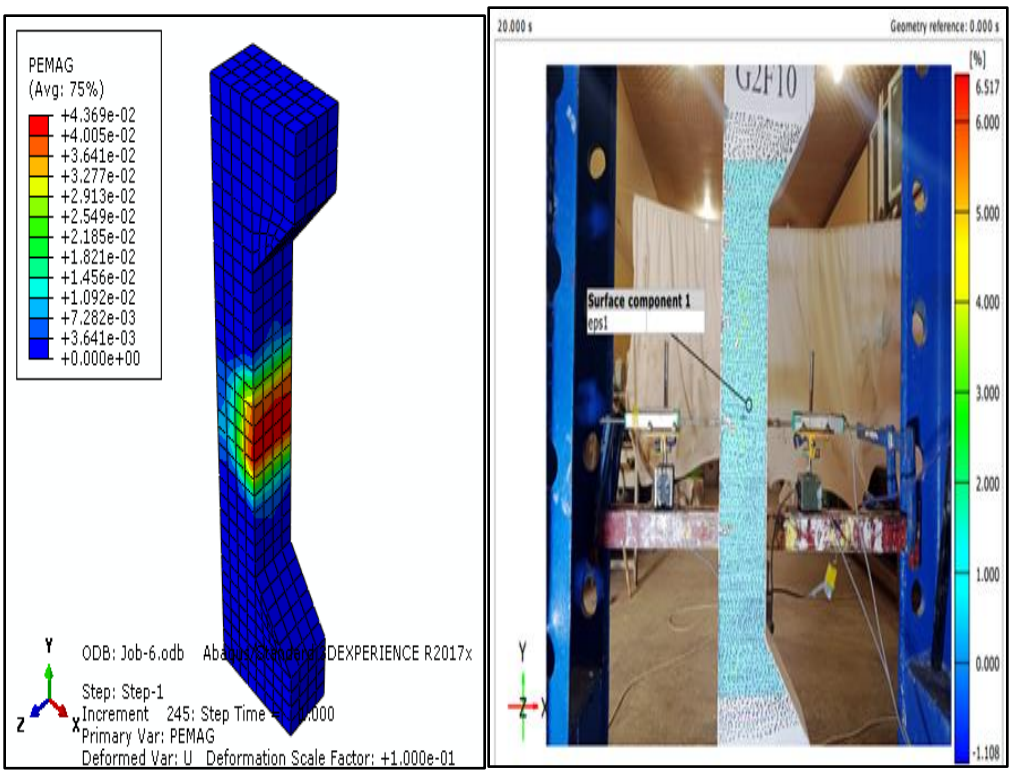

Figure (5-27): Plastic strain distribution of G2F10 column.

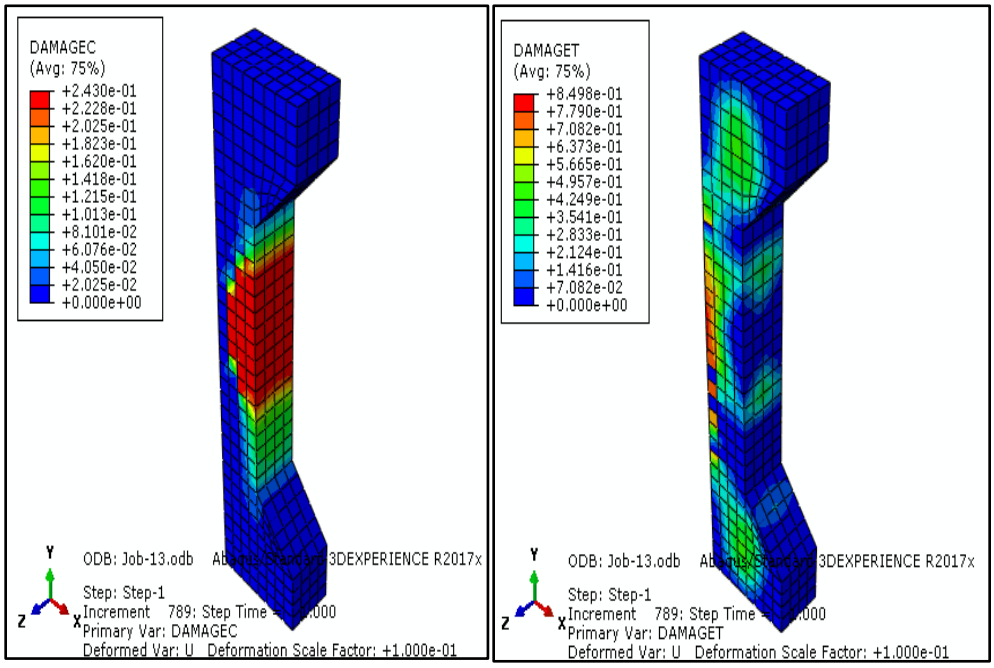

Figure (5-28): Concrete damage plasticity distribution (tensile and compressive damage variable) of G1F10 column.

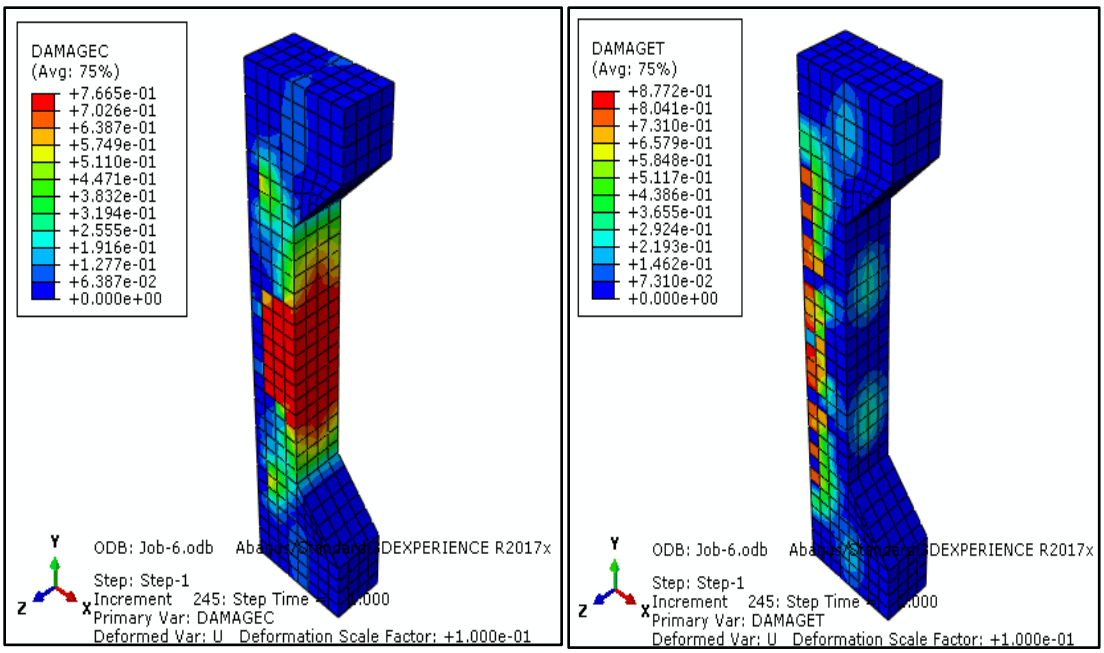

Figure (5-29): Concrete damage plasticity distribution (tensile and compressive damage variable) of G2F10 column.

5-6-4 Analytical Results of Rubberised Concrete Specimens (with 15% of rubber)

This composed of two columns (G1F15 and G2F15), were replaced the fine aggregate by 15% of rubber with different eccentricity (45, and 75) mm, respectively. Table (5-1) shows the outcomes of these columns' ultimate load, axial displacement, and lateral displacement. According to the results of column (G1F15) from group (1), the ultimate load from the FE model, which was 200.167 kN, was less than the ultimate load from the experimental data, which was 204.53 kN by (2.133%). The service lateral displacement of this model was (1.18) % correspondingly more than that of the experimental column. The service axial displacement of this model was (6.15) % correspondingly less than that of the experimental column. Whereas the ultimate load from the FE model, which was 140.807 kN, was higher than the ultimate load from the experimental data, which was 138.58 kN, according to the results of the column (G2F15) from group (2) by

(1.607%). The service lateral displacement of this model was (17.045) % correspondingly less than that of the experimental column. While the service axial displacement of this model was (35.97) % correspondingly more than that of the experimental column. Additionally, it should be noted that for G1F15 and G2F15, the numerical values of ductility in the (axial or lateral) displacement of this column specimens are higher than the experimental values by (2.56 and 35.97) % or (1.18 and 17.045) %, as shown in Table (5-2). Finite element results of load displacement for column specimens (G1F15 and G2F15) from both groups (1 and 2) are compared with experimental data in Figures (5-30), (5-31), (5-32), and (5-33), respectively. Figures (5-34) and Figure (5-35), which depict the failure modes for columns specimens of both groups (1 and 2) resulting from FEA generated from plastic strain, respectively. An acceptable match can be shown when comparing the load-displacement curves produced from the experimental data with those achieved from the finite element models. The distinction is that the post-peak deformations following failure loads as depicted in the figures were not recorded in the analytical results. The failure in the mid-height region and the area close to the corbel column can be seen in Figures (5-36) to (5-37), and this is nearly equivalent to the experiment specimen.

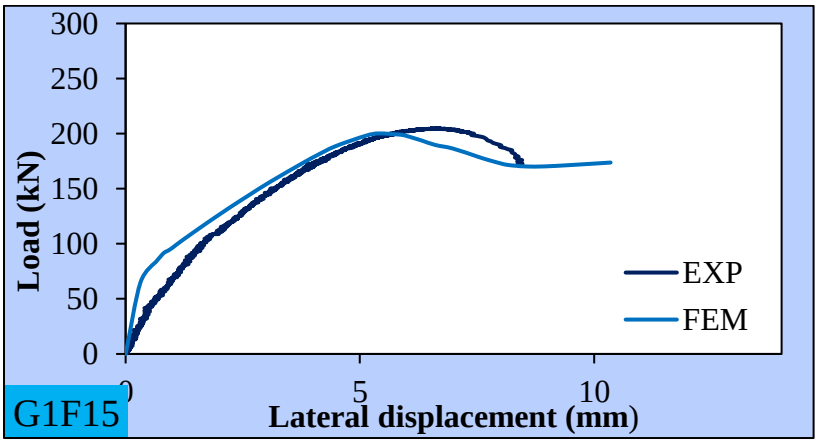

Figure (5-30): Load-lateral displacement relationship for G1F15 specimens.

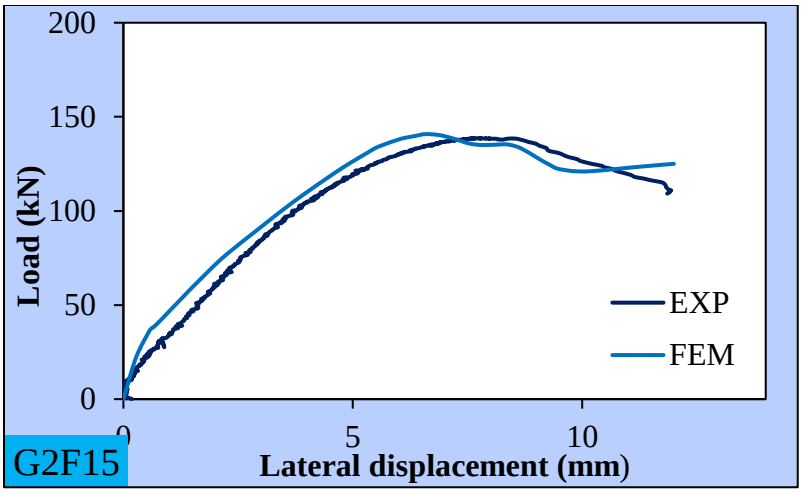

Figure (5-31): Load-lateral displacement relationship for G2F15 specimens.

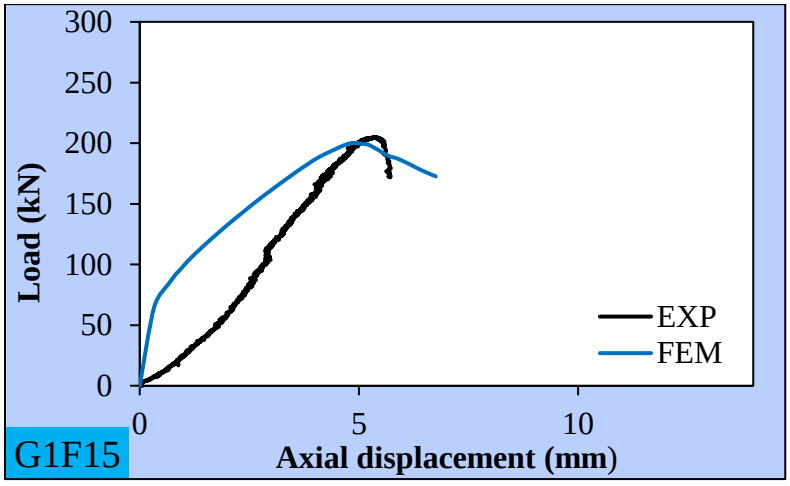

Figure (5-32): Load-axial displacement relationship for G1F15 specimens.

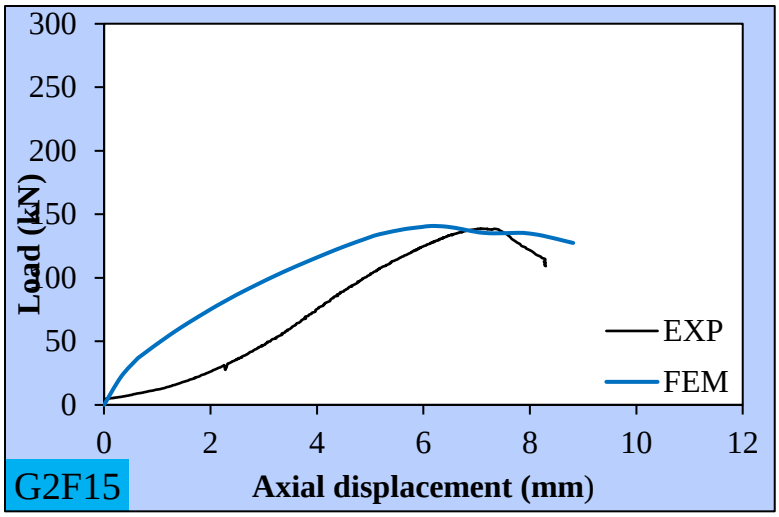

Figure (5-33): Load-axial displacement relationship for G2F15 specimens.

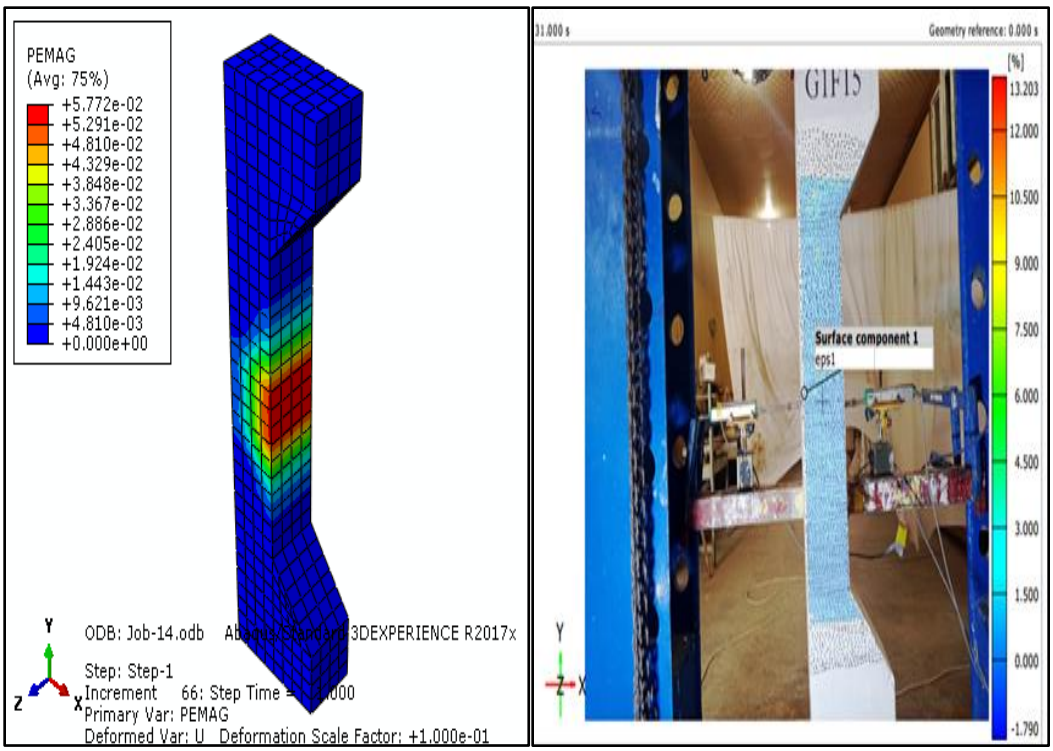

Figure (5-34): Plastic strain distribution of G1F15 column.

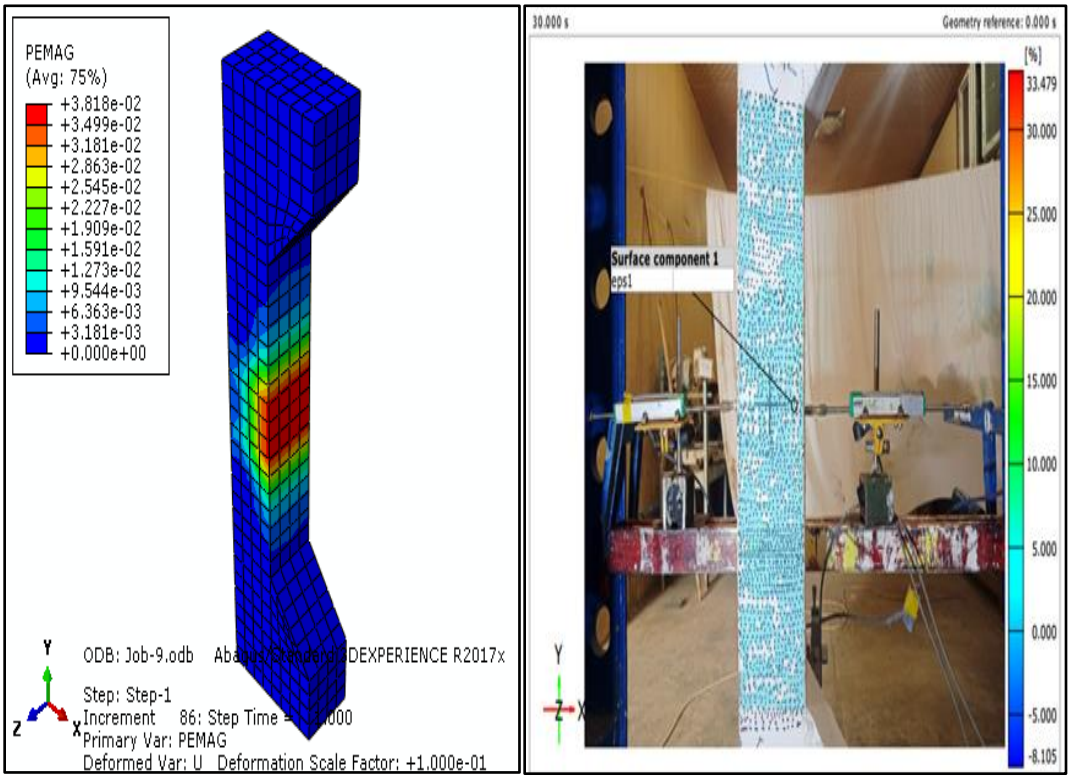

Figure (5-35): Plastic strain distribution of G2F15 column.

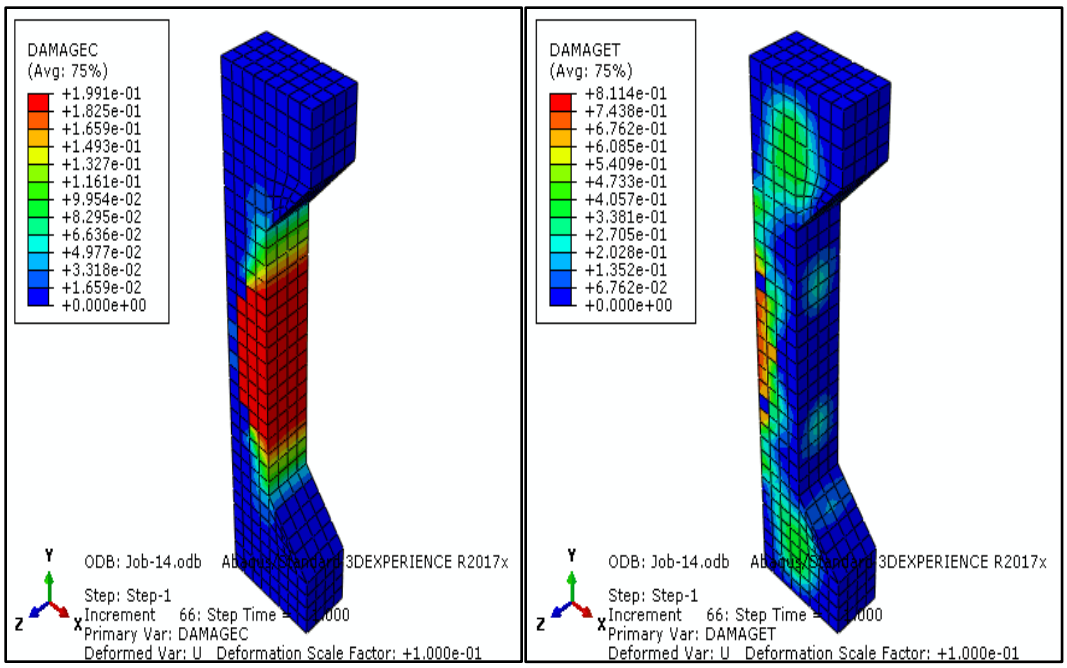

Figure (5-36): Concrete damage plasticity distribution (tensile and compressive damage variable) of G1F15 column.

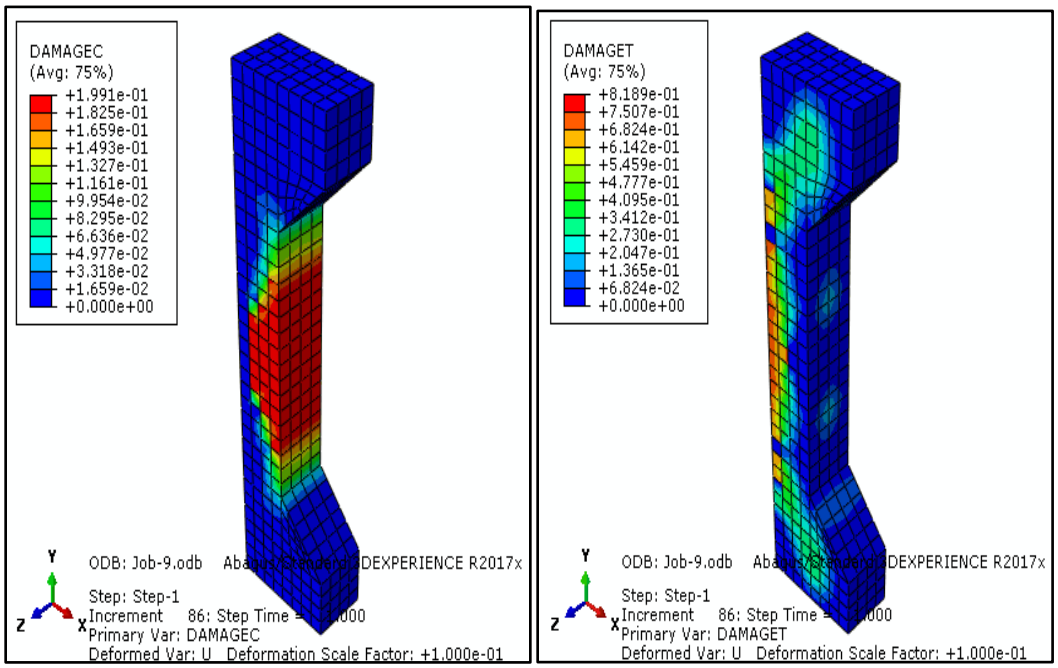

Figure (5-37): Concrete damage plasticity distribution (tensile and compressive damage variable) of G2F15 column.

5-7 Parametric Study

This section's main goal is to investigate how numerous important elements affect the behavior of normal and rubberized concrete columns. Due to time constraints, costs, and the difficulties of testing such a large number of models, experimental work was unable to fully examine all of the significant parameters. Therefore, the effect of some parameters that were not executed in the experimental program was studied. These parameters are as follow: -

1- Percentage of steel reinforcement.

2- Support condition.

5-7-1 Percentage of steel reinforcement

The ratio of reinforcement, in terms of load bearing capability, is one of the most significant elements affecting all structural parts, especially in places subjected to tension stresses, like the columns in this study where it has eccentric load. We tested two groups of specimens in the experimental models with the same reinforcement ratio and number of bars (use 4Ø10 for all specimens). In addition to the ratio employed in the experimental models and with the same number of reinforcing bars, two additional steel percentages are discussed in this section. Where the armament is (4Ø8, 4Ø14). The outcomes of the numerical analysis of the model groups mentioned above are shown in Table (5-3). According to Figures (5-38), (5-39), and (5-40), increasing the steel ratio of the column from (0.021 to 0.043) mm resulted in the following: a significant increment in the maximum load of about (20.49) % for G1N specimens, about (29.26) % for G1F10 specimens, and about (20.20) % for G1F15 specimens, respectively; a definite increase in axial deformations at ultimate loads of about (8.38) % for G1N specimens, about (6.74) % for the G1F15 specimen, but noted a decrease approximately (13.80) % for the G1F10 specimen. At ultimate loads, there is a noticeable decrease in lateral

displacement of about (15.04) % for the G1N specimen, and approximately (8.05) % for the G1F10 specimen, and about (18.22) % for the G1F15 specimen. While decreasing the steel ratio of the column from (0.021 to 0.014) mm resulted in the following: a significant decrement in the maximum load of about 15.24% for G1N specimens, about (20.28) % for G1F10 specimens, and about (32.46) % for G1F15 specimens, respectively; a definite increase in axial deformations at ultimate loads of about (8.86) % for G1N specimens, and about (6.55) % for the G1F15 specimen, there is a noticeable decrease approximately (17.33) % for the G1F10 specimen. At ultimate loads, there is a noticeable increase in lateral displacement of about (8.99) % for the G1N specimen, there is a noticeable decrease approximately (10.74) % for the G1F10 specimen, and about (18.97) % for the G1F15 specimen. The ratio 0.043 has more stiffness than other ratios and this stiffness clear in Figure (5-38). The load capacity of the three models with varying steel ratio and its impact on the capacity of normal and rubberized columns are shown in Figure (5-40). Figures (5-41) to (5-49) shown the variation of displacement and plastic strain (PEMAG) for control column (G1N) and rubberised columns (G1F10), and (G1F15) with different steel ratio.

Table (5-3): Analysis of the reinforcement ratio parameter's results.

Columns Symbol	Steel ratio (mm)	Load Carrying Capacity Pu (kN)	Percentage of reduction	Ultimate lateral deformation (mm)	Percentage Difference	Ultimate axial deformation (mm)	Percentage Difference %
G1N	0.021	274.36	….	6.78	….	6.32	….
	0.043	330.60	20.49	5.76	-15.04	6.85	8.38
	0.014	232.55	-15.24	7.45	8.99	6.88	8.86
G1F10	0.021	217.48	…..	6.33	…..	6.23	….
	0.043	281.12	29.26	5.82	-8.05	5.37	-13.80
	0.014	173.37	-20.28	5.65	-10.74	5.15	-17.33
G1F15	0.021	204.53	….	6.64	….	5.34	….
	0.043	245.84	20.20	5.43	-18.22	5.70	6.74
	0.014	138.128	-32.46	5.38	-18.97	5.69	6.55

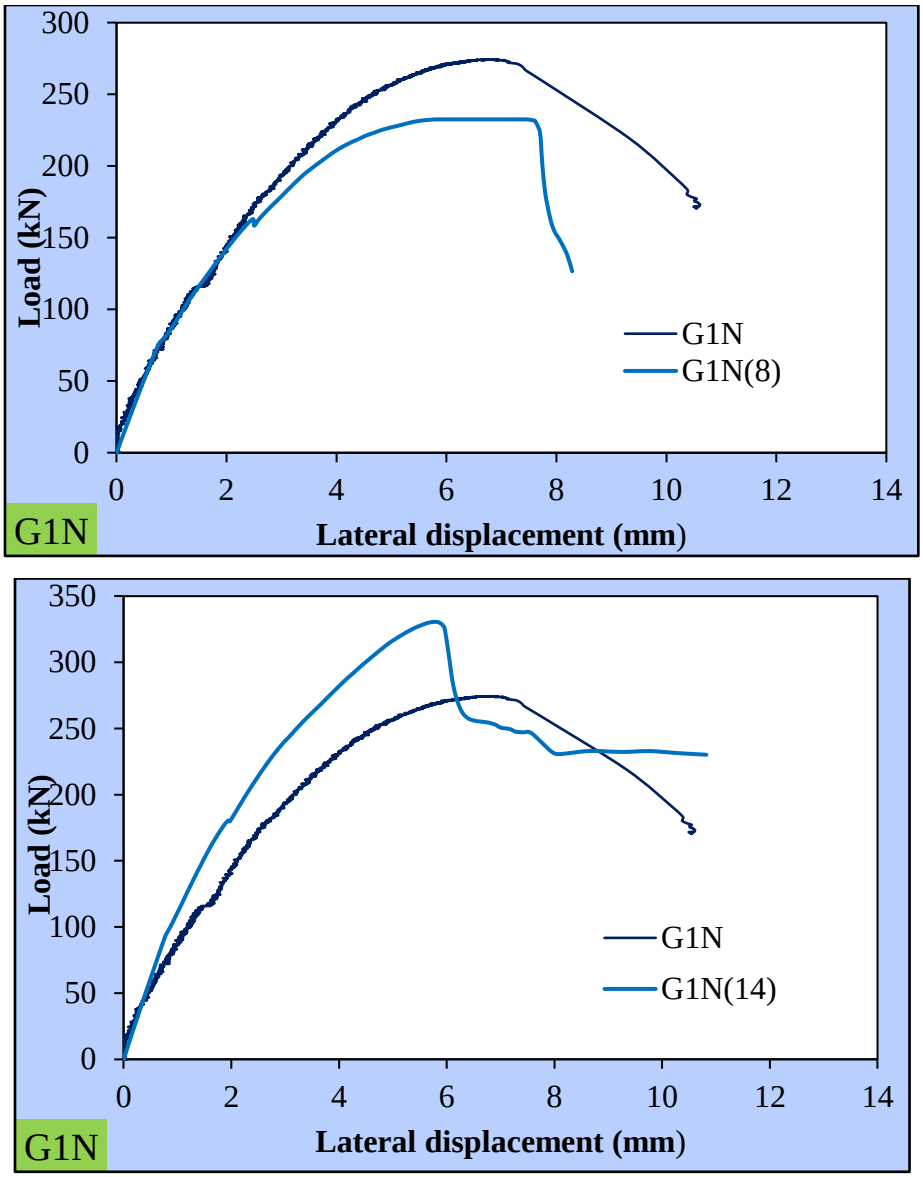

Figure (5-38): Load-Lateral displacement relationship for control columns (G1N) with different reinforcement ratio.

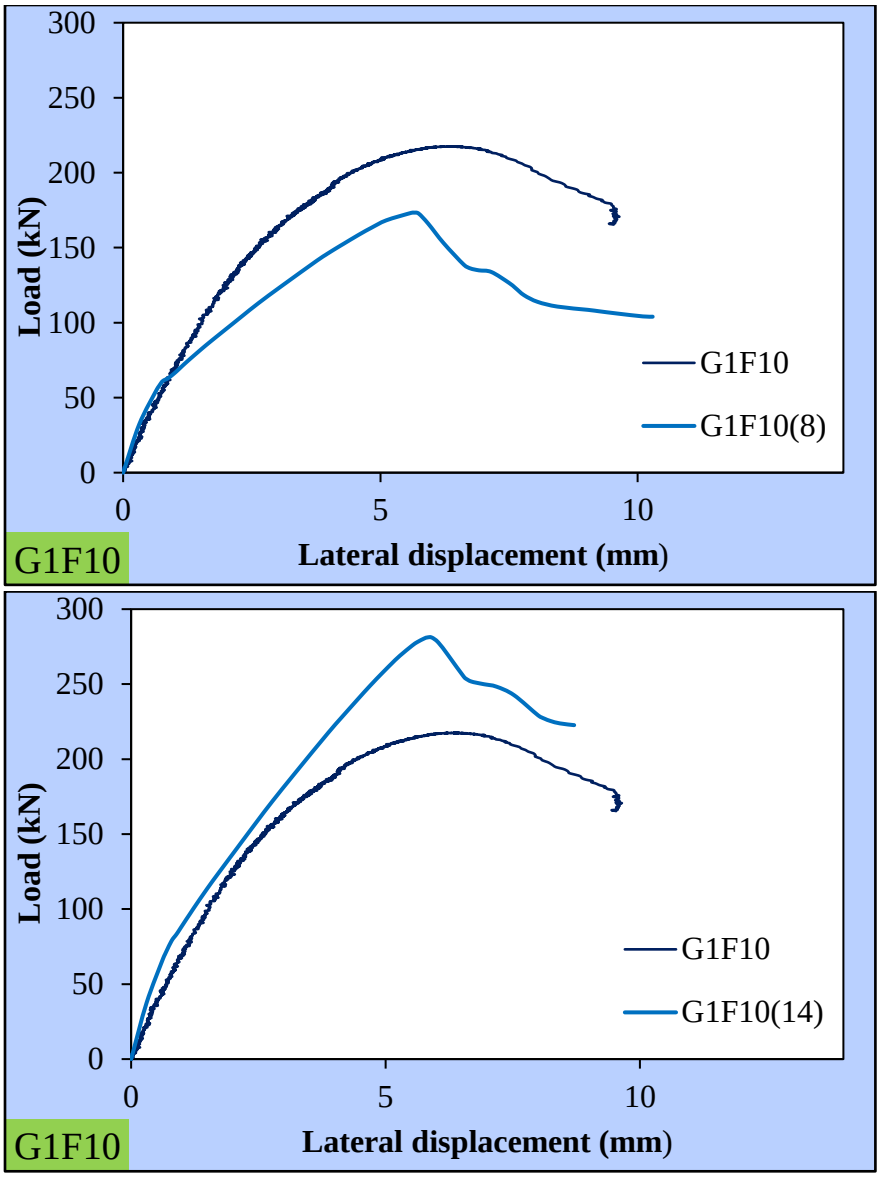

Figure (5-39): Load-Lateral displacement relationship for rubberised columns (G1F10) with different reinforcement ratio.

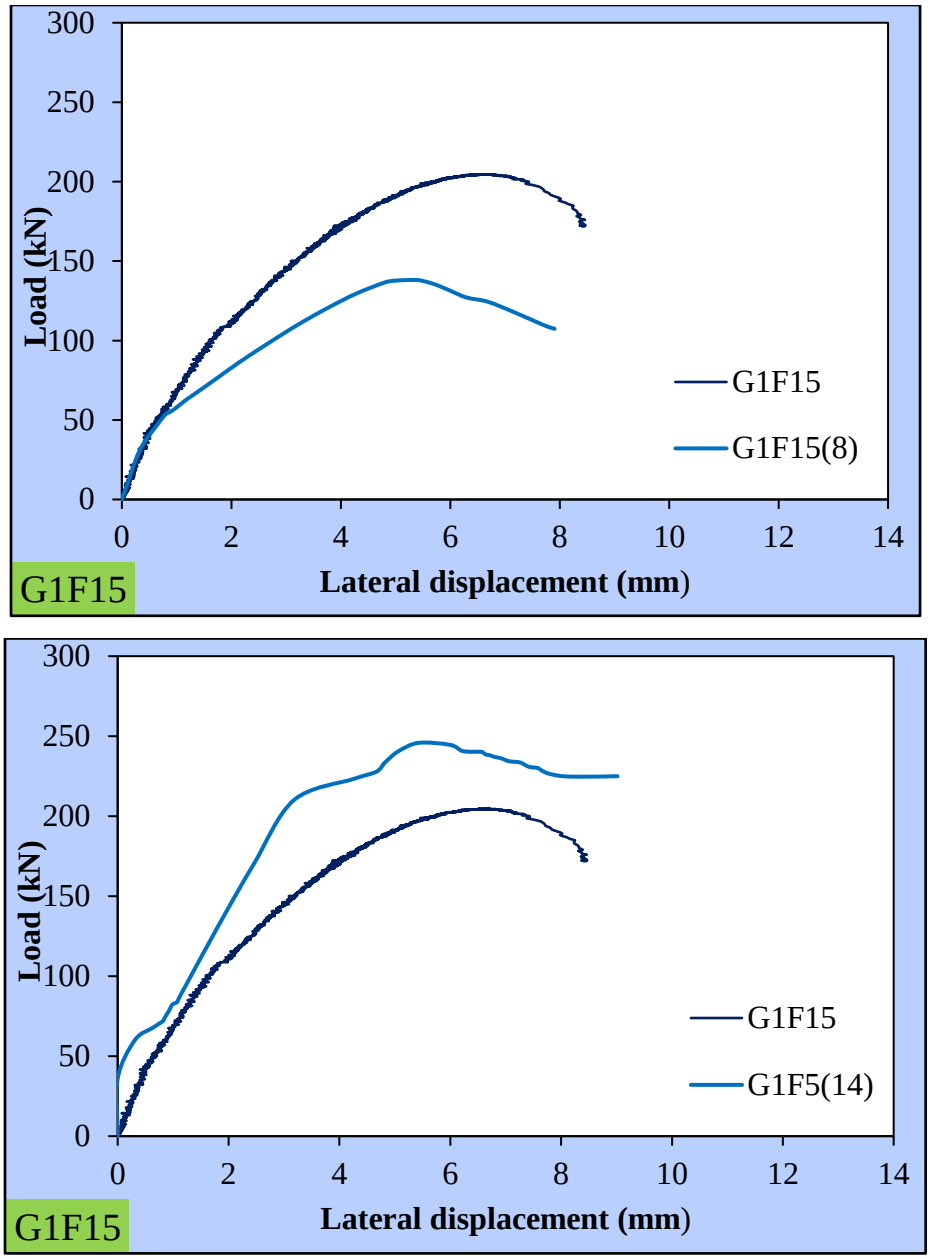

Figure (5-40): Load- Lateral displacement relationship for rubberised columns (G1F15) with different reinforcement ratio.

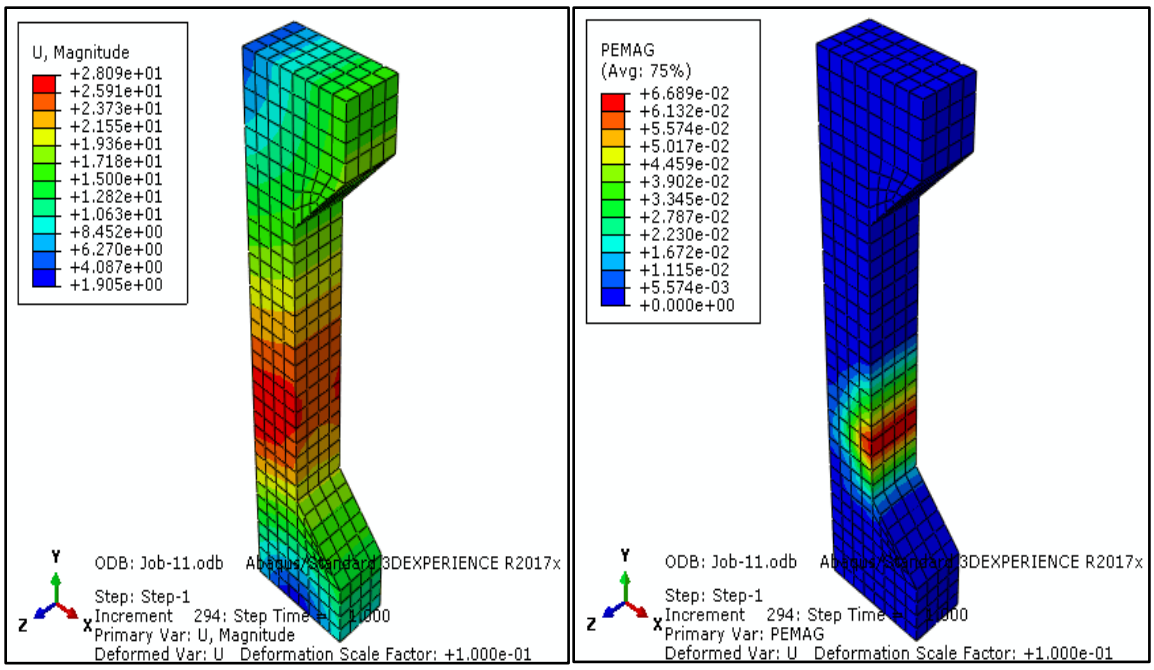

Figure (5-41): Variation of displacement and plastic strain (PEMAG) for control column G1N with (0.021) reinforcement ratio.

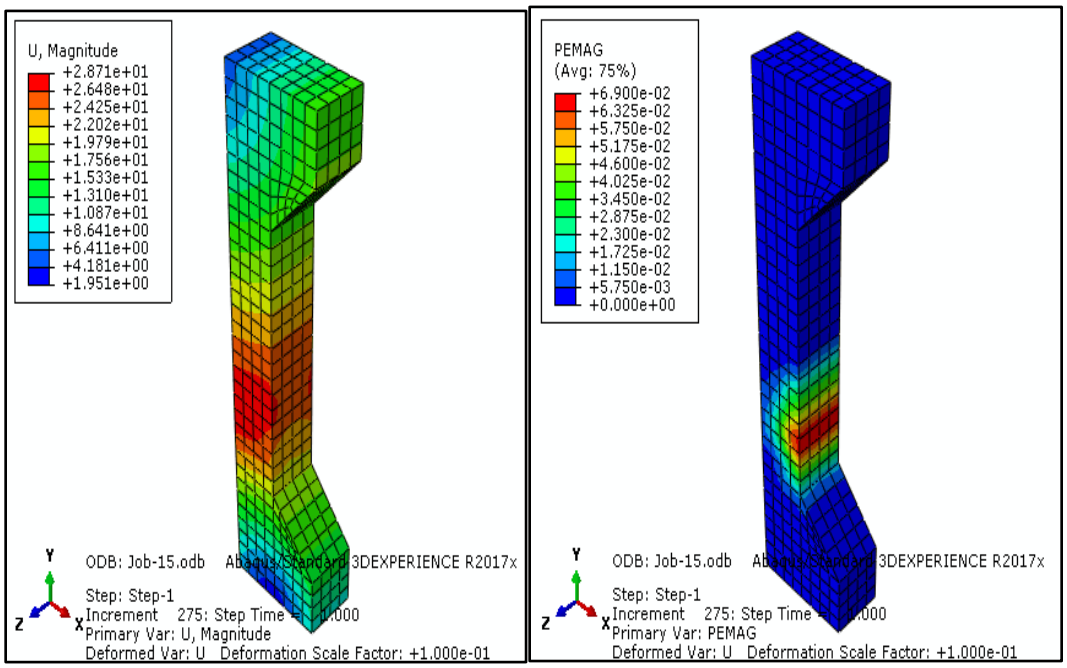

Figure (5-42): Variation of displacement and plastic strain (PEMAG) for control column G1N with (0.014) reinforcement ratio.

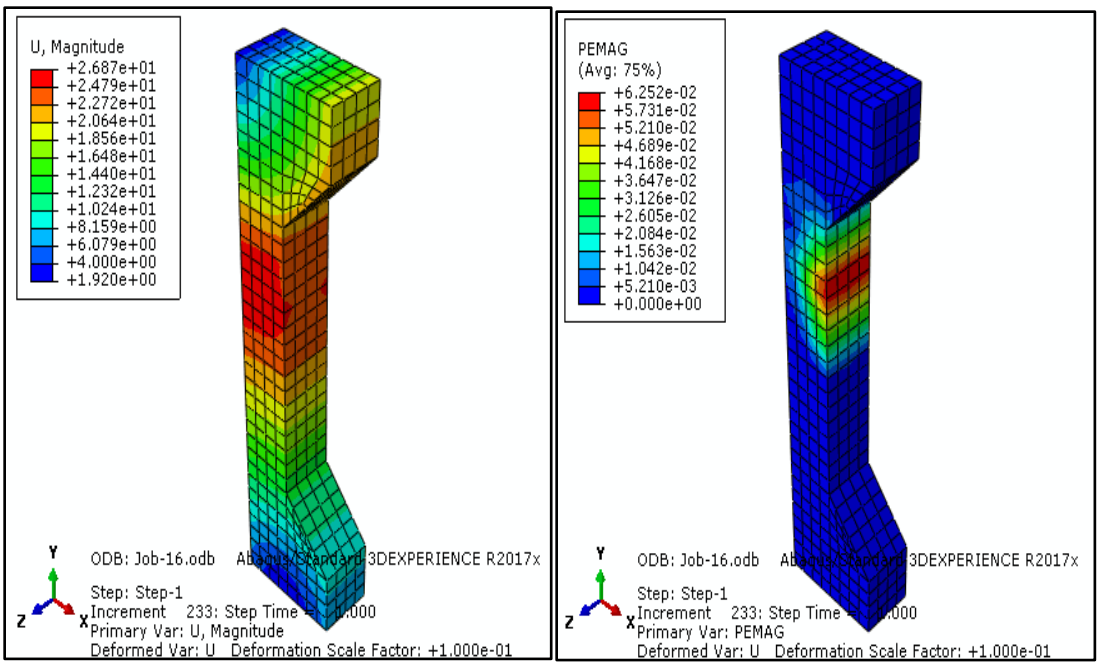

Figure (5-43): Variation of displacement and plastic strain (PEMAG) for control column G1N with (0.043) reinforcement ratio.

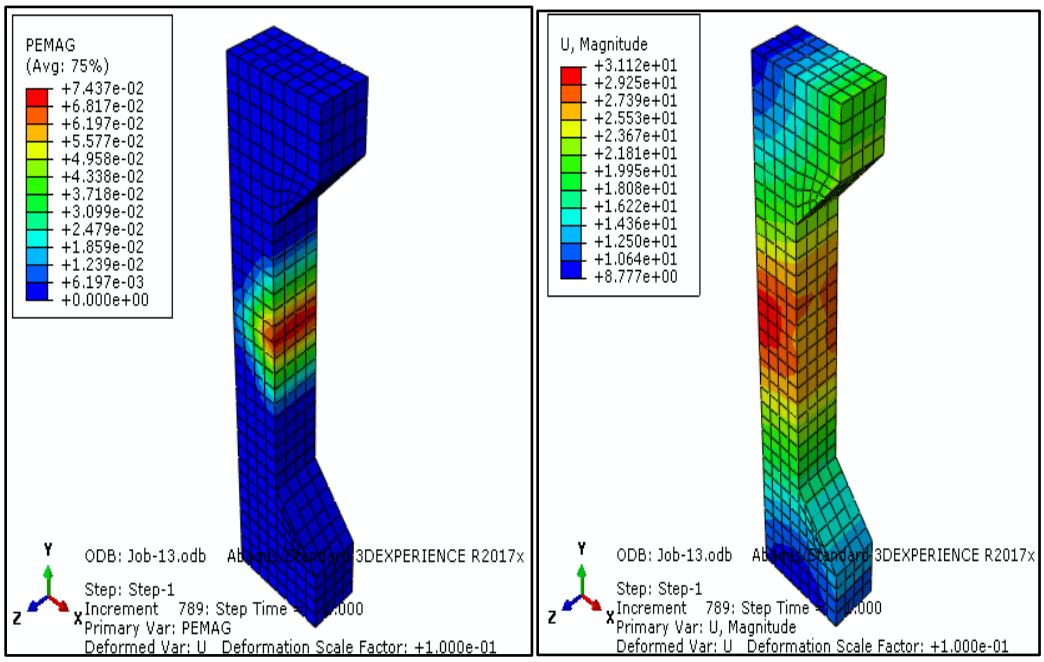

Figure (5-44): Variation of displacement and plastic strain (PEMAG) for column G1F10 with (0.021) reinforcement ratio.

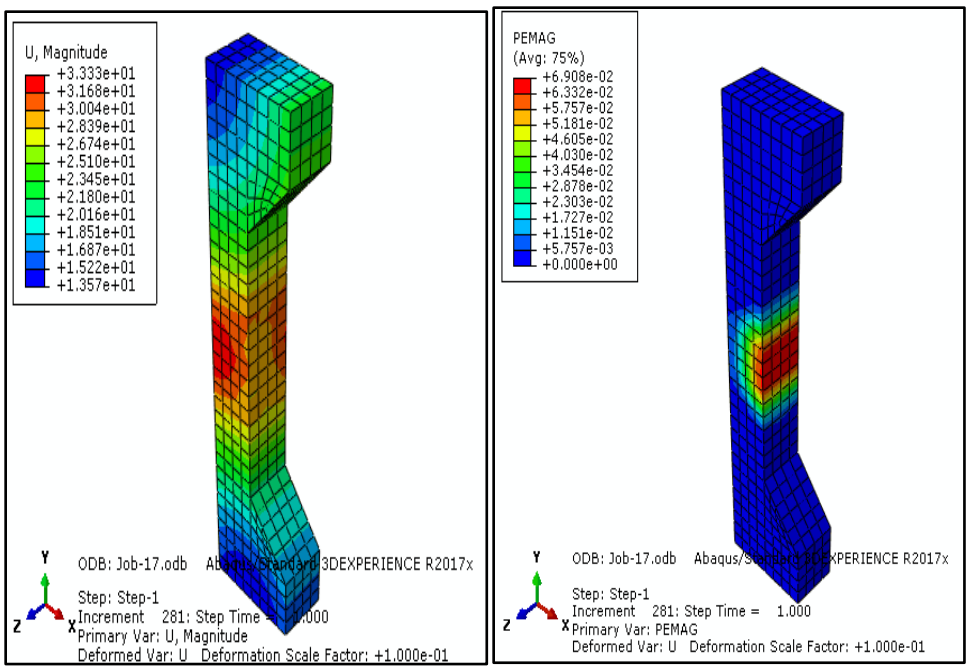

Figure (5-45): Variation of displacement and plastic strain (PEMAG) for column G1F10 with (0.014) reinforcement ratio.

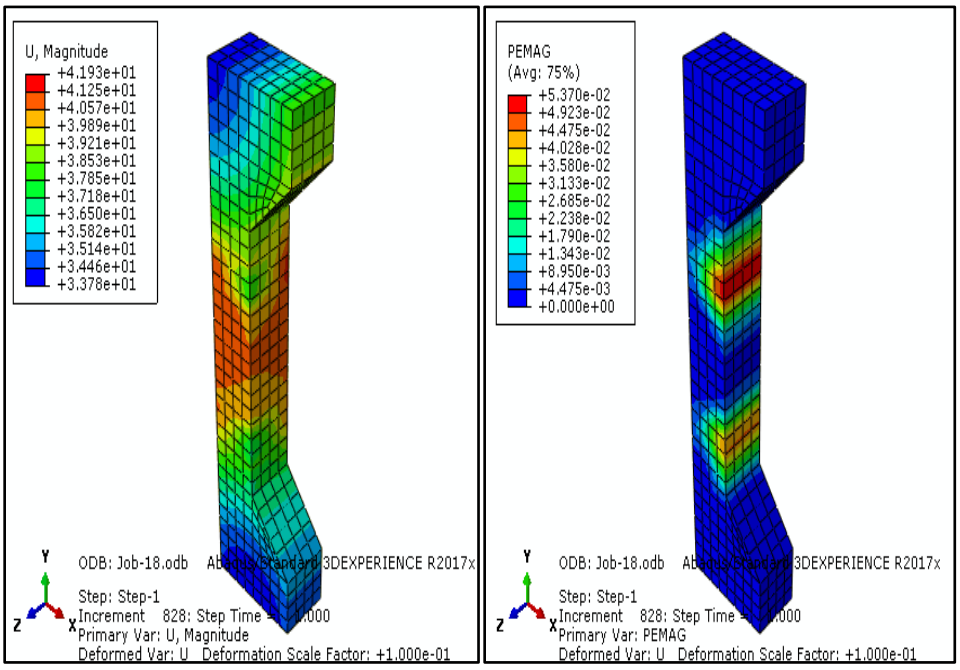

Figure (5-46): Variation of displacement and plastic strain (PEMAG) for column G1F10 with (0.043) reinforcement ratio.

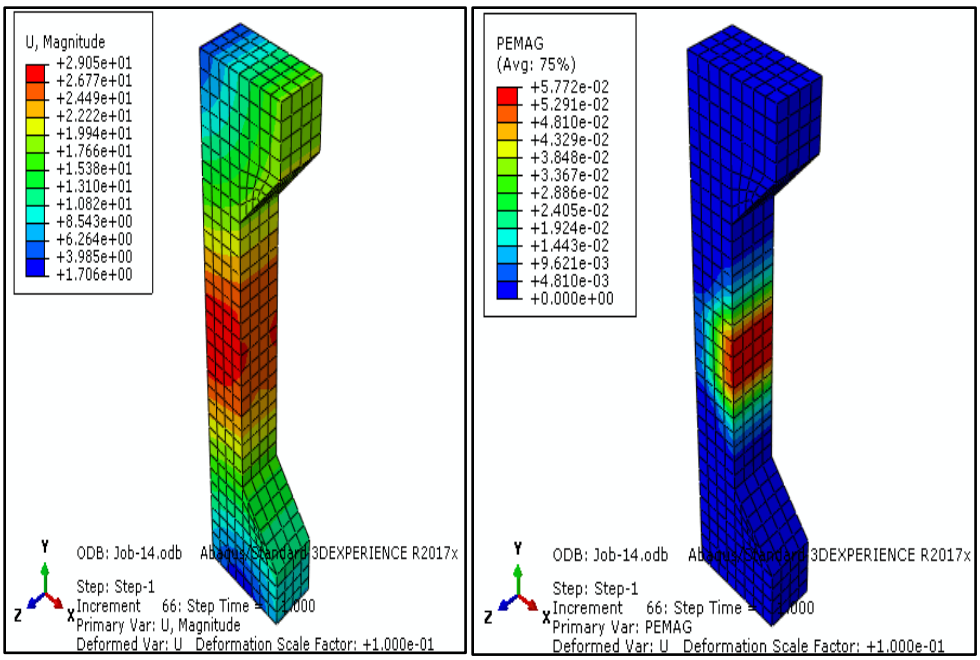

Figure (5-47): Displacement and plastic strain (PEMAG) change of G1F15 column with reinforcement ratio (0.021).

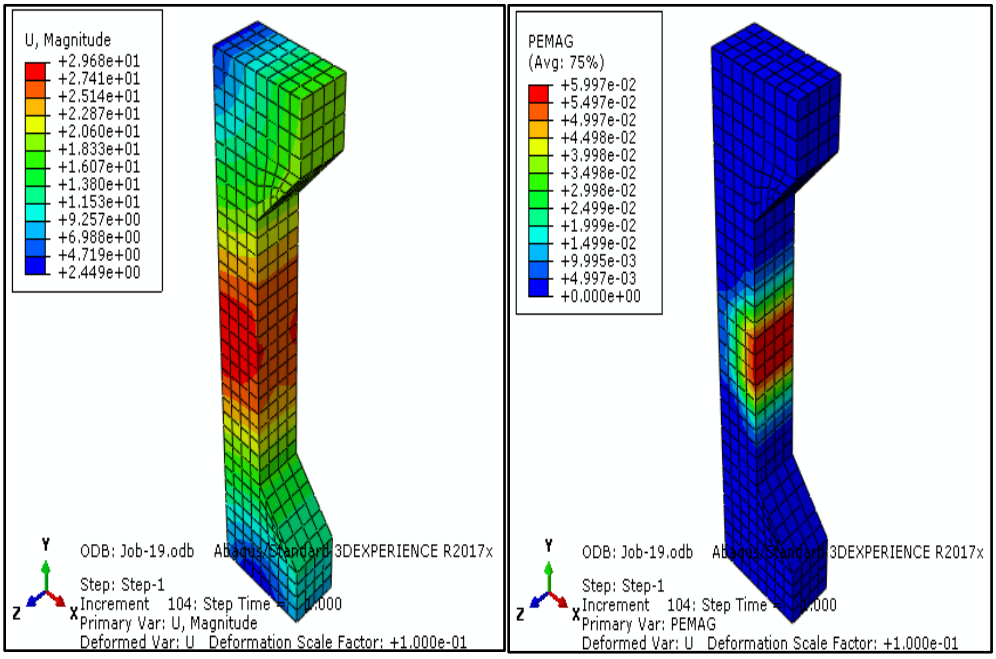

Figure (5-48): Displacement and plastic strain (PEMAG) change of a G1F15 column with reinforcement ratio (0.014).

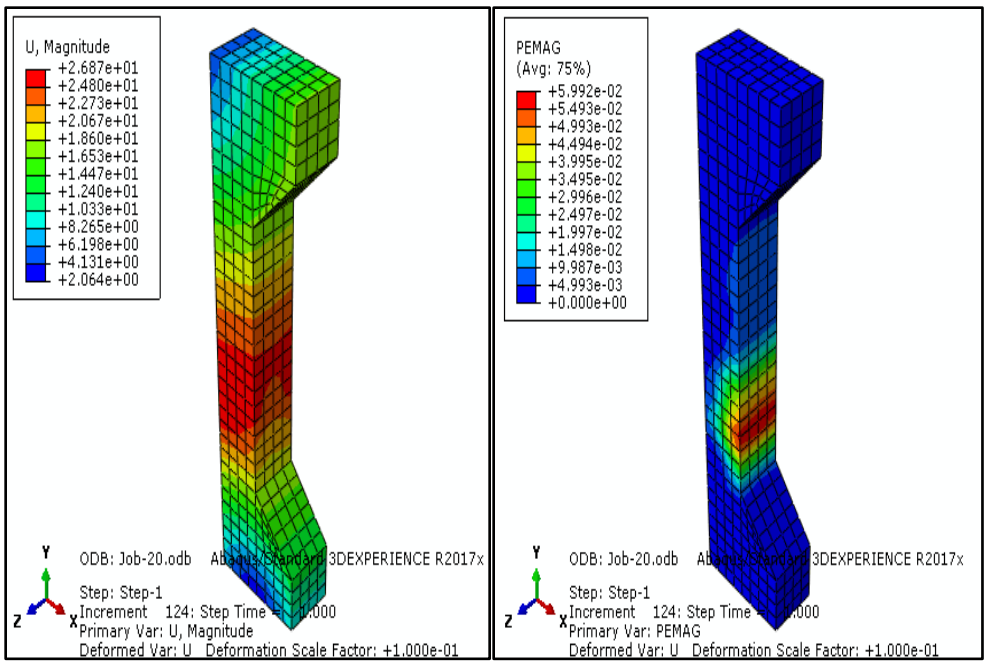

Figure (5-49): Displacement and plastic strain (PEMAG) change of a G1F15 column with reinforcement ratio (0.043).

5.8.2 Support condition

Both the model simulation in the first section of this chapter and the experimental study's support condition are hinge-hinge. This section focuses on analysing the impact of additional support conditions like fixed-fixed and fixed-hinge. The findings of the numerical analysis of models under chosen support conditions are presented in Table (5-4). Compared to other supports, fixed-fixed condition has more stiffness and weight carrying capacity, whereas fixed-hinge support is the weaker of the two. According to the Figures from (5-50) to (5-52), the results were that the changing support condition of columns from hinge-hinge to fixed-fixed led to: a clear decrease of the maximum load about (4.99)% for control column (G1N), about (6.08)% for rubberised column(G1F10), and about (32.46)% for rubberised column (G1F15), a clear decrease in axial and deformations at ultimate loads about (6.78)% for control column, about (3.09)% for rubberised column (G1F10), and about (18.67)% for rubberised column

(G1F15), respectively, and a clear increase in lateral displacement at ultimate loads about (23.89)% for control column (G1N), about (0.16)% for rubberised column(G1F10), but decreased about (8.98)% for rubberised column (G1F15), respectively.

While the results were that the changing support condition of columns from hinge-hinge to fixed-hinge led to: a large decrease of the maximum load about (4.89)% for control column (G1N), about (6.13)% for rubberised column (G1F10), and about (18.26)% for rubberised column (G1F15), a clear decrease in axial and deformations at ultimate loads about (8.11)% for control column, about (2.577)% for rubberised column (G1F10), and about (19.72)% for rubberised column (G1F15), respectively, and a clear increase in lateral displacement at ultimate loads about (23.89)% for control column (G1N), but decrease about (0.16)% for rubberised column (G1F10), and about (21.34)% for rubberised column (G1F15), respectively. Figures from (5-53) to (5-58) show the significant effect of support condition on the behaviour, failure criteria, and displacement of RC column.

Table (5-4): Results of analysis support conditions parameter.

Columns Symbol	Support Condition	Load Carrying Capacity Pu (kN)	Percentage of reduction %	Ultimate axial deformation (mm)	Percentage Difference %	Ultimate lateral deformation	Percentage Difference %
G1N	Fixed-fixed	260.66	-4.99	6.32	-6.78	7.83	23.89
	Fixed -hinge	260.94	-4.89	6.23	-8.11	7.83	23.89
	Hinge -hinge	274.36	……	6.78	……	6.32	……
G1F10	Fixed-fixed	204.256	-6.08	5.64	-3.09	6.24	0.16
	Fixed -hinge	204.138	-6.13	5.67	-2.577	6.22	-0.16
	Hinge -hinge	217.48	……	5.82	……	6.23	……
G1F15	Fixed-fixed	138.128	-32.46	5.40	-18.67	4.86	-8.98
	Fixed -hinge	167.17	-18.26	5.33	-19.72	4.20	-21.34
	Hinge -hinge	204.53	……	6.64	……	5.34	……

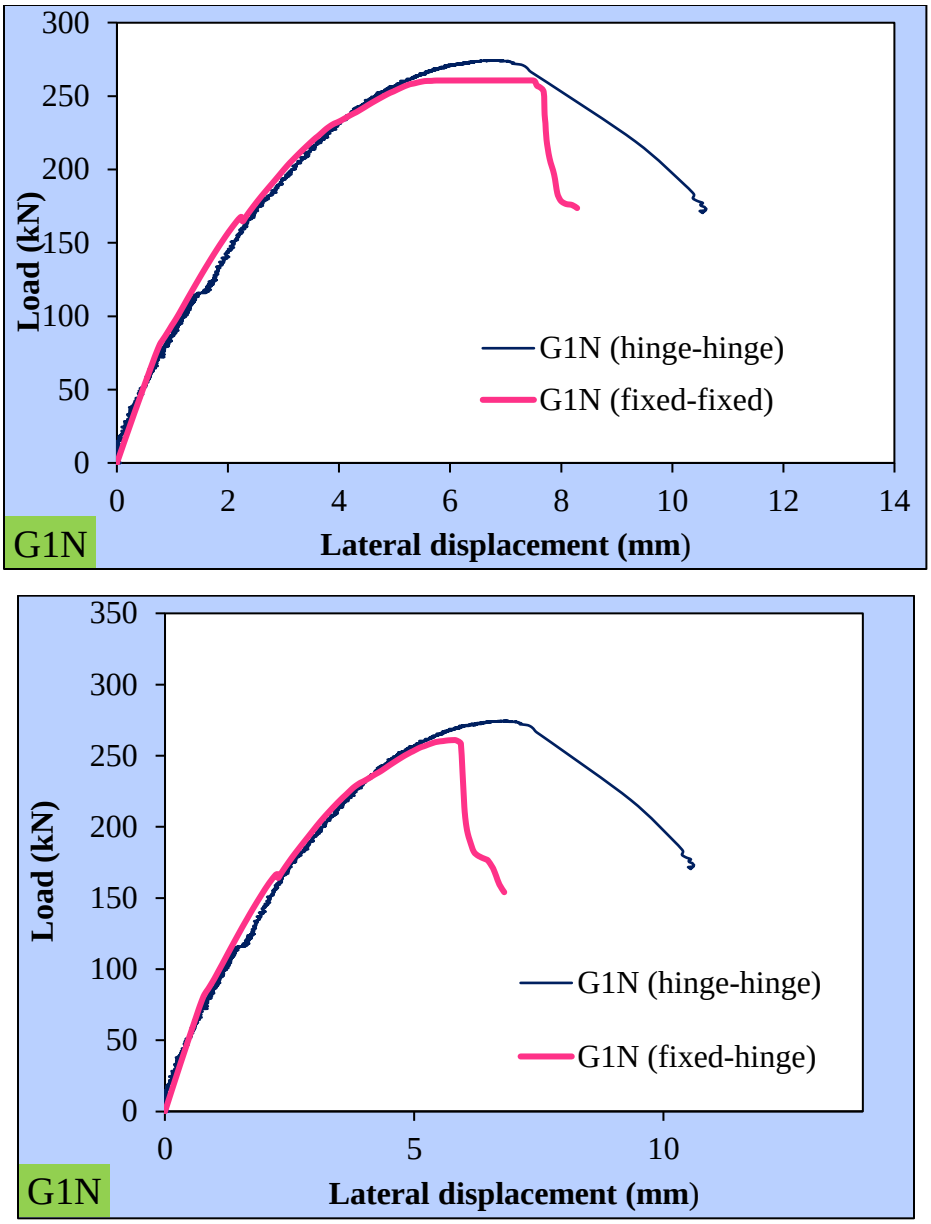

Figure (5-30): Load-lateral displacement relationship for control columns (G1N) with different support condition.

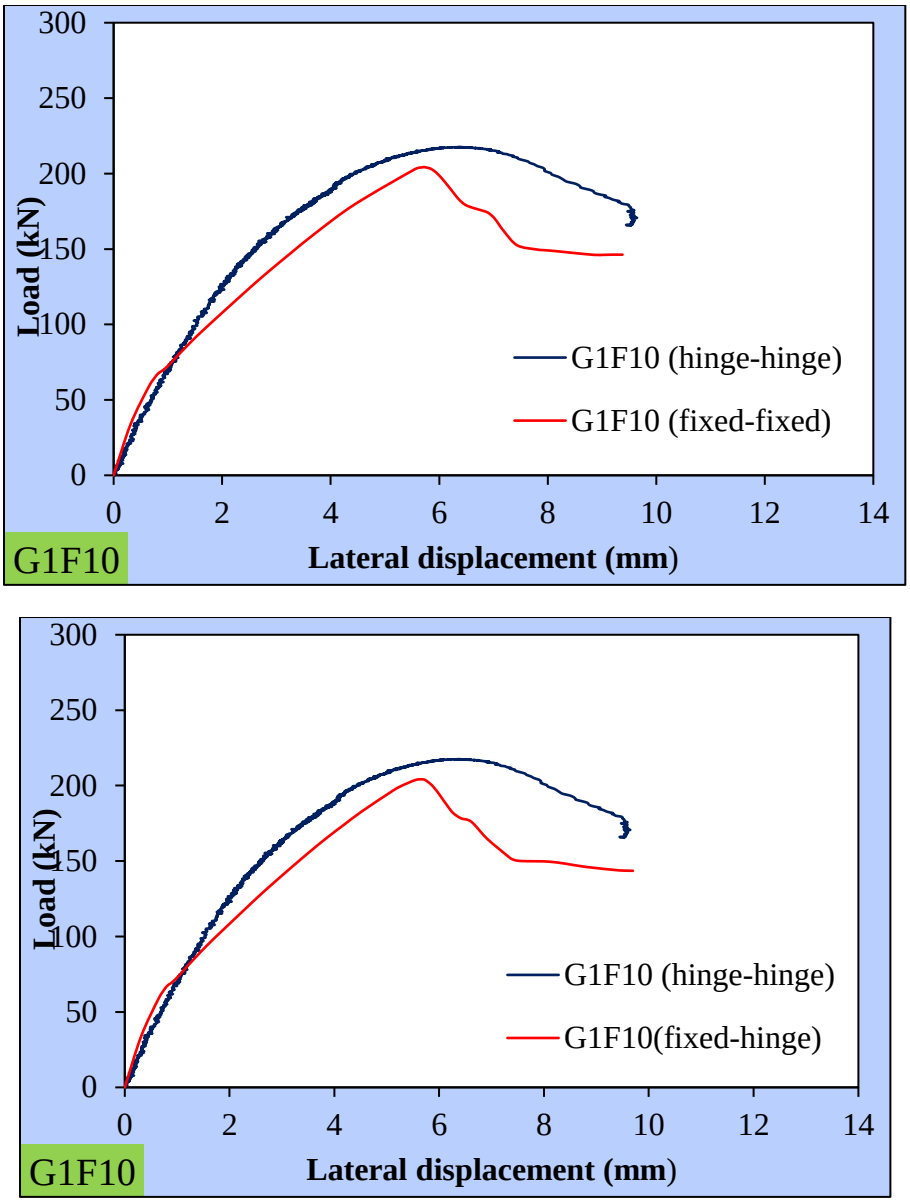

Figure (5-51): Load-lateral displacement relationship for rubberised columns (G1F10) with different support condition.

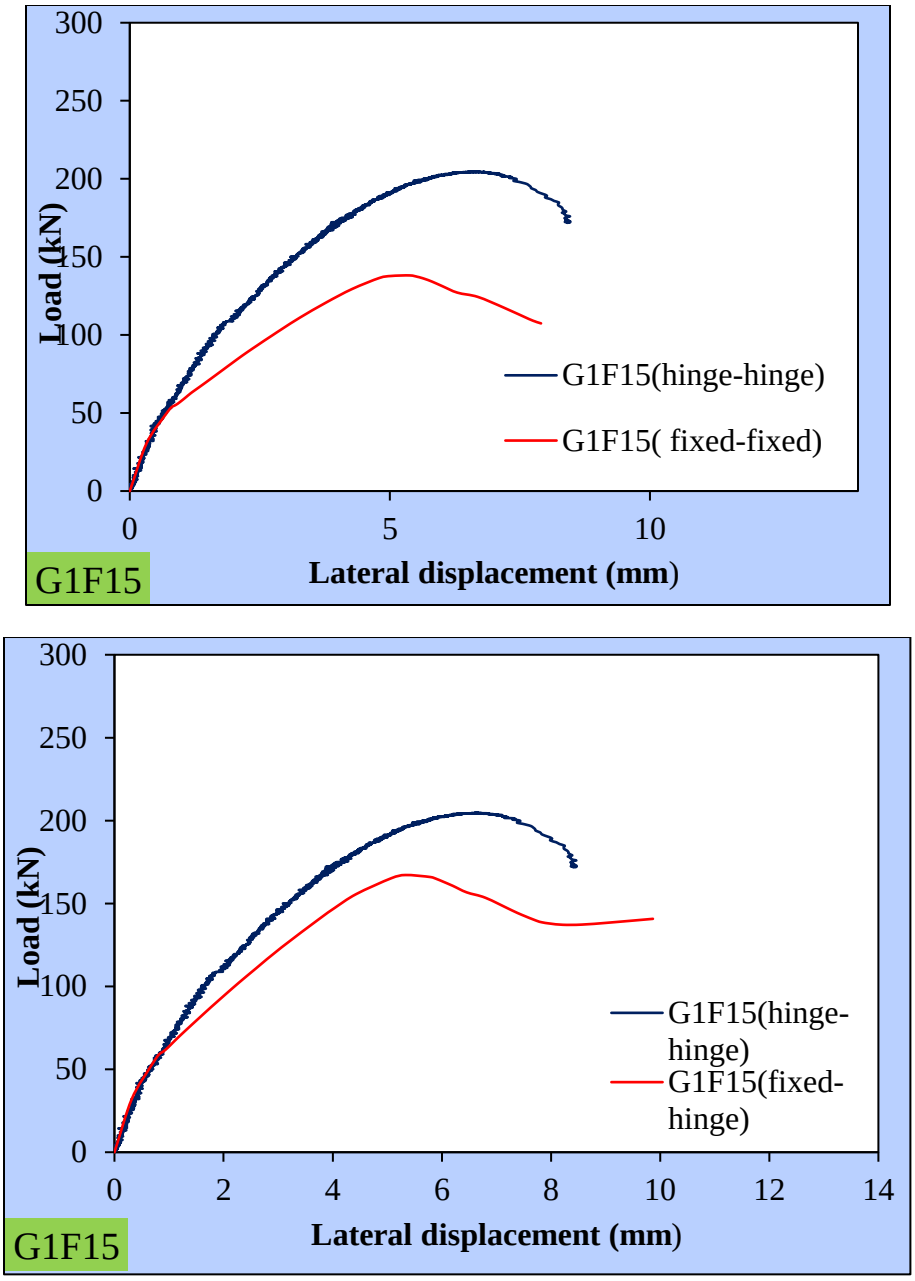

Figure (5-52): Load-lateral displacement relationship for rubberised columns(G1F15) with different support condition.

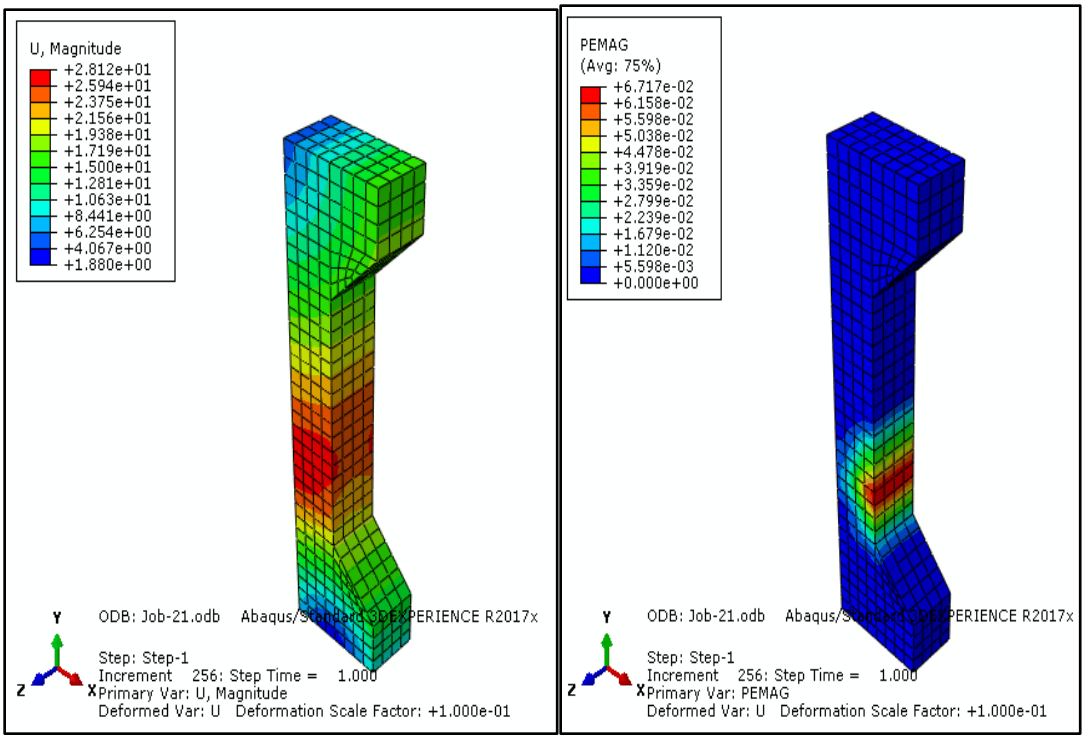

Figure (5-53): Variation of displacement and plastic strain (PEMAG) for control columns (G1N) with fixed –fixed support.

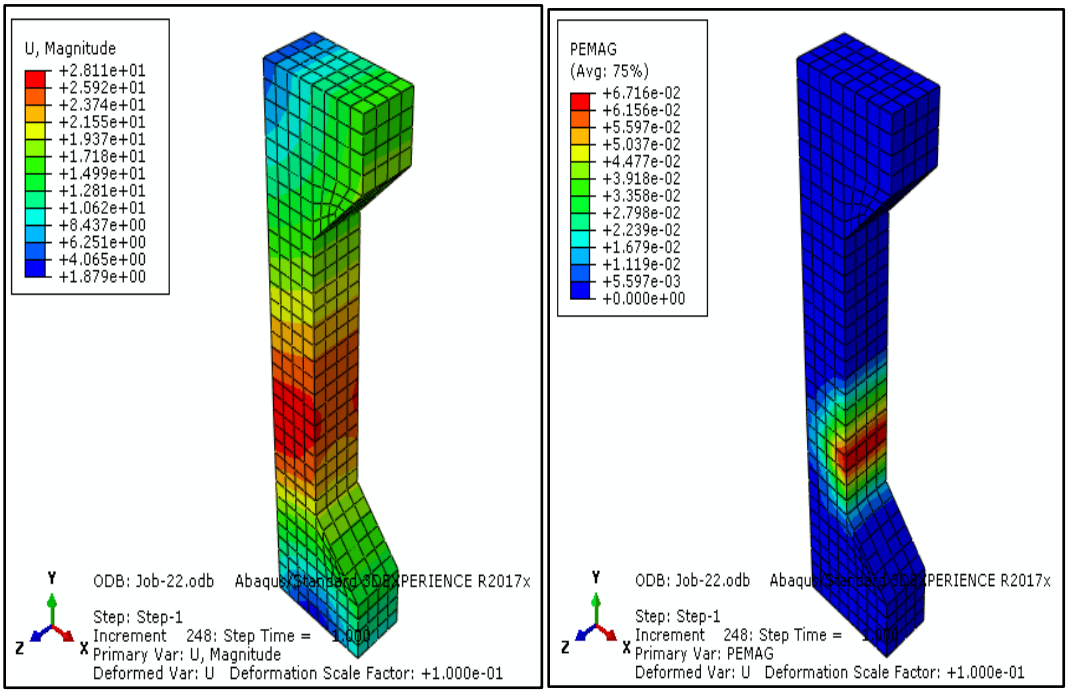

Figure (5-54): Variation of displacement and plastic strain (PEMAG) for control columns (G1N) with fixed –hinge support.

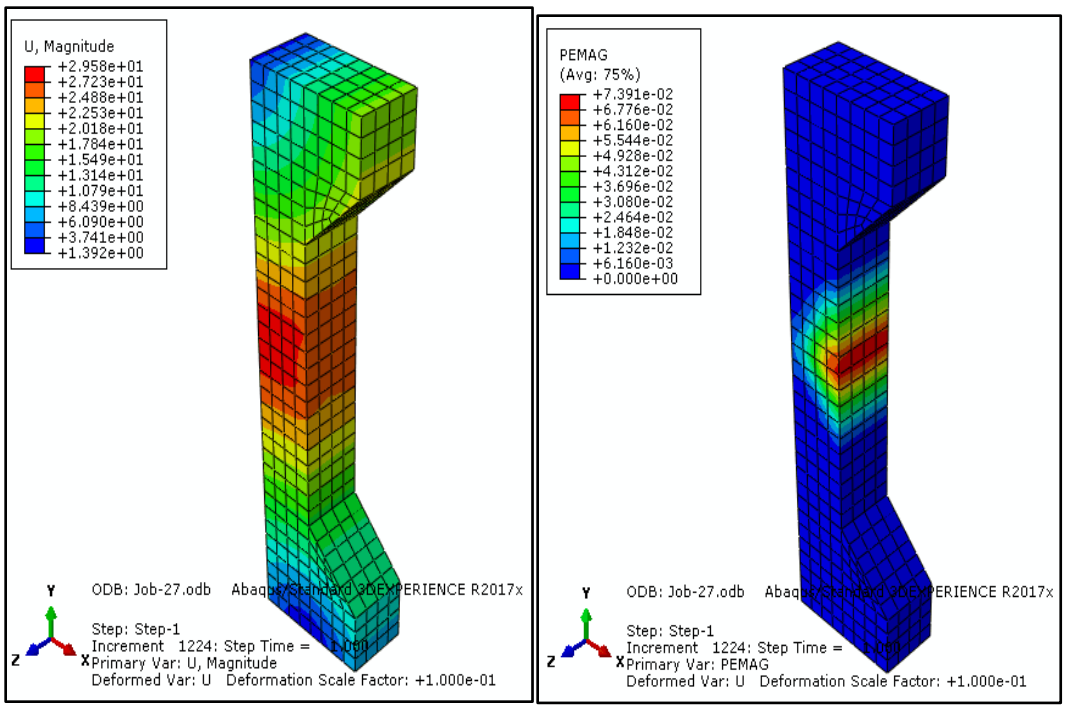

Figure (5-55): Variation of displacement and plastic strain (PEMAG) for rubberised columns (G1F10) with fixed –fixed support.

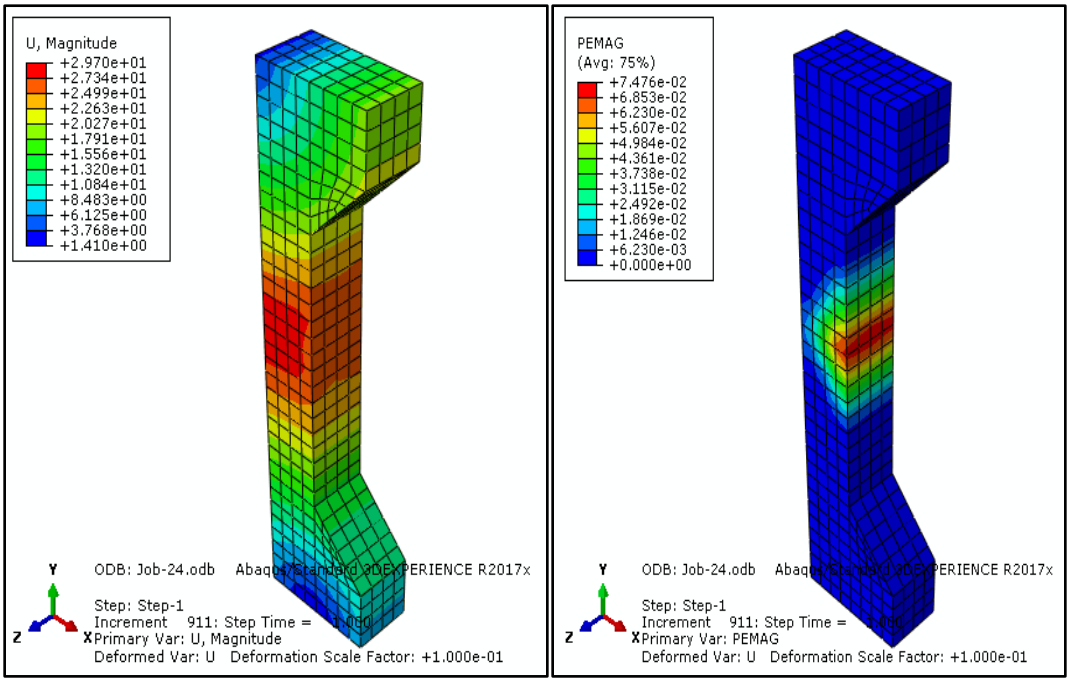

Figure (5-56): Variation of displacement and plastic strain (PEMAG) for rubberised columns (G1F10) columns with fixed –hinge support.

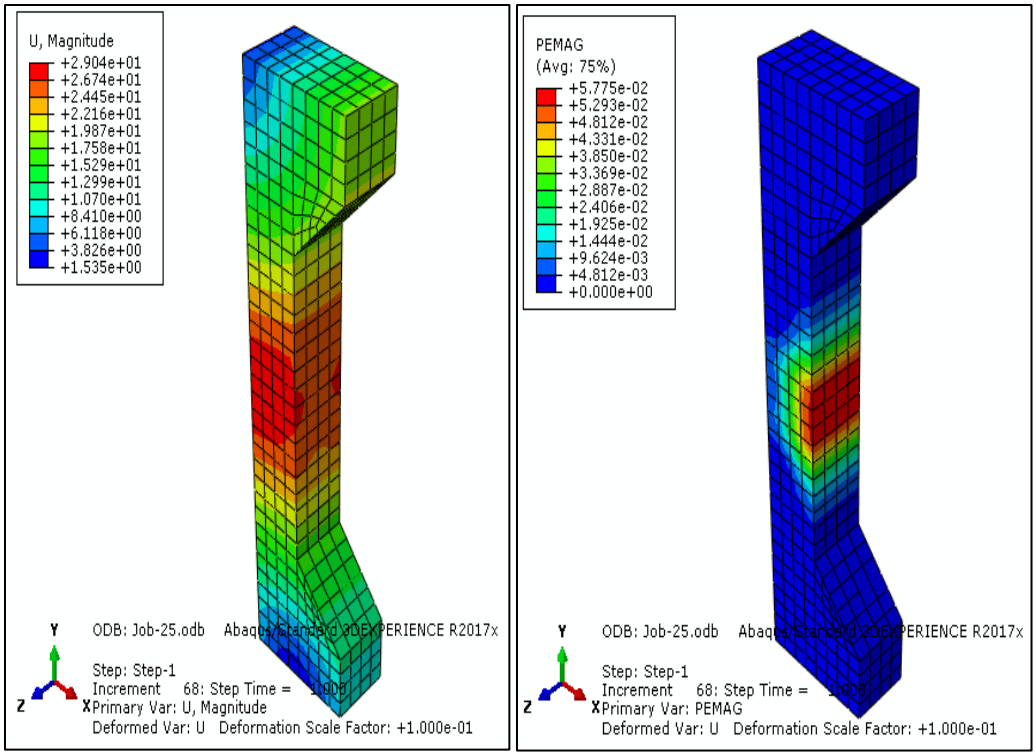

Figure (5-57): Variation of displacement and plastic strain (PEMAG) for rubberised columns (G1F15) columns with fixed –fixed support.

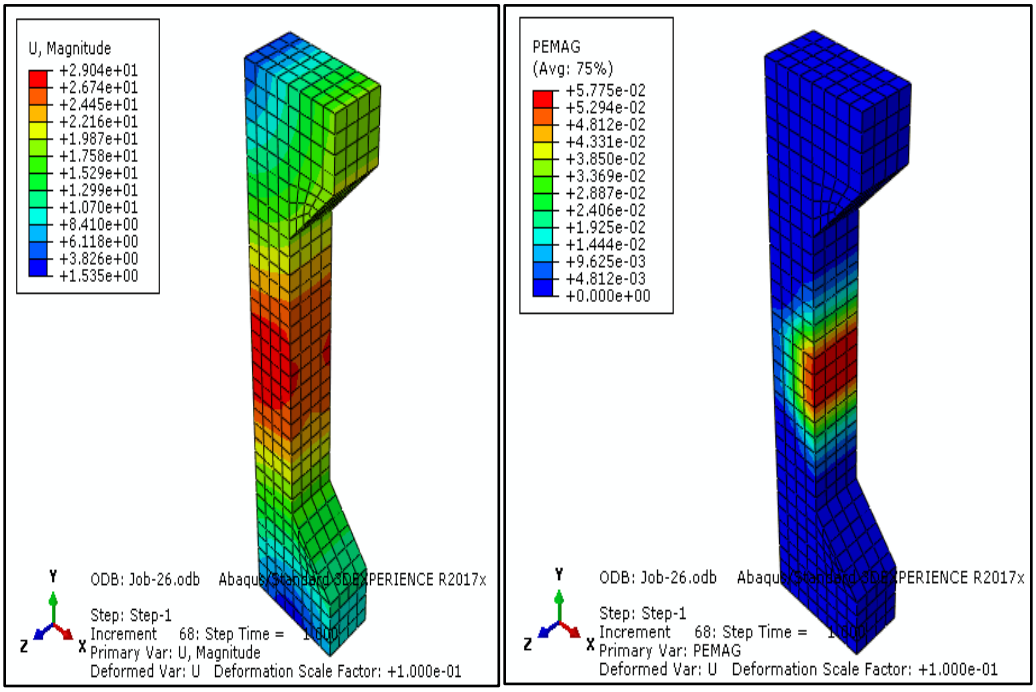

Figure (5-58): Variation of displacement and plastic strain (PEMAG) for rubberised columns (G1F15) columns with fixed –hinge support.

Chapter Six

Conclusions and Suggestions for Future Work

6-1 Introduction:

The primary findings of this study are presented in this chapter along with experimental and analytical conclusions and recommendations for future investigations.

6-2 Conclusions

The conclusion that can be drawn from experimental and numerical study is as follows:

6-2-1 Fresh Properties of Rubberized Concrete mixes

1- The same standard methods used for regular ordinary concrete can be employed to mix rubberized concrete.

2- By increasing the volume ratio of rubber substitute to natural aggregate, the workability is reduced. Compared to conventional concrete, the slump value of the mixture with 15% rubber particles instead of fine aggregate (F15) was increased by about 10%. Compound F10 also has a 10% lower setpoint compared to conventional compounds.

6-2-2 Hardened properties of rubberized concrete mixes

1. The number of blows from the blow initiating the initial fracture to the final crack increased slightly as waste tire rubber replacement increased, indicating that rubberized concrete is more ductile than regular concrete and that concrete brittleness has decreased.
2. The mechanical characteristics and behavior of the rubberized concrete are impacted by the presence of rubber. When crumb rubber was used in place

of the natural aggregates in the reference mixture, the fc′, ft, and fr decreased. When the replacement ratio for wasted tire rubber increased, a slow and continual loss of mix strength occurred. The mechanical parameters of rubberized concrete containing 15% crumb rubber are reduced by (33.49 and 28.10) % for compressive strength and splitting strength, respectively, compared to standard concrete mixtures.

3. The maintenance performance of the old tire replacement rate (5) % is close to that of ordinary concrete, and the ductility and energy absorption are better.

6-2-3 Experimental work of rubberised concrete columns behavior

Experimental work of rubberised specimens' behavior:

1- Rubber can be used to produce sustainable reinforced concrete columns with accepted structural response.
2- The failure load of the reinforced concrete columns reduces with the ratio of changing the crumb rubber instead of the fine aggregate.
3- Using of rubber delays instead of natural aggregate retards the first flexural and diagonal crack initiating in the rubberised concrete columns.
4- Increasing the proportion of crumb rubber from 0% to 15% reduces the width of ultimate failure cracks while increasing the frequency of cracks after rubber substitution.
5- The ultimate load capacity decrease with increasing rubber content from 0 % to 15 % with the two value of eccentricities (45 and 75) mm by (25.45 and 12.88) %, respectively. Also, with the increasing eccentricity (e) from 45 mm to 75 mm, the ultimate load capacity decreased by (42.02, 40.41, 36.52, and 32.24) % for the columns without rubber, columns with 5%

rubber, and columns with 10% rubber, and columns with 15 % rubber, respectively.

6- the ratio of crumb rubber to fine aggregate substitution reduces the failure load of reinforced concrete columns, as well as, a significant development in cracking load, and ductility compared with the same specimen without replacement.

7- The rubberized members generated a relatively soft post-peak response, indicating a more ductile reaction as compared to conventional RC, according to the test results. Show a modification in ductility ratio in lateral displacement with a percentage of crumb rubber of 15% by around (100.64 and 109.33) % for specimens (G1F5, and G2F5) with eccentricities of (45 and 75) mm, respectively. Therefore, it is important to determine the effect of this local material behaviour on the overall ductility of the reinforcement.

8- While the stiffness of the column specimens that were replaced with rubber after applying load at various levels deteriorated dramatically as the applied load level increased. For specimens loaded with 15% of crumb rubber with eccentricities of 45 mm and 75 mm, The lateral displacement stiffness decreased by (87.73 and 86.07) % with increasing load and increasing rubber content, respectively.

9- The ultimate capacity provided by the American (ACI 318-9) is underestimated and more cautious.

6-2-4 Conclusions from Numerical Study

1- 3D Nonlinear Finite Element Analysis (FEA) Using the computer program ABAQUS/Standard (6.14), it is possible to compare the experimental

results of the analysis with simulations based on maximum failure loads. The difference is approximately (7.19%).

2- For the majority of the chosen column specimens, the numerical failure modes of the FE analysis that were derived from plastic strain were close to the failure modes in the experimental test.

3- For the concrete column with or without rubber, measurements of the mechanical characteristics of the concrete using disintegration tests in conjunction with the ABAQUS program provided satisfactory estimates for the load-displacement response, and ultimate load.

4- The result of the control column (G1N) from the group (1), shows the ultimate load (261.348 kN) from the FE model is close with the ultimate load of (274.36) kN from the experimental data.

5- The ultimate load from the FE model, which was 269.106 kN, was higher than the final load from the experimental data, which was 258.06 kN by (4.280%), according to the results of column (G1F5) from group (1) with eccentricity 45mm.

6- The load-displacement relationships of columns with 5% crumb rubber which created the impression that experimental columns were stiffer than numerical analytical columns.

7- The increase in rubber content led to decrease the ultimate load of columns, leading to most damage in RuC column, thus reduced the capacity of tested columns.

8- The maximum strain was in the middle third of the column, and this failure approximated that of the tested column when spalling occurred in the center of the RuC column's compression face. As was the case in the tested column where the shape of failure varied from column to column

depending on its case of replacement of rubber, this strain was spread on the column by various percentages.

9- Whereas the ultimate load from the FE model, which was 140.807 kN, was higher than the ultimate load from the experimental data, which was 138.58 kN, according to the results of the column (G2F15) from group (2) by (1.607%). The service lateral displacement of this model was (17.045) % correspondingly less than that of the experimental column. While the service axial displacement of this model was (35.97) % correspondingly more than that of the experimental column.

10- increasing the steel ratio of the column from (0.021 to 0.043) mm resulted in the following: a significant increment in the maximum load of about (20.49) % for G1N specimens, about (29.26) % for G1F10 specimens, and about (20.20) % for G1F15 specimens, respectively.

11- While decreasing the steel ratio of the column from (0.021 to 0.014) mm resulted in the following: a significant decrement in the maximum load of about 15.24% for G1N specimens, about (20.28) % for G1F10 specimens, and about (32.46) % for G1F15 specimens, respectively

6-3 Suggestions for Future Work

A number of suggestions for future research are listed below. These suggestions may lead to more understanding of the performance of columns with adding rubber:

1- Studying the behavior of various rubberized structural elements, such as slabs and beam-column connectors.
2- Studying the behavior of rubberized columns with different amount of rubber under axial load.
3- In order to prevent shear failure at the ends and corbel of columns, additional tests on rubberized column specimens with different amounts of transverse reinforcement near the top and bottom are required.
4- Using columns with other materials to produce rubberized concrete such as shredded or fiber waste tire rubber, tests should be conducted with such this material to compared with those conducted in this study.
5- It suggests that future research focus on more essential experimental tests on the service features of rubberized concrete, such as fire resistance and sound thermal insulation.
6- The influence of the eccentricity of the pre-applied load by fire exposure on column behavior requires additional investigation.
7- Various supporting conditions may be considered on the performance of columns that replaces natural aggregate by rubber.

REFERENCES

[1] ACI 318-14, *ACI 318-14 - Building Code Requirements for Structural Concrete*. 2014.

[2] C. W. Dolan and A. H. Nilson, *Design of concrete structures*. 2016. doi: 10.1201/9781315368221-12.

[3] N. B. M. Noor, "Physical performance and durability evalution of rubberized concrete," *Dr. Thesis*, pp. 1–38, 2014, [Online]. Available: http://eprints.uthm.edu.my/id/eprint/7821/1/NURAZUWA_BINTI_MD_NOOR.pdf

[4] S. Raffoul, R. Garcia, D. Escolano-Margarit, M. Guadagnini, I. Hajirasouliha, and K. Pilakoutas, "Behaviour of unconfined and FRP-confined rubberised concrete in axial compression," *Constr. Build. Mater.*, vol. 147, pp. 388–397, 2017, doi: 10.1016/j.conbuildmat.2017.04.175.

[5] F. Elshazly, S. Mustafa, and H. Fawzy, "Rubberized concrete properties and its structural engineering applications – An overview," *Egypt. J. Eng. Sci. Technol.*, vol. 30, no. 1, pp. 1–11, 2020, doi: 10.21608/eijest.2020.35823.1000.

[6] K. B. Najim and M. R. Hall, "Mechanical and dynamic properties of self-compacting crumb rubber modified concrete," *Constr. Build. Mater.*, vol. 27, no. 1, pp. 521–530, 2012, doi: 10.1016/j.conbuildmat.2011.07.013.

[7] E. Ozbay, M. Lachemi, and U. K. Sevim, "Compressive strength, abrasion resistance and energy absorption capacity of rubberized concretes with and without slag," *Mater. Struct. Constr.*, vol. 44, no. 7, pp. 1297–1307, 2011, doi: 10.1617/s11527-010-9701-x.

[8] S. Dass and A. Sharma, "Rubberize+d Concrete : Needs of Good

REFERENCES

Environment (Overview),” *Int. J. Emerg. Technol. Adv. Eng.*, vol. 3, no. 3, 2013.

[9] E. Ganjian, M. Khorami, and A. A. Maghsoudi, “Scrap-tyre-rubber replacement for aggregate and filler in concrete,” *Constr. Build. Mater.*, vol. 23, no. 5, pp. 1828–1836, 2009, doi: 10.1016/j.conbuildmat.2008.09.020.

[10] F. Aslani, Mechanical Properties of Waste Tire Rubber Concrete,” *J. Mater. Civ. Eng.*, vol. 28, no. 3, p. 04015152, 2016, doi: 10.1061/(asce)mt.1943-5533.0001429.

[11] M. M. R. Taha, A. S. El-Dieb, M. A. A. El-Wahab, and M. E. Abdel-Hameed, “Mechanical , Fracture , and Microstructural Investigations of Rubber Concrete,” *J. Mater. Civ. Eng.*, vol. 1561, no. October, pp. 640–649, 2008.

[12] F. Aslani, G. Ma, D. L. Yim Wan, and V. X. Tran Le, “Experimental investigation into rubber granules and their effects on the fresh and hardened properties of self-compacting concrete,” *J. Clean. Prod.*, vol. 172, pp. 1835–1847, 2018, doi: 10.1016/j.jclepro.2017.12.003.

[13] J. O. Akinyele, R. W. Salim, and W. K. Kupolati, “the Impact of Rubber Crumb on the Mechanical and Chemical Properties of Concrete,” *Eng. Struct. Technol.*, vol. 7, no. 4, pp. 197–204, 2016, doi: 10.3846/2029882x.2016.1152169.

[14] M. Gesoglu, E. Güneyisi, O. Hansu, S. Ipek, and D. S. Asaad, “Influence of waste rubber utilization on the fracture and steel-concrete bond strength properties of concrete,” *Constr. Build. Mater.*, vol. 101, pp. 1113–1121, 2015, doi: 10.1016/j.conbuildmat.2015.10.030.

[15] B. S. Thomas and R. C. Gupta, “Long term behaviour of cement concrete containing discarded tire rubber,” *J. Clean. Prod.*, vol. 102, pp. 78–

87, 2015, doi: 10.1016/j.jclepro.2015.04.072.

[16] F. Liu, W. Zheng, L. Li, W. Feng, and G. Ning, “Mechanical and fatigue performance of rubber concrete,” *Constr. Build. Mater.*, vol. 47, pp. 711–719, 2013, doi: 10.1016/j.conbuildmat.2013.05.055.

[17] B. S. Thomas and R. Chandra Gupta, “Properties of high strength concrete containing scrap tire rubber,” *J. Clean. Prod.*, vol. 113, pp. 86–92, 2016, doi: 10.1016/j.jclepro.2015.11.019.

[18] L. Li, S. Ruan, and L. Zeng, “Mechanical properties and constitutive equations of concrete containing a low volume of tire rubber particles,” *Constr. Build. Mater.*, vol. 70, pp. 291–308, 2014, doi: 10.1016/j.conbuildmat.2014.07.105.

[19] İ. B. Topçu and A. Unverdi, “Scrap tires/crumb rubber,” *Waste Suppl. Cem. Mater. Concr. Characterisation, Prop. Appl.*, pp. 51–77, 2018, doi: 10.1016/B978-0-08-102156-9.00002-X.

[20] A. P. C. Duarte, B. A. Silva, N. Silvestre, J. de Brito, E. Júlio, and J. M. Castro, “Tests and design of short steel tubes filled with rubberised concrete,” *Eng. Struct.*, vol. 112, pp. 274–286, 2016, doi: 10.1016/j.engstruct.2016.01.018.

[21] A. T. Noaman, B. H. Abu Bakar, and H. M. Akil, “Experimental investigation on compression toughness of rubberized steel fibre concrete,” *Constr. Build. Mater.*, vol. 115, pp. 163–170, 2016, doi: 10.1016/j.conbuildmat.2016.04.022.

[22] M. K. Batayneh, I. Marie, and I. Asi, “Promoting the use of crumb rubber concrete in developing countries,” *Waste Manag.*, vol. 28, no. 11, pp. 2171–2176, 2008, doi: 10.1016/j.wasman.2007.09.035.

[23] L. Zheng, X. S. Huo, and Y. Yuan, “Strength, Modulus of Elasticity,

and Brittleness Index of Rubberized Concrete," *J. Mater. Civ. Eng.*, vol. 20, no. 11, pp. 692–699, 2008, doi: 10.1061/(asce)0899-1561(2008)20:11(692).

[24] G. Li, S. S. Pang, and S. I. Ibekwe, "FRP tube encased rubberized concrete cylinders," *Mater. Struct. Constr.*, vol. 44, no. 1, pp. 233–243, 2011, doi: 10.1617/s11527-010-9622-8.

[25] M. Al-Fadhli, "Advantages of Concrete Mixing with Tyre Rubber," *J. Eng. Res. Appl. www.ijera.com*, vol. 7, no. 4, pp. 96–98, 2017, doi: 10.9790/9622-0704069698.

[26] R. H. Ghedan and D. M. Hamza, "Effect Of Rubber Treatment On Compressive Strength And Thermal Conductivity Of Modified Rubberized Concrete," *J. Eng. Dev.*, vol. 15, no. 4, pp. 21–29, 2011.

[27] A. R. Khalid and M. H. Hameed, "Rubberized concrete (rubcrete) - A novest approch," *1st Int. Multi-Disciplinary Conf. 2015*, no. November, pp. 4–10, 2015.

[28] K. Strukar, T. K. Šipoš, T. Dokšanović, and H. Rodrigues, "Experimental study of rubberized concrete stress-strain behavior for improving constitutive models," *Materials (Basel).*, vol. 11, no. 11, 2018, doi: 10.3390/ma11112245.

[29] A. Siddika, M. A. Al Mamun, R. Alyousef, Y. H. M. Amran, F. Aslani, and H. Alabduljabbar, "Properties and utilizations of waste tire rubber in concrete: A review," *Constr. Build. Mater.*, vol. 224, pp. 711–731, 2019, doi: 10.1016/j.conbuildmat.2019.07.108.

[30] J. Lv, T. Zhou, Q. Du, and K. Li, "Experimental and analytical study on uniaxial compressive fatigue behavior of self-compacting rubber lightweight aggregate concrete," *Constr. Build. Mater.*, vol. 237, p. 117623, 2020, doi: 10.1016/j.conbuildmat.2019.117623.

[31] A. A. Kadhim and H. M. K. Al-Mutairee, “An experimental study on behavior of sustainable rubberized concrete mixes,” *Civ. Eng. J.*, vol. 6, no. 7, pp. 1273–1285, 2020, doi: 10.28991/cej-2020-03091547.

[32] K. S. Son, I. Hajirasouliha, and K. Pilakoutas, “Strength and deformability of waste tyre rubber-filled reinforced concrete columns,” *Constr. Build. Mater.*, vol. 25, no. 1, pp. 218–226, 2011, doi: 10.1016/j.conbuildmat.2010.06.035.

[33] J. Xue and M. Shinozuka, “Rubberized concrete: A green structural material with enhanced energy-dissipation capability,” *Constr. Build. Mater.*, vol. 42, pp. 196–204, 2013, doi: 10.1016/j.conbuildmat.2013.01.005.

[34] O. Youssf, M. A. ElGawady, and J. E. Mills, “Experimental Investigation of Crumb Rubber Concrete Columns under Seismic Loading,” *Structures*, vol. 3, pp. 13–27, 2015, doi: 10.1016/j.istruc.2015.02.005.

[35] O. Youssf, M. Elgawady, and J. E. Mills, “Behaviour of Frp-Confined Crumb Rubber,” no. December 2018, 2015.

[36] A. Moustafa, A. Gheni, and M. A. ElGawady, “Shaking-Table Testing of High Energy–Dissipating Rubberized Concrete Columns,” *J. Bridg. Eng.*, vol. 22, no. 8, p. 04017042, 2017, doi: 10.1061/(asce)be.1943-5592.0001077.

[37] R. Hassanli, O. Youssf, and J. E. Mills, “Experimental investigations of reinforced rubberized concrete structural members,” *J. Build. Eng.*, vol. 10, pp. 149–165, 2017, doi: 10.1016/j.jobe.2017.03.006.

[38] R. Hassanli, O. Youssf, and J. E. Mills, “The Behaviour of Structural Members Made with Crumbed Rubber Concrete,” *28th Bienn. Natl. Conf. Concr. Inst. Aust.*, no. October, p. 10, 2017, [Online]. Available: https://www.researchgate.net/publication/320614160_The_Behaviour_of_St

ructural_Members_Made_with_Crumbed_Rubber_Concrete

[39] Li and Y. Li, "Experimental study on performance of rubber particle and steel fiber composite toughening concrete," *Constr. Build. Mater.*, vol. 146, pp. 267–275, 2017, doi: 10.1016/j.conbuildmat.2017.04.100.

[40] R. Hassanli, O. Youssf, and J. E. Mills, "Seismic Performance of Precast Posttensioned Segmental FRP-Confined and Unconfined Crumb Rubber Concrete Columns," *J. Compos. Constr.*, vol. 21, no. 4, p. 04017006, 2017, doi: 10.1061/(asce)cc.1943-5614.0000789.

[41] R. Hassanli, O. Youssf, J. E. Mills, R. Karim, and T. Vincent, "Performance of segmental self-centering rubberized concrete columns under different loading directions," *J. Build. Eng.*, vol. 20, no. May, pp. 285–302, 2018, doi: 10.1016/j.jobe.2018.08.003.

[42] A. Y. Elghazouli, D. V. Bompa, B. Xu, A. M. Ruiz-Teran, and P. J. Stafford, "Performance of rubberised reinforced concrete members under cyclic loading," *Eng. Struct.*, vol. 166, no. November 2017, pp. 526–545, 2018, doi: 10.1016/j.engstruct.2018.03.090.

[43] T. Pham, X. Zhang, and A. Karrech, "Dynamic Response of Rubberized Concrete Columns with and without FRP Confinement Subjected to Lateral Impact Dynamic Response of Rubberized Concrete Columns with and without FRP Confinement Subjected to Lateral Impact," no. July, 2018, doi: 10.1016/j.conbuildmat.2018.07.146.

[44] M. M. Al-Tayeb, B. H. Abu Bakar, H. M. Akil, and H. Ismail, "Performance of Rubberized and Hybrid Rubberized Concrete Structures under Static and Impact Load Conditions," *Exp. Mech.*, vol. 53, no. 3, pp. 377–384, 2013, doi: 10.1007/s11340-012-9651-z.

[45] A. P. C. Duarte, B. A. Silva, N. Silvestre, J. de Brito, E. Júlio, and J.

M. Castro, “Finite element modelling of short steel tubes filled with rubberized concrete,” *Compos. Struct.*, vol. 150, pp. 28–40, 2016, doi: 10.1016/j.compstruct.2016.04.048.

[46] B. Xu, D. V. Bompa, A. Y. Elghazouli, A. M. Ruiz-Teran, and P. J. Stafford, “Numerical assessment of reinforced concrete members incorporating recycled rubber materials,” *Eng. Struct.*, vol. 204, no. September 2019, 2020, doi: 10.1016/j.engstruct.2019.110017.

[47] I. M. H. Alshaikh, B. H. A. Bakar, E. A. H. Alwesabi, A. M. Zeyad, and H. M. Magbool, “Finite element analysis and experimental validation of progressive collapse of reinforced rubberized concrete frame,” *Structures*, vol. 33, no. June, pp. 2361–2373, 2021, doi: 10.1016/j.istruc.2021.06.008.

[48] A. M. Ali, S. R. Taai, E. K. Jaafar, H. N. G. AL-Maliki, H. M. Madhloom, and N. Al-ansari, “Nonlinear Simulation Analysis of Mechanical Behaviour of Rubberized Concrete,” *Int. J. GEOMATE*, vol. 22, no. 90, pp. 125–137, 2022, doi: 10.21660/2022.90.13.

[49] C. Liang, Y. Fu, C. Wang, Y. Gao, and J. Zhao, “Damping of rubberized recycled aggregate concrete and damping estimation of its elements by finite element analysis,” *Compos. Struct.*, vol. 281, no. August 2021, p. 114967, 2022, doi: 10.1016/j.compstruct.2021.114967.

[50] M. S. Gomaa and M. Elsayed, “Behavior of Short Reinforced Crumb Rubber Concrete Columns Subjected to Behavior of Short Reinforced Crumb Rubber Concrete Columns Subjected to Elevated Temperatures,” no. February, 2020.

[51] ACI 318-19, *Building Code (ACI 318-19) and Commentary on Building Code Requirements for Structural Concrete (ACI 318R-19)*. 2019.

[52] R. M. Waqas and F. Butt, “Behavior of quarry rock dust, fly ash and

slag based geopolymer concrete columns reinforced with steel fibers under eccentric loading," *Appl. Sci.*, vol. 11, no. 15, 2021, doi: 10.3390/app11156740.

[53] D. B. Le, S. D. Tran, J. L. Torero, and V. T. N. Dao, "Application of digital image correlation system for reliable deformation measurement of concrete structures at high temperatures," *Eng. Struct.*, vol. 192, pp. 181–189, 2019, doi: 10.1016/j.engstruct.2019.05.009.

[54] Iraqi Specification No.5 -1984, Portland cement, 1984.

[55] Iraqi Specification No.45-1984, Aggregate from natural sources for concrete and building construction, 1984.

[56] ASTM A615-16, "Standard Specification for Deformed and Plain Carbon Structural Steel Bars for Concrete Reinforcement", Annual Book of ASTM Standards, 2016.

[57] ACI Committee 211.1-91, "Standard Practice for Selecting Proportions for Normal Heavyweight, and Mass Concrete" (ACI 211.1 - 91).

[58] ASTM 143M-12, Standard Test Method for Slump of Hydraulic-Cement Concrete ASTM International, West Conshohocken, PA, USA, 2012.

[59] BS 1881 Part 116 (1989), "Method for Determination of Compressive Strength of Concrete Cube", British Standards Institution.

[60] ASTM Standard C496/ C496M: Standard Test Method for Splitting Tensile Strength of Cylindrical Concrete Specimens, ASTM International, West Conshohocken, PA, USA, 2009.

[61] ASTM C78-02, (2002), "Standard Test Method for Flexural Strength of Concrete (Using Simple Beam with Third-Point Loading", Annual Book of ASTM Standards, American Society for Testing and Materials.

REFERENCES

[62] O. Youssf, R. Hassanli, and J. E. Mills, “Mechanical performance of FRP-confined and unconfined crumb rubber concrete containing high rubber content,” *J. Build. Eng.*, vol. 11, pp. 115–126, 2017, doi: 10.1016/j.jobe.2017.04.011.

[63] V. Corinaldesi and J. Donnini, *Waste rubber aggregates*. Elsevier Ltd, 2018. doi: 10.1016/B978-0-08-102480-5.00004-X.

[64] D. V Bompa, A. Y. Elghazouli, B. Xu, and P. J. Stafford, “Experimental assessment and constitutive modelling of rubberised concrete materials,” vol. 137, pp. 246–260, 2017, doi: 10.1016/j.conbuildmat.2017.01.086.

[65] Lubliner, J., Oliver, J., Oller, S., & Oñate, E. “A plastic-damage model for concrete‖. International Journal of Solids and Structures, 25(3), pp. (299-326), (1989).

[66] ibbitt, Karlsson, & Sorensen, “ABAQUS User’s Manual”. Pawtucket, 6th Edition, (2010).

[67] Jankowiak, Tomasz, and Tomasz Lodygowski. "Identification of parameters of concrete damage plasticity constitutive model." Foundations of civil and environmental engineering6.1 (2005): 53-69.

[68] Malm, R., “Shear cracks in concrete structures subjected to in-plane stresses,” Lic. thesis, Royal Institute of Technology (KTH) (2006), Stockholm, Sweden.

[69] Birtel, V., and P. Mark. "Parameterised finite element modelling of RC beam shear failure." ABAQUS users’ conference. 2006.

[70] D. V Bompa, A. Y. Elghazouli, B. Xu, and P. J. Stafford, “Experimental assessment and constitutive modelling of rubberised concrete materials,” vol. 137, pp. 246–260, 2017, doi:

10.1016/j.conbuildmat.2017.01.086.

[71] Hordijk DA. Tensile and tensile fatigue behaviour of concrete; experiments, modelling and analyses. Heron 1992;37(1).

[72] ACI (American Concrete Institute). ACI 318M-14 building code requirements for structural concrete and commentary. Farmington Hills, MI.

[73] ACI (American Concrete Institute). ACI 318M-14 building code requirements for structural concrete and commentary. Farmington Hills, MI.

[74] William, K. J., and Warnke, E. P. (1975). "Constitutive model for the triaxial behavior of concrete." Proc, International Association for Bridge and Structural Engineering, vol. 19, 1-30.

[75] Schickert, G., and Winkler, H. (1979). "Results of tests concerning strength and strain of concrete subjected to multiaxial compressive stresses." Deutscher Ausschuss fur Stahlbeton, Heft 277, Berlin, West Germany.

[76] Elwi, A. A., and Murray, D. W. (1979). "A 3D hypoelastic concrete constitutive relationship." *J. Engrg. Mech. Div.*, ASCE, 105(4), 623-641.

[77] Jeffrey S. Russell. "Prestrectives in Civil Engineering". Commemorating the 150th Anniversary of the American Society of Civil Engineering, ASCE Publications, 2003.

[78] Muthuswamy, K.R,and Thirugnanam G.S. "Structural Behaviour of Hybrid Fibre Reinforced Concrete Exterior Beam-Column Joint Subjected to Cyclic Loading". International Journal of Civil and Structural Engineering, 2014.

APPENDIX A

Design of Control Columns

A-1 Design of Concrete Columns (4 ø10), *f*'c=30 MPa, fy=600 MPa

All columns were design according to ACI 318M-19 Code. The control columns were designed in such a way to ensure capacity. The control columns are without rubber (i.e., normal columns) as a reference column, all columns have a square cross-section of 120×120 mm, with a total length of 1000 mm. The distance between corbels (middle portion) is 520 mm and the dimensions of the corbel are 120×240×120 mm. All columns had a similar clear cover of 15 mm from each exterior concrete face to the longitudinal reinforcement, the details of reinforcement included (4ø10mm) diameter of deformed bars were provided as longitudinal reinforcement. Also, the columns have steel ties of diameter (**ø**4 mm) with spacing of 100 mm c/c (or 60 mm c/c).

According to the ACI 318M-19, the design calculation is induced, as follows:

● Longitudinal Reinforcement

A_g =120*120=14400 mm^2

A_{st} = 4* π/4*$(10)^2$ =314.16 mm^2

$\rho = A_{st}/ A_g$ =314.16 / 14400 =0.021

$0.01 \leq \rho \leq 0.08$ (Ok)

● Clear Spacing of Longitudinal Reinforcement

The greatest of { 40 mm ; $1.5\ d_b$; $4/3 * d_{agg}$ } **=40 mm**

● Max Spacing of transverse Reinforcement

The greatest of { $16\ d_b = 16*10 = 160$; $48\ d_{tie} = 48*4 = 192$; Least dimension=120 } **=120 mm**

use = 100 mm

A.2 Ultimate Strength Calculation

***For e=0**

h=120 mm

$P_o = 0.85 * f_C' * (A_g - A_{st}) + A_{st} * f_y$

$P_o = (0.85 * 30 * (0.12*0.12 - 314.159 * 10^{-6}) + 314.159 * 600 * 10^{-6}) * 10^3$

$=548\ kN$

$p_u = 0.65 * 548 = 356.2$ KN

***For e=45 mm**

h=120 mm

$\sum$ Force =0, $Pu' = 0.85 * f_C' * b * a + A_S' * f_y - A_S * f_S$ ……①

$Pu' = 0.85 * 30 * a * 0.12 + 157.1 * 10^{-6} * 600 - 157.1 * 10^{-6} * f_S$ …….. ①

$e' = e + h/2 - d'$

$e' = 45 + 120/2 - 24$

$e' = 81$ mm

$\sum M_{AS} = 0$

$Pu' * e' = 0.85 * f_c' * b * a * (d - a/2) + A_S' * f_y * (d - d')$ …… ②

$Pu' * 0.081 = 0.85 * 30 * 0.12 * a (0.096 - a/2) + 157.1 * 10^{-6} * 600 * (0.096 - 0.024)$

……②

From strain diagram:

$\varepsilon_s / (d-c) = \varepsilon_s / c$

$f_s = \varepsilon_s * E_s = 600 (B_1 * d/a - 1) = 600(0.85 * 0.096/a - 1)$ ……. ③

Solution of eq ①, ② and ③

$a = 0.057$ m

$f_s = 600(0.85 * 0.096/0.057 - 1) = 258.95$ Mpa

$Pu' = (0.85 * 30 * 0.057 * 0.12 + 157.1 * 10^{-6} * 600 - 157.1 * 10^{-6} * 258.95) * 10^3$

Pu′ = 228 kN

***For e=75 mm**

h=120 mm

$\sum$ Force =0, $Pu' = 0.85 * f_C * b * a + A_S' * f_y - A_S * f_S$ ……①

$Pu' = 0.85 * 30 * a * 0.12 + 157.1 * 10^{-6} * 600 - 157.1 * 10^{-6} * f_S$ ……...①

$e' = e + h/2 - d'$

$e' = 75 + 120/2 - 24$

$e' = 111$ mm

$\sum M_{AS} = 0$

$Pu' * e' = 0.85 * f_c' * b * a * (d - a/2) + A_S' * f_y * (d - d')$ …… ②

$Pu' * 0.111 = 0.85 * 30 * 0.12 * a (0.096 - a/2) + 157.1 * 10^{-6} * 600 * (0.096 - 0.024)$ ……②

From strain diagram:

$\varepsilon_s / (d-c) = \varepsilon_s / c$

$f_s = \varepsilon_s * E_s = 600 (B_1 * d/a - 1) = 600(0.85 * 0.096/a - 1)$ ……. ③

Solution of eq ①, ② and ③

$a = 0.0444$ m

$f_s = 600(0.85 * 0.096/0.0444 - 1) = 502.70$ MPa

$Pu' = (0.85 * 30 * 0.0444 * 0.12 + 157.1 * 10^{-6} * 600 - 157.1 * 10^{-6} * 502.70) * 10^3$

$Pu' = 151$ kN

A.3 Design of corbel

A-When (f_c' =30 MPa), e=45 mm

$Pu = 228$ KN / 2 $= 114$ KN $= Vu$

$Mu = Vu * a + Nu * (h-d)$

Mu= 114 * 0.060 + 0.2 * 114 * (0.24- 0.225)

=6.84 +0.342=7.182 KN.m

A_f =Mu/ Φ* f_y *la =7.182 *10^6/ (0.75*600*0.9*225)

=79 mm^2

A_n =Nu/ Φ* f_y =0.2 *114 *10^3/ (0.75*600)

=51 mm^2

A_{vf} =Vu/ Φ* f_y *μ =114 *10^3/ (0.75*600* 1.4)

= 181 mm^2

$A_s = A_f + A_n$

=79 + 51 = 130 mm^2

A_s = ⅔ A_{vf} + A_n

=⅔* 181 +51 = 172 mm^2

use A_S= 172 mm^2

Use 3 ø10 = 235.62 > 172 mm^2 (ok)

Ah = 0.5 (A_s- A_n)

=0.5 (172 -51) = 61mm^2

Use 4 ø4 =101 mm^2 > 61 mm^2 (ok) (Closed)

2/3*d=2/3*225=150/4= 37.5

Use 5 ø 4 @ 40 mm (closed)

Appendix B

Modeling of Material Properties in FEA

B.1 Introduction

ABAQUS is a complex finite element (FE) package widely used in civil Engineering practice. In particular, it is used for modeling of reinforced concrete structures. Smeared crack concrete model, brittle crack concrete model, and concrete damaged plasticity (CDP) model are the three material models available in ABAQUS for the analysis of concrete. In the current study, the concrete damaged plasticity model out of the three concrete models is chosen because it takes concrete's tensile cracking and compressive crushing into account as potential failure mechanisms. The behavior and characteristics of the concrete and other materials used in this investigation, as well as the CDP model employed in ABAQUS, are all explained below.

B.2 Concrete Damage Plasticity (CDP)

CDP can represent all structural types of reinforced or unreinforced concrete, as well as other quasi-brittle materials, exposed to monotonic, cyclic, or dynamic stresses. This model is based on a linked damage plasticity theory, and the multi-axial behavior of concrete in the damaged plasticity model is governed by a yield surface presented by **[65],** as shown in Figure (B-1). The principal failure mechanisms in this model are tensile cracking and compressive crushing of concrete. In addition, this model takes into account material degradation for both tension and compression behavior.

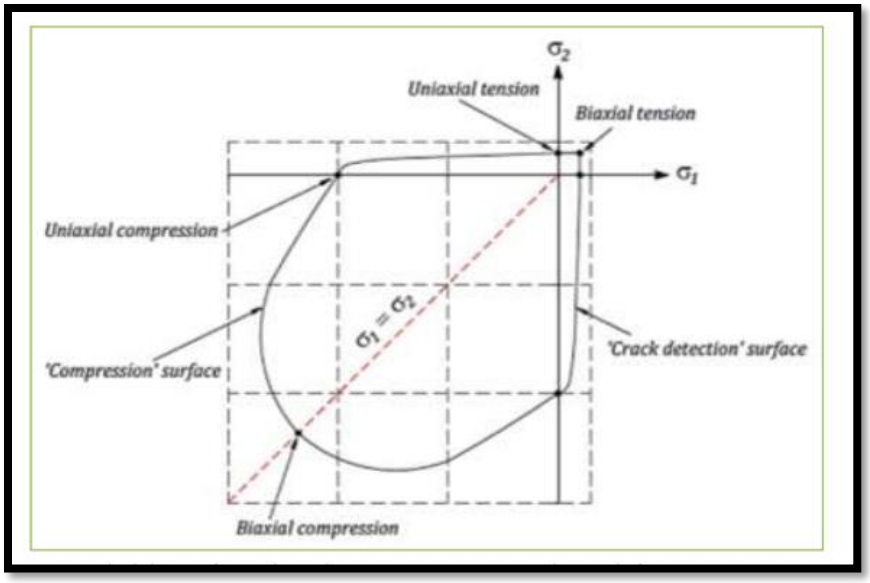

Figure (B-1): Yield surface in plane stress reproduced from (Lubliner et. al., 1989) [65].

B.3 UNIAXIAL BEHAVIOR OF CONCRETE

B.3.1 Uniaxial Behavior of normal strength Concrete

B.3.1.1 Uniaxial Tensile Behavior for normal strength Concrete

Under uniaxial tension, as can be seen in Figure (B-2), the stress increases with a linear elastic relationship with strain up to the ultimate tensile strength (ft), and then micro-cracks from microscopically with a tension softening response. There are three different methods to define tension softening response in ABAQUS: stress-strain, stress-displacement, or by use of fracture energy Gf **(Hibbitt, et.al, 2010**) **[66]**.

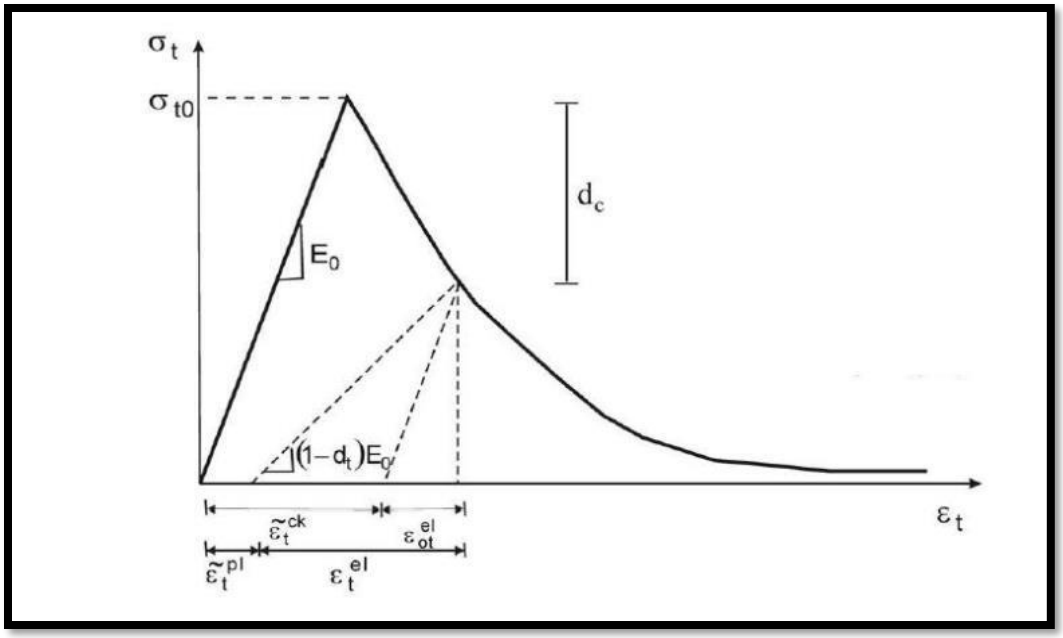

Figure (B-2): Uniaxial tensile behavior of concrete [67].

To define the tensile stress-strain relation of concrete in ABAQUS, user should input young's modulus (E_0), stress (σ_t), cracking strain (ε_t^{cr}) values and the damage parameter values (dt) for the relevant grade of concrete. The cracking strain (ε_t^{cr}) should be calculated from the total strain using Eq. (B-1) below:

$$\varepsilon_t^{cr} = \varepsilon_t - \varepsilon_{ot}^{el} \qquad \text{(B-1)}$$

Where, $\varepsilon_{ot}^{el} = \sigma_t / E_0$, the elastic strain corresponding to the undamaged material, and ε_t = total tensile strain.

B.3.1.2 Uniaxial Compression Behavior for normal strength Concrete

Under uniaxial compression, there is a linear elastic relationship between stress-strain until initial yield. After losing stiffness due to bond failure between the aggregates and the cement paste, the behavior becomes

non-linear. In stresses greater than ultimate strength, stress hardening and strain softening defines plastic response. In other words, compressive stress decreases while the corresponding strain increases. The uniaxial compressive behavior of concrete is depicted in Figure (B-3).

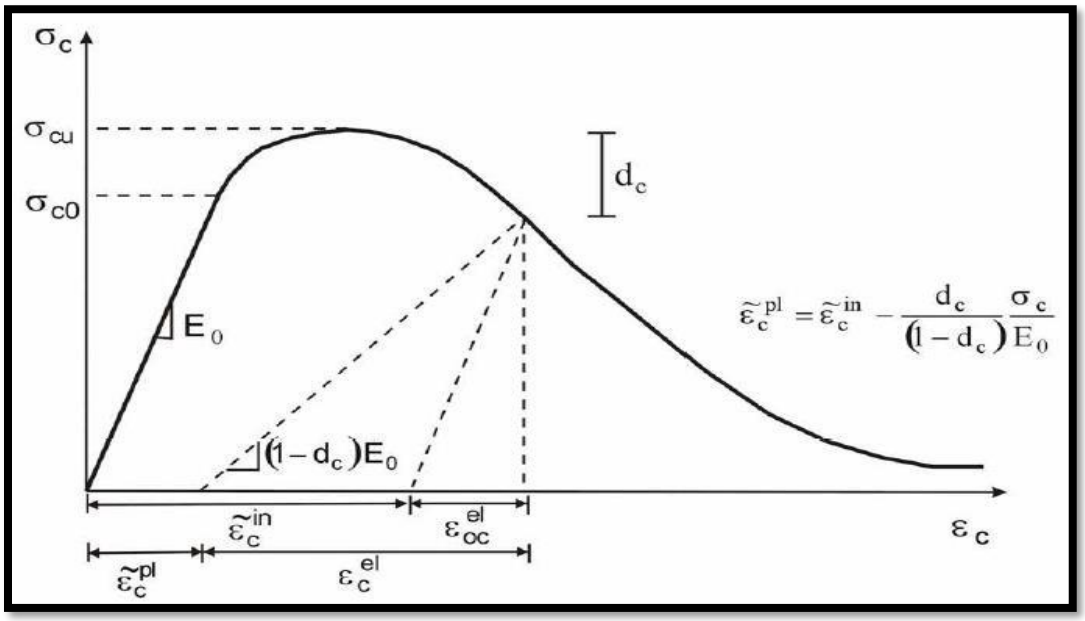

Figure (B-3): Uniaxial compressive behavior of concrete reproduced from [68].

To define the compression stress-strain relation of concrete in ABAQUS, user needs to enter the stresses (σc), inelastic strains (ε_c^{in}) correspond to stress values, and damage properties (dc) with inelastic strains in tabular format. Therefore, total strain values should be converted to the inelastic strains using Eq. (B-2):

$$\varepsilon_c^{in} = \varepsilon_c - \varepsilon_{oc}^{el} \qquad \text{(B-2)}$$

Where, $\varepsilon_{oc}^{el} = \sigma_c / E_0$, the elastic compression strain corresponding to the undamaged material, and ε_c= total compression strain.

Compression and tension damage parameters describing crushing and cracking behavior were defined as tables within CDPM. The following equations developed by **(Birtel and Mark) [69]** were successfully used in obtaining the compression and damage parameters. Damage parameters take values ranging from 0 (no damage) to 1 (fully damaged), representing the level of damage. E_c^{-1}

$$dc = 1 - \frac{\sigma c \, E_c^{-1}}{\varepsilon_c^{pl}\left(\frac{1}{bc}-1\right)+\sigma c \, E_c^{-1}} \quad (B-3)$$

$$dt = 1 - \frac{\sigma t \, E_c^{-1}}{\varepsilon_{ct}^{pl}\left(\frac{1}{bt}-1\right)+\sigma t \, E_c^{-1}} \quad (B-4)$$

$$\varepsilon_c^{pl} = b_c \, \tilde{\varepsilon}_c^{in} \quad (B-5)$$

$$\varepsilon_t^{pl} = b_t \, \tilde{\varepsilon}_t^{ck} \quad (B-6)$$

The coefficients b_c and b_t take values between 0 and 1. Birtel and Mark **[69]** suggested bc=0.7 and bt=0.1.

Further, corrective measures should be taken to ensure that the plastic strain values calculated using (eq. B-5 and eq. B-6) are neither negative nor decreasing with increased stresses **[66]**.

B.3.2 Uniaxial Behavior of Rubberized Concrete

B.3.2.1 Uniaxial Compression Behavior for Rubberized Concrete

Rubberized concrete (RC) behaves differently under loads from normal concrete and high compressive strength concrete. There have been numerous studies about the mechanical characteristics of RC, but relatively few have explained its behavior. Constitutive uniaxial models were created in order to simulate the

behavior of concrete under a single axial stress quantitatively. It should be mentioned that there are further constitutive models that describe the behavior of concrete under different stress states and for different purposes, but they have not been created for rubberized concrete due to a lack of experimental data. based on the experimental results of numerous studies, variations in the mixture proportions, additives, etc., have an impact on concrete behavior, namely the uniaxial curve's shape. Because of this, no one constitutive model can be used to explain the behavior of all varieties of concrete, and for rubberized concrete, only a few models have been proposed. Both the volume of rubber and the size of the rubber particle are taken into account by these models. To obtain a stress-strain curve as in Figure (B-4), input data in models are peak compressive stress *fc*, peak strain ε_c and elastic modulus *Ec* of normal concrete (NC) which are used to calculate peak compressive stress f_{rc}, peak strain ε_{rc} and elastic modulus *Erc* of rubberized concrete (RC). However, researchers considered different parameters while developing constitutive models described with a stress factor σ/frc.

Bompa et al. **[6]** presented a constitutive model for rubberized concrete which uses equations that they proposed to estimate the elastic modulus and peak compressive stress of rubberized concrete. The constitutive model considers the volumetric rubber ratio ρ_{vr} up to 0.65 (65% of volumetric rubber replacement with mineral aggregate) and size of replaced mineral aggregate $d_{g,repl}$ with factor λ. The constitutive model has three parts; first up to the proportionally limit $\varepsilon_{rc,el}$ (1), second up to the peak strain ε_{rc} (ascending part of the curve) (2), and third after the peak strain (descending part of the curve) (3) which depends on the post-peak crushing energy $gc,2$.

Peak compressive stress for rubberized concrete:

$$\sigma = E_{rc}\varepsilon_{rc,1},\cdots\varepsilon_{rc} \leq \varepsilon_{rc,el} \tag{B-7}$$

$$\frac{\sigma}{f_{rc}} = \left[\frac{5}{3} \times \left(\frac{\varepsilon-\varepsilon_{rc,el}}{\varepsilon_{rc}}\right) - \left(\frac{\varepsilon-\varepsilon_{rc,el}}{\varepsilon_{rc}}\right)^2 + \frac{0.3f_{rc}}{f_{rc}}\right],\ \varepsilon\,\epsilon\left(\varepsilon_{rc,el},\ \varepsilon_{cr}\right) \tag{B-8}$$

$$\frac{\sigma}{f_{rc}} = \left[\frac{1}{8} \times \left(\frac{f_{rc}}{g_{c,2}} - 1\right)\left(\frac{\varepsilon-\varepsilon_{rc1,2}}{\varepsilon_{rc}}\right)^2 - \frac{6}{8}\left(\frac{f_{rc}}{g_{c,2}} - 1\right)\left(\frac{\varepsilon-\varepsilon_{rc1,2}}{\varepsilon_{rc}}\right) + \frac{f_{rc,2}}{f_{rc}}\right],\ \varepsilon\,\epsilon\left(\varepsilon \geq \varepsilon_{rc}\right) \tag{B-9}$$

$$\frac{f_{rc,2}}{f_{rc}} = \left[\frac{5}{3} \times \left(\frac{\varepsilon_{rc}-\varepsilon_{rc,el}}{\varepsilon_{rc}}\right) - \left(\frac{\varepsilon_{rc}-\varepsilon_{rc,el}}{\varepsilon_{rc}}\right)^2 + \frac{0.3f_{rc}}{f_{rc}}\right] \tag{B-10}$$

$$f_{rc} = \frac{1}{1+2\left(\frac{3\lambda\rho_{vr}}{2}\right)^{3/2}} f_c \tag{B-11}$$

$$\lambda = \begin{cases} 2.43 \rightarrow\ d_{g,repl}\,\epsilon\,(0,5) \\ 2.90 \rightarrow\ d_{g,repl}\,\epsilon\,\left(0, d_{g,max}\right) \\ 2.08 \rightarrow\ d_{g,repl}\,\epsilon\,\left(5, d_{g,max}\right) \end{cases} \tag{B-12}$$

$$E_{rc} = 12\left(f_{rc}/10\right)^{2/3} \tag{B-13}$$

$$\varepsilon_{rc,el} = 0.3f_{rc}/E_{rc} \tag{B-14}$$

$$\varepsilon_{rc1,2} = \frac{4}{3(1-\rho_{vr})}\varepsilon_{rc} \tag{B-15}$$

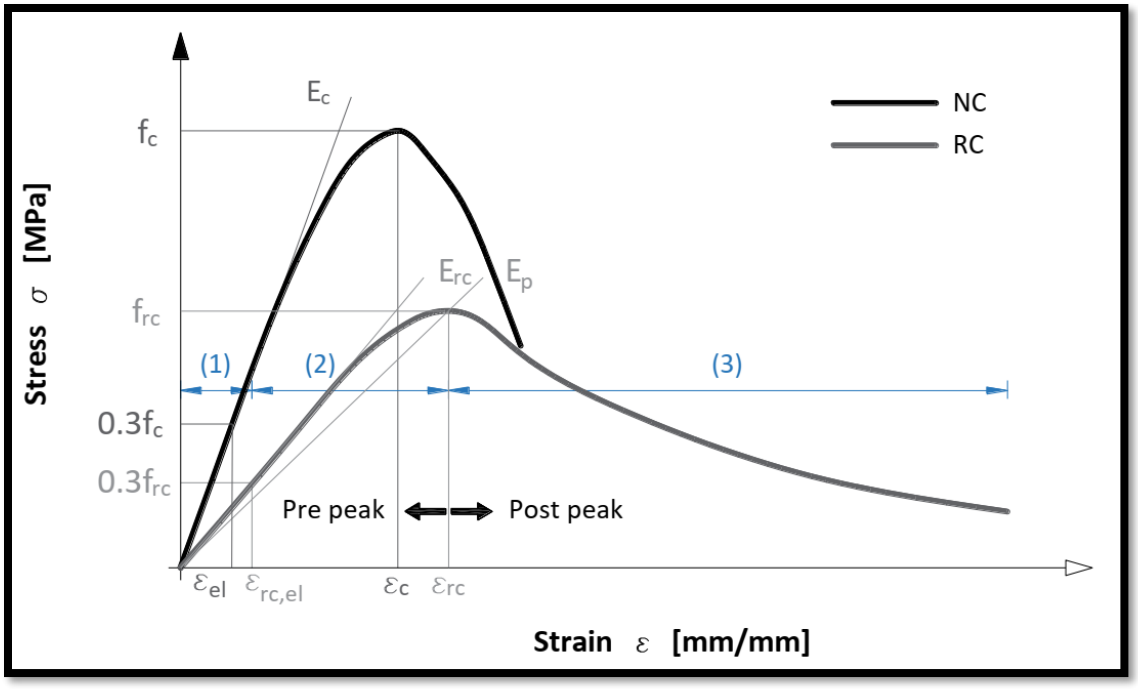

Figure (B-4): Stress-strain curve which describes mechanical parameters needed for establishing constitutive model of rubberized concrete.

B.3.2.2 Uniaxial Tension Behavior for Rubberized Concrete

The uniaxial tensile behavior of RC considered in this study follows a linear stress-strain relationship up to the tensile strength f_{ct}, and an exponential decay function for the softening behavior as shown in Eq. (B-16) with $f_{ct} = 0.3 \times f_c \text{^} 1/2$ and constitutive parameters $c1$ = 3, $c2$ = 6.93 **[70][71]**. In the decay function, the tensile stress-crack opening width w relationship is a function of both the tensile strength fct and maximum crack opening width $w_{max,r}$. The latter is determined using Eq. (B-17) **[72]**, which accounts for the influence of rubber content ρ_{vr}. The cracking opening width is transformed to strain with the consideration of the characteristic length lm, and damage parameters are employed in the softening regime. Beyond $w_{max,r}$, the damage tension scalar is subsequently held constant to preserve a residual stiffness and strength **[73]**.

$$\sigma_t/f_{ctr} = [1 + (c_1 w/w_{\max,r})^3] \exp(-c_2 w/w_{\max,r}) - (w/w_{\max,r})(1 + c_1{}^3) \exp(-c_2) \quad \text{(B-16)}$$

$$w_{\max,r} = w_{\max,0} + 0.3\rho_{vr} \ \text{(in mm)} \quad \text{(B-17)}$$

where 0.18mm

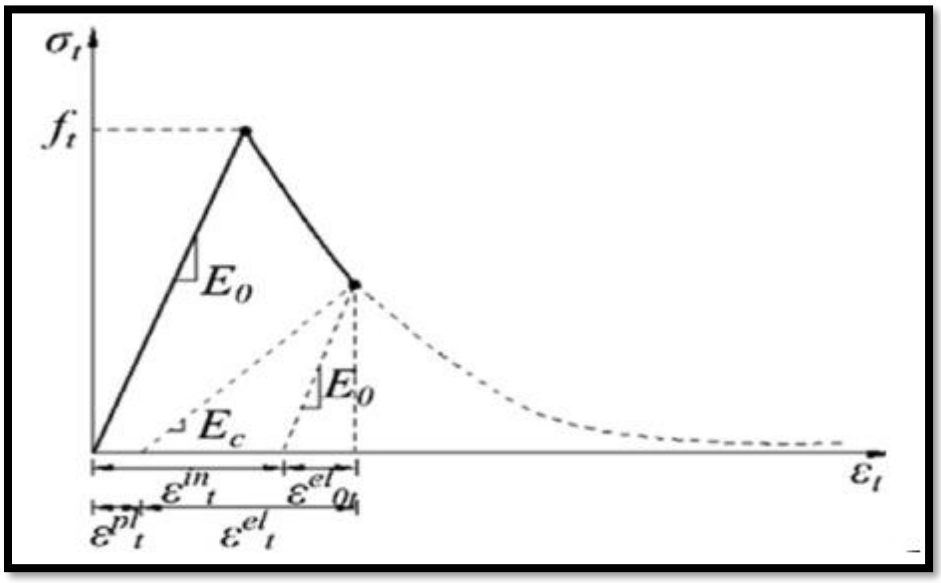

Figure (B-5): Material modelling with CDP uniaxial tension

B.4 Concrete Damaged Plasticity Definitions

In order to describe strength with the equation for triaxial stress as input to the finite element program ABAQUS, a set of five parameters are required to completely describe the plastic behavior of concrete;

Ψ: is the dilation angle, where it should be defined to calculate the inclination of the plastic flow potential in high confining pressures measured in (p-q) plane, as shown in Figure (B-6). In higher level of confinement stress and plastic strain, dilation angle is decreased. Maximum value of it equal (56.3^o) and minimum value is close to (zero). Upper values represent a more ductile behavior and lower values

show a more brittle behavior. According to (**Malm, 2006**) **[68]** the effect of the dilation angle in values between $30^o \leq \psi \leq 40^o$.

ε: is the flow potential eccentricity. It is a small positive number, which defines the range that the plastic potential function closes to the asymptote as shown in Figure (B-6). The default value in ABAQUS is (0.1) and indicates that the dilation angle is almost constant in a wide range of confining pressure. In higher value of (ϵ), with reduction of confining pressure, the dilation angle increases more rapidly. Very small values of in comparison with the default value may cause convergence problems in cases with low confining pressure, due to very tight flow potential curvature at the point of intersection with the (p-axis) **(Malm, 2006) [68].**

Fb0/fc0: is the proportion of initial equibiaxial compressive yield stress and initial uniaxial compressive yield stress. The default value in ABAQUS is (1.16)

K: is the ratio of the second stress invariant in the tensile meridian to compressive meridian for any defined value of the pressure invariant at initial yield. It is used to define the multi-axial behavior of concrete and is ($0.5<Kc\leq1$). The default value in ABAQUS is (0.667).

μ: is the viscosity parameter. According to (Malm, 2006) μ=10-7 is recommended because in comparison with characteristic time increment it should be small.

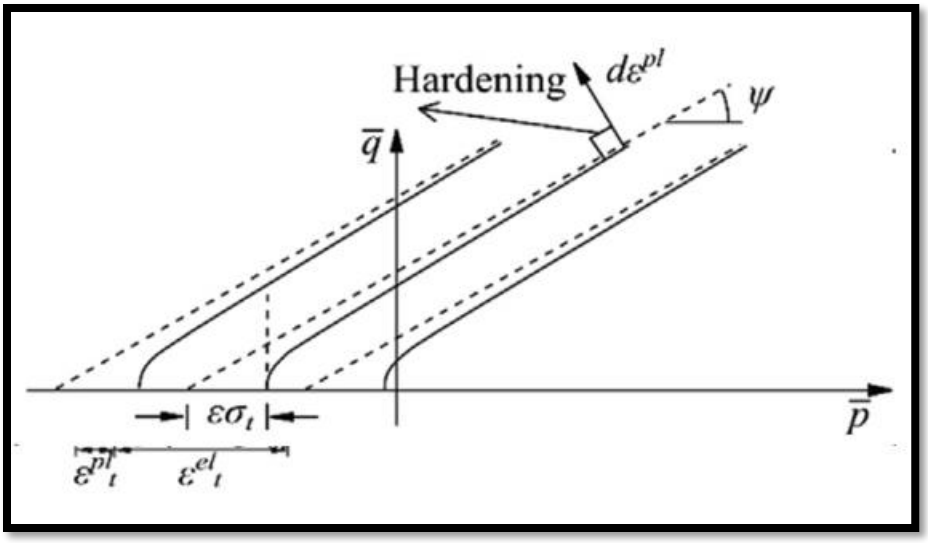

Figure (B-6): Hyperbolic plastic flow rule reproduced from **(Malm, 2006**) **[68]**.

B.5 Material Properties for FEM

B.5.1 Concrete Model Properties

The modulus of elasticity E_0 in the concrete damaged plasticity model, the Poisson's ratio v, and the compressive and tensile strengths of concrete are the concrete material parameters that should be used. To determine the confined concrete compressive strength f'_{cc}, a constitutive model involving a specified ultimate strength surface for multiaxial compressive stresses is used in this model. The "five-parameter" multiaxial failure surface described by **William and Warnke (1975) [74]** is adopted, since it provides excellent agreement with triaxial test data. The calculated ultimate strength surface based on the triaxial tests of **Schickert and Winkler (1977) [75]** is adopted here. Details of the calculations have been given by **Elwi and Murray (1979) [76]**. When the confined concrete core is placed in triaxial compression with equal effective lateral confining stresses f'_l from spirals or circular hoops, it can be shown that the confined compressive strength given is

$$f'_{cc} = f'_{co}\left(-1.254 + 2.254\sqrt{1 + \frac{7.94f'_l}{f'_{co}}} - 2\frac{f'_l}{f'_{co}} \right) \quad \text{(B-18)}$$

where f'_{co} = unconfined concrete compressive strength; and f'_l is given by below:

$$f'_l = \frac{1}{2} k_e \rho_s f_{yh} \quad \text{(B-19)}$$

On the other hand, tensile stress-strain (σ-ε) relationship was assumed linear up to the uniaxial tensile strength and then determined using the equation (B-20).

$$\varepsilon_t = \frac{f_t}{E_o} \quad \text{(B-20)}$$

B.5.2 Steel Reinforcement Model Properties

The required input parameters for material definition of steel bars, includes density, elastic and plastic behavior. Elastic behavior of steel material is defined by specifying young's modulus (*Es*) and Poisson's ratio (*v*) of which typical values are 200000 MPa and 0.3, respectively. Plastic behavior is defined in a tabular form, included yield stress and corresponding plastic strain. According to **(Hibbit et al.) [66]** defined. Input values of stress in each point for an isotropic material are calculated according to Eqs. (B-21) and (B-22). A higher number of input points lead to results that are more accurate.

$$\sigma_{true} = \sigma_{nominal}\,(1 + \varepsilon_{nominal}) \quad \text{(B-21)}$$

$$\sigma_{in}^{pl} = ln\,(1 - \varepsilon_{nominal}) - (\sigma_{true}/E_s) \quad \text{(B-22)}$$

B.5.3 Steel Plate Model Properties

The steel plates were modeled using an isotropic linear elastic material model by Eq. (B-23) with solid elements for all models. The assumption for the material of loading and supporting plates is to avoid problems in solution due to the large deformations that will be developed or stress singularity in the plates.

fs= E$s\varepsilon s$ (MPa), $\varepsilon s \leq \varepsilon y$ ……(B-23)

الخلاصة

الغرض من هذه الدراسة هو التحقق من سلوك الأعمدة الخرسانية المسلحة باستخدام قدر كبير من إعادة التدوير وإعادة استخدام فتات المطاط كبديل لجزيئات الركام. تتكون هذه الدراسة من جزأين: الأول هو العمل التجريبي ، والذي يتضمن إعداد واختبار ثمانية نماذج أعمدة خرسانية ، مقسمة إلى مجموعتين لدراسة تأثير: (استبدال الركام الناعم بفتات المطاط بثلاث نسب مختلفة بالحجم (5٪ ، 10٪ ، 15٪) ، الانحراف المركزي للحمل المطبق) ، على حمل التكسير ، قابلية التحمل النهائية ، التشوه ، نمط التكسير ، الليونة ، الصلابة ، ونمط الفشل. تم إجراء الاختبارات على ثمانية أعمدة مربعة ذات محتوى مطاطي متنوع. جميع نماذج الأعمدة لها نفس الأبعاد (120 * 120 * 1000) ملم ، وتم اختبارها تحت الحمل اللامركزي.

يؤثر وجود المطاط على الخواص الميكانيكية وسلوك الخرسانة المطاطية. بالمقارنة مع الخلطات الخرسانية العادية ، تقل الخواص الميكانيكية للخرسانة المطاطية المحتوية على 15٪ مطاط بنسبة (33.49 و 28.10)٪ لمقاومة الانضغاط وقوة الانشطار على التوالي. من ناحية أخرى ، تقل قدرة الحمل القصوى مع زيادة محتوى المطاط من 0٪ إلى 15٪ مع انحرافات (45 و 75) ملم بنسبة (25.45 و 12.88)٪ على التوالي. أيضًا ، مع زيادة الانحراف من 45 ملم إلى 75 ملم ، انخفضت سعة الحمولة النهائية حوالي (42.02 ، 40.41 ، 36.52 ، 32.24)٪ للأعمدة بدون المطاط ، والأعمدة بنسبة 5٪ من المطاط ، والأعمدة بنسبة 10٪ وأعمدة من المطاط بنسبة 15٪ على التوالي. وقد لوحظ أن نسبة المطاط إلى استبدال الركام الناعم تقلل من حمل الفشل في أعمدة الخرسانة المسلحة ، بالإضافة إلى تطور هام في حمل التكسير والليونة مقارنة مع نفس العينة بدون استبدال. بينما تدهورت صلابة عينات العمود التي تم استبدالها بالمطاط بعد تطبيق الحمل على مستويات مختلفة بشكل كبير مع زيادة مستوى الحمل المطبق.

يستخدم القسم الثاني من الدراسة نهج العناصر المحدودة غير الخطية ثلاثية الأبعاد لتصوير السلوك اللاخطي للمواد باستخدام تطبيق الكمبيوتر ABAQUS / القياسي 6.14 والطرق العددية للتحليل الرياضي لفحص الأعمدة المختبرة.

من حيث استجابة الحمل والتشوه والحمل النهائي وانتشار التشقق تمت مقارنة النتائج النظرية والنتائج التجريبية التي تم الحصول عليها. أظهرت نتائج نموذج العناصر المحدودة فرقًا في الحمل النهائي بحوالي (4.743٪) للخرسانة العادية (مع انحراف حوالي 45 ملم) واتفاق معقول مع البيانات التجريبية.

اشتملت الدراسة البارامترية على تأثيرات العوامل المختلفة: النوع الخرساني بنسب مختلفة من التسليح. بالإضافة إلى النسبة المستخدمة في النماذج التجريبية وبنفس العدد من قضبان التسليح ، تمت مناقشة نسبتين إضافيتين من حديد التسليح في هذه الدراسة ، حيث أدت زيادة نسبة حديد التسليح للعمود من (0.021 إلى 0.043) إلى ما يلي: زيادة ملحوظة في الحمل الأقصى بحوالي (20.49)٪ للعينة (بدون مطاط مع انحراف 45 ملم) ، حوالي (29.26)٪ للعينة (مع 10٪ من فتات المطاط ومع انحراف 45 ملم) ، وحوالي (20.20)٪ لعينة G1F15 (مع 15٪ من فتات المطاط ومع انحراف 45 ملم) ، على التوالي. بينما أدى انخفاض نسبة حديد التسليح للعمود من (0.021 إلى 0.014) إلى ما يلي: انخفاض ملحوظ في الحمل الأقصى بحوالي 15.24٪ للعينة (بدون مطاط ومع انحراف 45 ملم) ، حوالي (20.28)٪ للعينة. العينة (مع 10٪ من فتات المطاط ومع انحراف 45 ملم) ، وحوالي (32.46)٪ للعينة (مع 15٪ من فتات المطاط و انحراف 45 ملم) ، على التوالي.

جمهورية العراق

وزارة التعليم العالي والبحث العلمي

جامعة بابل

السلوك الإنشائي لأعمدة الخرسانة المسلحة والمطاطية المستدامة

اطروحة مقدمة لكليَّةِ الهندسة – جامعةِ بابل كجزء مِنْ متطلبات الحصول على درجةِ الماجستير في الهندسة المدنيةِ (الإنشاءات)

من قبل

تبارك حسين عبود

بكالوريوس علوم في الهندسة المدنية (2018) م

أشراف

الأستاذ الدكتور: حيدر محمد كاظم المطيري

الاستاذ المساعد الدكتور: ماجد محمد علي كاظم